INVESTIGATION OF REDOX-ACTIVE RUTHENIUM(II) POLYPYRIDYL

COMPLEXES AS POTENTIAL ANTI-CANCER DRUGS

By

ABHISHEK YADAV

Presented to the Faculty of the Graduate School of

The University Of Texas at Arlington in Partial Fulfillment

of the Requirements

for the Degree of

DOCTOR OF PHILOSOPHY

THE UNIVERSITY OF TEXAS AT ARLINGTON

December 2008

ACKNOWLEDGEMENTS

I would like to take this opportunity to express my sincere gratitude to my Ph.D. advisor Prof Frederick M. MacDonnell for all his support and guidance throughout the course of my graduate work. Fred has been an inspiring leader and a very supportive and understanding mentor. Always bursting with energy and new ideas, he has taught me to work with ease in a highly dynamic multidisciplinary environment interfacing inorganic chemistry and biological sciences. I feel his guidance, support, understanding, infinite patience and constant encouragement have been instrumental in bringing my graduate research study where it is today. Working with Fred made me more independent and responsible which I believe is the most important aspect in anyone's career. Also, I thank him for his support for the industrial internship at Bristol-Myers Squibb, New York. My sincere thanks go to my supervisor in internship, Dr. Nicholas Abu-Absi, who taught me a lot about working in an industrial environment.

I would like to give my special thanks to professors of my dissertation committee, Prof Sanjay Awasthi and Prof. Kevin Schug for their valuable advice throughout these years.

I would also like to express my sincere thanks to past committee members Prof. Rasika Dias and (Late) Prof. Dmitry Rudkevich. A special thanks to Dr.

Norma Tacconi for her endless support throughout my Ph.D. period. Also notable thanks go to Dr. Sanjay Awasthi's research group Dr. Sharad Singhal, Dr. Sushma Yadav and Jyotsana Singhal for all the help they gave in carrying out my biological experimental work. I am very much indebted to the post-docs of my lab colleagues, Dr. Shreeyukta Singh and Dr. Manas Saha for sharing their copious knowledge and teaching.

Special thanks go out to all past and present members of Dr. MacDonnell's research group, Dr. Thamara Janaratne, Dr. Kelly W. Wouters, Alper Yarasik, Rungano Chitakunye, Fiona Ongeri, Cale McCalister, Arthi Krishnan, Nancy R. Diaz, David Boston and Joseph Aslan for their help and support in the lab.

Personally I would also like to thank Dr. Liping Tang from Biomedical Engineering for allowing me to use his tissue culture facility and Mr. Alphas Wicker from Biology Department to help me in carrying out the animal work.

I would like to thank all the staff in Department of Chemistry; Rita S. Anderson, Erin M. Hampe, Ruth Handley, Deborah Cookie, Autumn Huddlestone, Brian Edwards, Charles Savage, James Garner, Jill Howard, Nancy Boone and Yvonne Russell as well as the staff in graduate school especially Ginger Dickens for assisting me with everything possible in my graduate studies. I would also like to thank Satu O. Birch from international office for helping a lot in my paper work.

iv

Lastly a special note of thanks goes to two of my friends, Preeti Sejwal in Syracuse University for helping me in all aspects in my life and Sabuj Mukherjee who is like a brother to me and whose sympathetic understanding and unwavering co-operation gave me the support I needed the most in Arlington, without both of them besides me completing this dissertation would have been a very difficult endeavor.

I would like to make a special mention of my mom-dad and my sisters who have offered me unconditional love throughout these years none of this would have been possible without them.

One more thing I would like to add is that to achieve something in life you have to devote yourself entirely into it, for that you need to make a lot of critical decisions and sometimes make sacrifices too, it is you who know if it is worth a sacrifice.

The years I spent here will be with me throughout my life and I cherish that.

November 7, 2008

ABSTRACT

INVESTIGATION OF REDOX-ACTIVE RUTHENIUM(II) POLYPYRIDYL

COMPLEXES AS POTENTIAL ANTI-CANCER DRUGS

Abhishek Yadav, Ph.D.

The University of Texas at Arlington, 2008

Supervising Professor: Frederick M. MacDonnell

Stereospecific binding of ruthenium metallointercalators with DNA is of particular interest because of the potential for improved targeting of specific sites in DNA. The present studies are focused on new metallointercalator, ruthenium (II) polypyridyl complex $[(phen)_2Ru(tatpp)(phen)_2]Cl_4$, $[P_p]^{4+}$, and it's structural analog $[Ru(phen)_2(tatpp)]Cl_2$, $[MP_p]^{2+}$; the latter contains a redox active bridging ligand tatpp (where tatpp = 9,11,20,22-tetraazatetrapyrido[3,2-a:2',3'-c:3",2"-l:2''',3'''-n]-pentacene and phen = 1,10-phenanthroline). Complex $[P_p]^{4+}$ exists as a mixture of $\Delta\Delta-$, $\Lambda\Lambda-$ and $\Delta\Lambda-$ stereisomers whereas $[MP_p]^{2+}$ exists as a pair of enantiomers $\Delta-$ and $\Lambda-$. Previously our lab has shown promising cytotoxicity of

these ruthenium(II) complexes against cancer cell lines (NSCLC). Also preliminary animal toxicity studies (mice) have shown these cationic complexes are well tolerated. These ruthenium(II) polypyridyl complexes target the DNA and bring about DNA damage under hypoxic conditions.

The present studies are focused towards establishing a complete structure-activity relationship based on cytotoxicity and animal toxicity. The promising results in this screen led us to also study the antitumor activity of these ruthenium complexes in syngeneic mouse melanoma as well as lung cancer xenograft model. A novel free-radical based mechanism of DNA cleavage is proposed that is unique in that it is significantly more effective under hypoxic conditions.

Chapter 2 discusses the studies aimed towards determining the mechanism of DNA cleavage of $[P_p]^{4+}$ and some related complexes. These studies support the role of a carbon-centered radical species in the cleavage mechanism as demonstrated by EPR and electrochemistry experiments.

Chapter 3 describes the effects different structural parameters have on the cytotoxicity of these complexes against two non-small cell lung cancer cell lines (NSCLC- H358 and H226) and, in certain cases, against two normal, healthy cell lines, HUVEC and HAVSMC. The most antipromising activity was shown by complex with a longer bridging redox active ligand tatpp ($\Delta\Delta-[P_p]^{4+}$ and $\Delta-[MP_p]^{2+}$) with an IC_{50} value of about 10 µM, very rare for this class. In addition, the chapter also discusses the results from a NCI-60 panel prescreen of two

promising complexes. These complexes were submitted to this free testing

through the Developmental Therapeutics Program of the National Cancer

Institute and the results are presented.

Chapter 4 describes the toxicology and pharmacology of many of the

ruthenium complexes studied in chapter 3. In the first experimental design, a

murine structure-toxicity screen was performed on the more promising

complexes from the cytotoxicity studies. Structural features leading to less

toxicity were identified. The two chiral complexes $\Delta\Delta-[P_p]^{4+}$ and $\Delta-[MP_p]^{2+}$ was

shown to have low animal toxicity in the screen with MTD as high as 100 mg/Kg

for both the complexes. The biodistribution of the rac/mix- ruthenium complexes

$[Ru_p]^{2+}$, $[Z_p]^{4+}$ and $[P_p]^{4+}$ were examined by sacrificing mice which had been given

i.p. injections of these complexes at doses below the maximum tolerable dose.

Mice were sacrificed at different times after dosing to follow the fates of the drugs

temporally. Selected organs were collected by dissection and the ruthenium

content analyzed using graphite furnace atomic absorption spectroscopy. It was

found that the complexes were not accumulated in the organs and were mainly

excreted.

Chapter 5 examines the in-vivo anti-tumor activity of the most promising

lead complexes identified in chapters 3 and 4. $\Delta\Delta-[P_p]^{4+}$ and $\Delta-[MP_p]^{2+}$ were

further examined for their ability to inhibit tumor growth in mice. Both complexes

showed the ability to slow or stop tumor progression in both a syngeneic mouse

melanoma model and in a xenograft human lung carcinoma model in nude mice.

These striking results suggest these complexes have excellent potential for further development as anti-cancer drugs.

TABLE OF CONTENTS

LIST OF ILLUSTRATIONS

LIST OF TABLES

CHAPTER 1

RUTHENIUM(II) POLYPYRIDYL COMPLEXES AS POTENTIAL ANTI-CANCER

AGENTS WITH A NOVEL HYPOXIA SENSITIZING MECHANISM

1.1 Cancer: Basic Facts

Cancer is a group of diseases characterized by uncontrolled growth and spread
of abnormal cells. According to a 2008 report published by the National Cancer
Institute it was estimated that approximately 10.8 million Americans with a history
of cancer were alive in January 2004. Another finding in this report is that the
five year survival rate has increased to 66% for all types of cancer diagnosed
between 1996 and 2003. This is up from 50% in 1975-1977.[1] Much of this
increase is due to new and better drugs which have led to researchers continued
interest in this field.

One of the prime molecular targets for anti-cancer drugs is DNA and
several classes of anticancer drugs are known to interact with DNA in vivo.
These drugs can be distinguished on the basis of their interaction with DNA;
some form noncovalent complexes with DNA such as anthracycline drugs like
doxorubicin while others like cisplatin and mitomycin C form covalent linkages

with DNA. Another important class of drugs are those that cause DNA backbone

cleavage, such as bleomycin and neocarzinostatin.[2]

1.2 Biological Activity of Ruthenium(II) Polypyridyl Complexes

The recent interest in ruthenium polypyridyl complexes and biological systems

started with the use of simple trischelate complexes such as $[Ru(phen)_3]^{2+}$ as

probes for DNA.[3] These complexes are stable and have a number of properties

which make them useful probes for DNA. $[Ru(phen)_3]^{2+}$ is strongly luminescent

and partially intercalates into the DNA double helix resulting in changes in

luminescence.[4] Subsequently, it has been shown that by replacing the phen

ligand with larger planar aromatic ligands such as dppz and bdppz (Figure 1.1)

can lead to complexes with much higher DNA binding affinities and which fully

intercalate into the DNA base-pairs.[5-7]
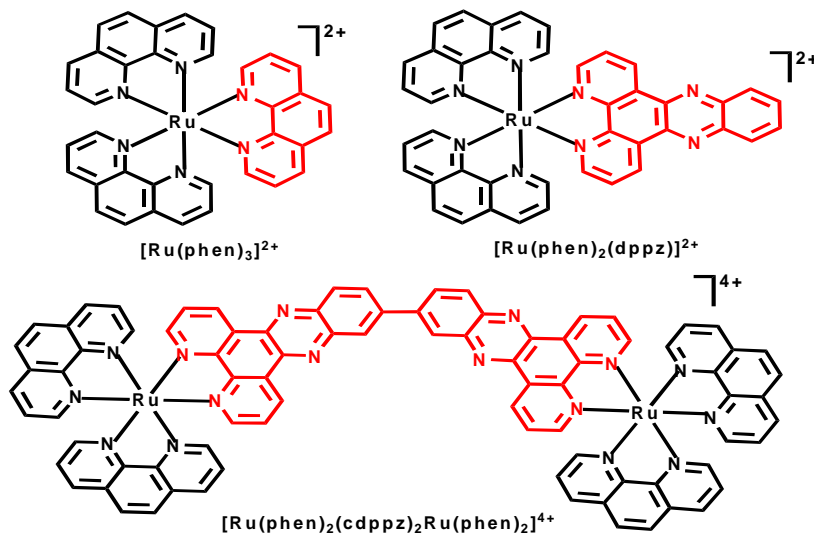
Figure 1.1: Ru(II) polypyridyl complexes as chemotherapeutic agents

2

Despite the interesting biological activity in vitro, these complexes were generally considered poor candidates for drugs because early studies revealed the $[Ru(phen)_3]^{2+}$ complexes to be acutely toxic to mice at relatively low doses.[8] The toxicity was attributed to inhibition of acetylcholinesterase (AChE), a central enzyme in the breakdown of the neurotransmitter, acetylcholine.[9] In vitro studies confirmed the inhibition of AChE by metal complexes of phenanthroline, bipyridyl and terpyridyl. Dwyer and co-workers examined the biodistribution and metabolism of the radiolabeled cationic complex, $[^{106}Ru(phen)_3]^{2+}$ after i.p. injection in mice.[10] It was found that there was little accumulation of the complex in any organ and that the bulk of the complex is excreted in urine. Subsequent tests revealed the excreted complex is not metabolized to any significant extent in the process.

These early studies also showed the chirality of these complexes to have a significant effect on their biological activity. Studies with enantiopure $\Delta-[Ru(phen)_3]^{2+}$ and $\Lambda-[Ru(phen)_3]^{2+}$ showed the $\Delta-$ enantiomer to be less toxic in mice and rats, less inhibitory towards AChE, and less quickly absorbed in the blood in mice.[10] Other studies have shown that the cytotoxicity of mer-$[Ru(terpy)Cl_3]$ in both murine and human tumor cell lines is correlated with their DNA binding ability.[11]

Ruthenium complexes, such as $[Ru(phen)_2(dppz)]^{2+}$, have been shown to bind by intercalation as well as electrostatics.[12] To illustrate this additional binding mode, consider that the binding constants for $\Delta-$ and $\Lambda-$

3

$[Ru(phen)_2dppz]^{2+}$ are 3.2 X 10^6 M^{-1} and 1.7 X 10^6 M^{-1} respectively[13] which is approximately three orders of magnitude higher than those with no intercalation. As can be seen, the chirality affects the binding ability of $[Ru(phen)_2(dppz)]^{2+}$ but not dramatically. The enantiomeric selectivity is attributed to unfavorable steric interactions between the non-intercalated phenanthroline ligands in the $\Delta-$ isomer with the phosphate backbone which is minimized if the metal complex binds in the major groove of DNA. Interestingly, these metallointercalators show some sequence selectivity with the $\Delta-$ enantiomer preferring GC tracts. Another example of intercalation is the dimeric Ru(II) complex shown in Figure 1.1 in which two Ru(II) ions are connected by two planar dppz ligands and thus possessing an overall 4+ charge. The dimer $[(phen)_2Ru(\mu-c_4(cpdppz)_2Ru(phen)_2]^{4+}$ has a DNA binding constant on the order of 10^{12} M^{-1}.[6] This complex is reported to have promising antitumor activity against platinum resistant tumor types in vitro.[14]

Preliminary work in our lab showed that the dinuclear ruthenium(II) polypyridyl complex shown in Figure 1.2 has good cytotoxicity towards NSCLC H358 and H226 cancer cells.[15,16]
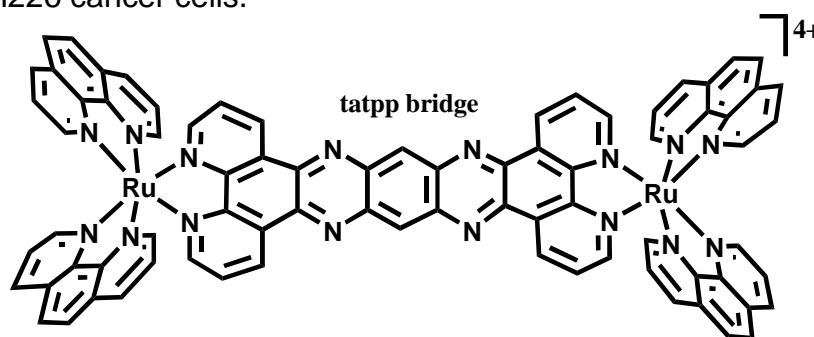
Figure 1.2: Dinuclear Ru(II) polypyridyl complex, $[(phen)_2Ru(tatpp)Ru(phen)_2]^{4+}$, $[P_p]^{4+}$

During these studies it was also discovered that the cationic complex, $[(phen)_2Ru(tatpp)Ru(phen)_2]^{4+}$, $[P_p]^{4+}$ was not acutely toxic to mice with a maximum tolerable dose of 67 mg/kg and was able to partially inhibit tumor growth (isogenic, orthotopic mouse melanoma model) in vivo. In our lab, Krishnan et. al. also established some structure-activity relationships for the complex $[P_p]^{4+}$ and other ruthenium(II) polypyridyl complexes in cytotoxicity assays.[16]

Complex $[P_p]^{4+}$ is known to intercalate and bind DNA tightly ($K_b = 1.1 \times 10^8$ M^{-1} at 25 mM NaCl).[17,18] The strong interaction with DNA is not unusual for this class of cationic, intercalating complexes and it clearly has a number of structural similarities to many known metallointercalators.

Janaratne and coworkers also examined the ability of a number of Ru(II) trisdiimine monomers and dimers to cleave DNA in vitro.[19] None of the complexes examined showed any DNA cleavage activity in phosphate buffer. However, when a reducing agent, glutathione (γ–glutamylcysteinylglycine, GSH) (Figure 1.3) was added to the assay, the complex $[P_p]^{4+}$ gave an appreciable amount of single-strand cleavage in a cleavage assay with supercoiled plasmid DNA.
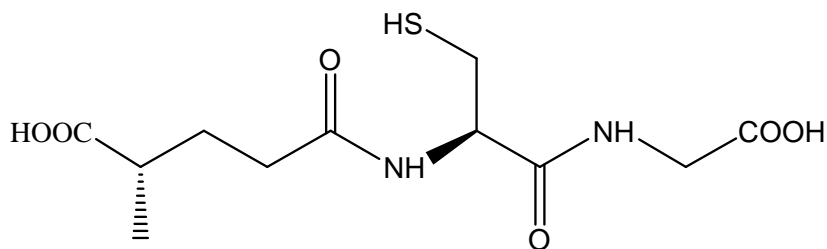
Figure 1.3: Chemical structure of glutathione

Surprisingly, the DNA cleavage activity of $[P_p]^{4+}$ was not due to the activation of O_2. In fact, cleavage assays performed under anaerobic conditions showed the reduced complex causes more cleavage than when under aerobic conditions.[20] This highly unusual result suggested that an unusual cleavage mechanism was occurring. Subsequent studies revealed that at pH 7, GSH reduces $[(phen)_2Ru(tatpp)Ru(phen)_2]^{4+}$, $[P_p]^{4+}$, to $[(phen)_2Ru(H_2tatpp)Ru(phen)_2]^{4+}$, $[H_2P_p]^{4+}$ and this species alone is responsible for the DNA damage.

1.3 Scope of Dissertation

The basic structural features of the ruthenium complexes under study are sketched in Figure 1.4. Each complex is centered around a bridging, planar aromatic bridging ligand (BL) which is either tatpp or tpphz. The BL is coordinated to one or two Ru(II) ions which themselves have an additional two terminal ligands (TL). In this study the TL's are limited to 1,10-phenanthroline (phen) or 2,2'-bipyridine (bpy). As the coordination environment about each Ru(II) ion consists of three diimine ligands the Ru center is chiral and exists in either the $\Delta-$ or $\Lambda-$ absolute configuration. These stereoisomers are stable and can be prepared in diastereomeric and enantiomeric pure form.

6
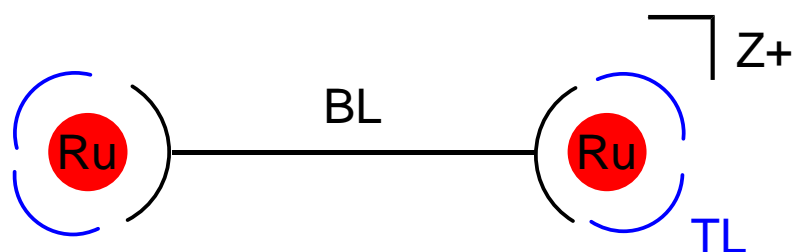
Figure 1.4: Schematic representation of Ru(II) polypyridyl complexes

Chapter 2 discusses the studies aimed towards determining the mechanism of DNA cleavage of $[P_p]^{4+}$ and some related complexes. These studies support the role of a carbon-centered radical species in the cleavage mechanism. Furthermore, a structure-activity study helped determine the essential pharmacophore in these complexes. For example, it appears that the tatpp unit is the essential pharmacophore as complexes with shorter, related tpphz and dppz ligands do not show any DNA cleaving activity with or without GSH. Of the three ligands, tatpp, tpphz and dppz, only tatpp is reduced at modest, biologically accessibly potentials suggesting that the redox chemistry of the tatpp ligand is essential for activity. Questions regarding the role of the Ru(II) ions and their ancillary phenanthroline ligands were addressed. Are both Ru(II) ions required? It is clear that one important role for the Ru(phen)$_2$$^{2+}$ fragments present in $[(phen)_2Ru(tatpp)Ru(phen)_2]^{4+}$, $[P_p]^{4+}$ is to solubilize the otherwise insoluble tatpp ligand.

Chapter 3 describes the effects different structural parameters have on the cytotoxicity of these complexes against two cancer cell lines and, in certain

cases, against two normal, healthy cell lines. The new data along with that obtained previously by Janaratne[15] and Krishnan[16] are presented to give a complete structure-activity study of these complexes with respect to cytotoxicity in vitro.

The first structural feature examined was the BL. Complexes containing either the tatpp or the tpphz ligand were compared for cytotoxicity. Both BL's require coordination to Ru(II) or other metal ions to form water soluble compounds and cannot be studied alone. Once coordinated the two ligands have one important difference, aside from their obvious difference in length: tatpp is redox-active in these complexes and is readily reduced by common cellular reductants, such as glutathione; the tpphz ligand, in contrast, is not reduced under the same conditions and thus complexes of this 'shorter' tpphz ligand are can thus serve, to some degree, as a non-redox active control. For completeness the mononuclear complexes: $[Ru(phen)_3]^{2+}$, $[Ru_p]^{2+}$ and $[Ru(bpy)_3]^{2+}$, $[Ru_b]^{2+}$ in both racemic and enantiopure forms, were included in this study.

The second structural feature investigated was the need for two metal ions in each complex. Complexes containing a single Ru(II) ion have been prepared and examined to determine the advantages or disadvantages of one versus two metal centers.

The third structural feature varied was the type of TL used to complete the coordination sphere of the Ru(II) ions. Phen and bpy are structurally similar bidentate diimine ligands that would be expected, a proiri, to have minimal

8

influence on the observed biological activity. However, a study on the cytotoxicity of Ru(II) complexes differing only in phen or bpy showed this small change can dramatically affect the observed activity.

Finally, the chirality about the Ru(II) centers was examined to determine the importance of stereochemistry. Initial studies were performed with racemates for the mononuclear Ru(II) complexes and with diastereotopic mixtures for the dinuclear complexes.

Chapter 3 also contains a detailed description of the synthesis and characterization of the ruthenium complexes investigated in the structure-activity cytotoxicity screen. Using stereospecific synthetic techniques developed in this lab[21-24], the $\Delta-$ and $\Lambda-$ enantiomers for monomeric complexes were prepared and subsequently tested for differences in tumor and healthy cell cytotoxicity and animal toxicity. Similarly, the $\Delta\Delta-$, $\Lambda\Lambda-$ and meso $\Delta\Lambda-$ dinuclear complexes were prepared in enantiopure form a subject to biological testing.

In addition, the above chapter also discusses the results from a NCI-60 panel prescreen of two promising complexes. These complexes were submitted to this free testing through the Developmental Therapeutics Program of the National Cancer Institute and the results are presented.

Chapter 4 describes the toxicology and pharmacology of many of the ruthenium complexes studied in chapter 3. In the first experimental design, a murine structure-toxicity screen was performed on the more promising complexes from the cytotoxicity studies. Structural features leading to less

9

toxicity were identified. The biodistribution of the complexes $[Ru_p]^{2+}$, $[Z_p]^{4+}$ and

$[P_p]^{4+}$ were examined by sacrificing mice which had been given i.p. injections of

these complexes at doses below the maximum tolerable dose. Mice were

sacrificed at different times after dosing to follow the fates of the drugs

temporally. Selected organs were collected by dissection and the ruthenium

content analyzed using graphite furnace atomic absorption spectroscopy.

Chapter 5 examines the in-vivo anti-tumor activity of the most promising

lead complexes identified in chapters 3 and 4. $\Delta-[MP_p]^{2+}$ and $\Delta\Delta-[P_p]^{4+}$ were

examined for their ability to inhibit tumor growth in mice. Both complexes

showed the ability to slow or stop tumor progression in both a syngeneic mouse

melanoma model and in a xenograft human lung carcinoma model in nude mice.

These striking results suggest these complexes have excellent potential for

further development as anti-cancer drugs.

1.4 Nomenclature

The following shorthand notation was developed to quickly denote and identify a

particular stereoisomer for a given tatpp or tpphz monomer or dimer. The

shorthand is best illustrated by example. The dinuclear ruthenium(II) complex

$[(phen)_2Ru(tatpp)Ru(phen)_2]^{4+}$ would be denoted as $[P_p]^{4+}$ with the capitol bold P

indicative of a dinuclear complex with the tatpp BL. The identical dinuclear

complex with the tpphz BL, $[(phen)_2Ru(tpphz)Ru(phen)_2]^{4+}$, would be denoted

$[Z_p]^{4+}$ (Figure 1.5).
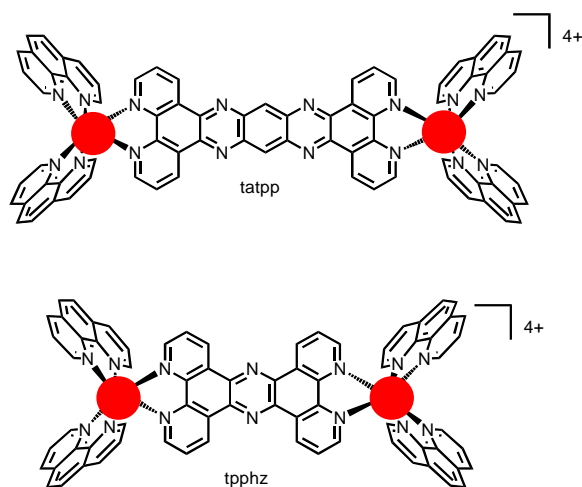
Figure 1.5: Dinuclear Ru(II) complexes of tatpp and tpphz

The subscript ($_p$) indicates the terminal ligands are phenanthroline. A subscript ($_b$) indicates the TL's are bipyridine e.g., $[Z_b]^{4+}$ would be for $[(bpy)_2Ru(tpphz)Ru(bpy)_2]^{4+}$. Complexes containing only one ruthenium ion are indicated as $[MP]^{2+}$ or $[MZ]^{2+}$ for the monometallated complexes of tatpp and tpphz, respectively. Thus $[MP_b]^{2+}$ and $[MZ_b]^{2+}$ are shorthand notation for the complexes $[(bpy)_2Ru(tatpp)]^{2+}$ and $[(bpy)_2Ru(tpphz)]^{2+}$, respectively. Most often, the compounds were used as racemates for mononuclear complexes $[MP]^{2+}$ and $[MZ]^{2+}$ or as diastereotopic mixtures for the dinuclear complexes ($[P]^{4+}$ and $[Z]^{4+}$). In the absence of a stereochemical descriptor before the $[P]^{4+}$, $[Z]^{4+}$, $[MP]^{2+}$ or $[MZ]^{2+}$, the complex can be assumed to be a racemate for $[MP]^{2+}$ and $[MZ]^{2+}$ or a mixture for $[P]^{4+}$ and $[Z]^{4+}$. If the complex is a particular stereoisomer, the stereochemical descriptors $\Delta-$ and $\Lambda-$ are used to indicate the absolute chirality at one or both metal sites. For example, $\Delta-[(phen)_2Ru(tatpp)]^{2+}$ and

11

$\Delta\Delta-[(\text{phen})_2\text{Ru(tatpp)Ru(phen)}_2]^{4+}$ would be denoted as $\Delta-[\text{MP}_p]^{2+}$ and $\Delta\Delta-[\text{P}_p]^{4+}$, respectively. In cases where it is necessary to specify that the complex is present as a racemate or diastereotopic mixture the prefixes rac-$[\text{MP}_p]^{2+}$ and mix-$[\text{P}_p]^{4+}$ are used to avoid ambiguity. In all cases, we have kept the superscript $(^{2+ \text{ or } 4+})$ to indicate the overall charge of the complex as it is important to keep the fact that these complexes are cationic in mind.

CHAPTER 2

MECHANISM OF DNA CLEAVAGE BY RUTHENIUM(II)

POLYPYRIDYL COMPLEXES

2.1 Introduction

The use of transition-metal complexes in medicine has enjoyed extensive
attention due to the tremendous success of cisplatin as a chemotherapeutic
agent[25] and the ability of many metal complexes to interact with and damage
cellular structures, particularly DNA.[12,26-30] While cisplatin is known to form
covalent adducts with adjacent GG bases, there are a number of transition metal
complexes that show strong interactions with DNA through non-covalent
interactions. In particular, transition metal polypyridyl complexes have also been
extensively studied for their stereospecific interactions since the early reports of
interaction of $[Fe(bpy)_3]^{2+}$ with $\beta-$DNA by Norden and Tjerneld.[31] Complexes
with three neutral diimine chelate ligands possess an overall positive charge,
helical chirality and can readily be isolated in enantiopure form which makes
them excellent candidates for probing helical conformation of DNA.[32,33] The
incorporation of large planar aromatic diimine ligands, such as those shown in
Figure 2.1 leads to an additional mode of interaction, namely intercalation, which
greatly increases their binding affinity.[6,13,33-35]
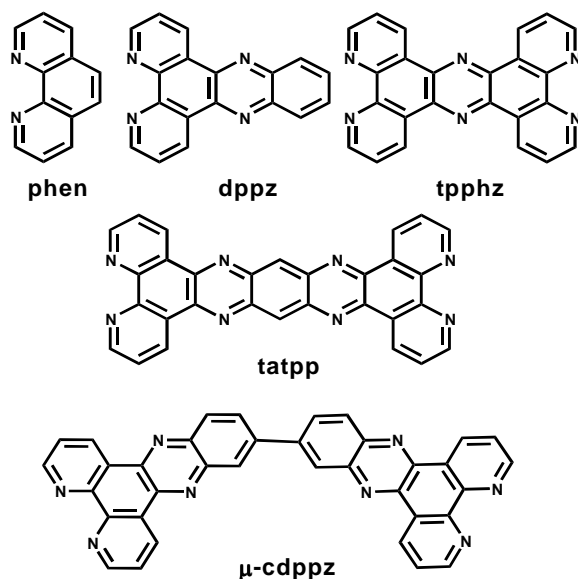
Figure 2.1: Bridging ligands

Several of these intercalating ligands, such as tpphz, tatpp, and μ–cdppz, can bind a second metal center to form dinuclear complexes. Norden has shown that the dinuclear complex, $[(phen)_2Ru(\mu–cdppz)Ru(phen)_2]^{4+}$ which has two bulky metal complexes on each end of the intercalating ligand, can slowly thread its way through the DNA double-strand to form very stable [dimer-DNA] complex $(K_b \sim 10^{11} \ M^{-1})$.[6]

Table 2.1 lists a number of ruthenium-trisdiimine complexes, their reported DNA binding constants, the proposed mode of binding and the method by which the K_b was determined. As can be seen, simple trisdiimine complexes (e.g. trisbpy and trisphen) have a binding constant on the order of $10^3 \ M^{-1}$ which is attributed largely to their divalent charge. Addition of an intercalating diimine ligand increases the K_b by approximately 3 orders of magnitude to $\sim 10^6 \ M^{-1}$. Addition of a second metal center raises the binding constant even further, in part

due to their higher positive charge. For example, complex

$[(phen)_2Ru(tatpp)Ru(phen)_2]^{4+}$, $[P_p]^{4+}$ has a reported K_b on the order of

~10^8 M^{-1}.[17,18]

Table 2.1: Binding constants for metal complexes with CT-DNA

Complex	$K_b(M^{-1})$	Method and Analysis	Mode of Binding
$[Fe(bpy)_3]^{2+}$	1.1-1.4 X10^3	CV- Scatchard	Electrostatic
$[Fe(phen)_3]^{2+}$	7-15 X 10^3	CV- Scatchard	Electrostatic
$[Co(bpy)_3]^{3+}$	5.4-8.4 X10^3	CV- Scatchard	Electrostatic
$[Co(phen)_3]^{3+}$	2.8 X 10^4	CV- Scatchard	Intercalative
$[Os(bpy)_3]^{2+}$	5.0-7.3 X10^3	CV- Scatchard	Electrostatic
$[Ru(bpy)_3]^{2+}$	0.7 X 10^3	Dialysis-McGhee	Electrostatic
$[Ru(phen)_3]^{2+}$	3.1 X 10^3	Dialysis-McGhee	Electrostatic
$[Rh(phen)_3]^{2+}$	2.9 X 10^3	Quenching-Scatchard	Intercalative
$[Ru(bpy)_2(dppz)]^{2+}$	4.9 X 10^6	Emission- Scatchard	Intercalative
$[Ru(phen)_2(dppz)]^{2+}$	1.7-3.2 X 10^6	Emission- Scatchard	Intercalative
$[Ru(bpy)_2(phen)]^{2+}$	7.0 X 10^2	Dialysis-McGhee	Electrostatic
$[Ru(phen)_2(bpy)]^{2+}$	2.4 X 10^3	Dialysis-McGhee	Electrostatic
$[Ru(bpy)_2(DIP)]^{2+}$	1.7 X 10^3	Dialysis-McGhee	Intercalative
$[Ru(phen)_2(DIP)]^{2+}$	2.5 X 10^3	Dialysis-McGhee	Intercalative

Table 2.1- Continued

Complex	$K_b(M^{-1})$	Method and Analysis	Mode of Binding
$[Ru(bpy)_2(phi)]^{2+}$	16×10^4	Dialysis-McGhee	Intercalative
$[Ru(phen)_2(phi)]^{2+}$	110×10^3	Dialysis-McGhee	Intercalative
$[Ru_2(Me_2bpy)_4(bpm)]^{4+}$	$\sim 10^8$	^{1}H NMR	Intercalative
$[Ru_2(phen)_4(tatpp)]^{4+}$	$\sim 10^8$	Electrophoresis	Intercalative
$[Ru_2(phen)_4(bpdppz)]^{4+}$	$\sim 10^{12}$	^{1}H NMR	Threading

Studies with enantiopure ruthenium trisdiimine complexes show that in most cases, the $\Delta-$ enantiomer binds more tightly to the right-handed DNA double helix, than the $\Lambda-$ enantiomer, although the absolute chirality has a relatively minor overall impact on the binding constant. For example, the K_b's for $\Delta-[Ru_p]^{2+}$ and $\Lambda-[Ru_b]^{2+}$ are 4.9×10^4 M^{-1} and 2.8×10^4 M^{-1}, respectively and for $\Delta-$ and $\Lambda-[Ru (phen)_2 dppz]^{2+}$ are 3.2×10^6 M^{-1} and 1.7×10^6 M^{-1}, respectively.[13,36] In both cases, the $\Delta-$ enantiomer binds more tightly but by only a 2-fold difference. The enantiomeric selectivity is attributed to unfavorable steric interactions between the non-intercalated phenanthroline ligands in the $\Lambda-$ isomer with the phosphate backbone which is minimized if the metal complex binds in the major groove of $\beta-$DNA.[34] Interestingly, a number of these chiral complexes recognize different local structures along the DNA strand and hence

16

show sequence selectivity[32] for example, metallointercalators show some sequence selectivity with the $\Delta-$enantiomer preferring GC tracts.[37]

2.2 Mechanism of DNA Damage by Metal Complexes

There are a number of known mechanisms by which metal complexes can damage or cleave DNA. These include hydrolysis of the phosphodiester backbone,[38] formation of DNA-complex adducts, and oxidation of the DNA bases or sugars.[39,40] A large number of DNA-cleaving metal complexes oxidize DNA in an indirect way in that they react with dioxygen [O_2] to generate reactive oxygen species (ROS).[38, 41] These ROS include species such as superoxide radical and hydroxyl radical which have oxidizing potentials of 0.9 V and 2.4 V vs. NHE, respectively[42] and are capable of oxidizing DNA leading to DNA cleavage. The ·OH radical is capable of H-atom abstraction from the sugar moiety[43] which often leads to DNA strand sission[43]. Of the bases, guanine is the most easily oxidized with the major product formed being 8-OH-guanine.[44] An example of a complex which catalyzes this ROS activating mechanism is [Cu(phen)$_2$]$^{2+}$ which undergoes in situ reduction to form a Cu(I) complex which, in turn, reduces dioxygen to form ROS.[45, 46] As seen from this example, these complexes usually require a reducing agent to reduce the metal complex for reactivity with [O_2].

Complexes which generate carbon-centered radicals are less common and can also damage DNA by either abstracting a hydrogen atom from the sugar moiety or by attacking the guanine base forming 8-alkylpurines.[47] Mohler et. al.

17

demonstrated that a cyclopentadienyl-metal complex could cleave DNA by a mechanism involving homolysis of metal-alkyl bond to generate carbon-centered radical species.[48] There a few organic compounds that operates in a similar fashion including the ene-diyne antibiotics like neocarzinostatin and calicheamicin.[49,50]

There are a number of Ru-polypyridyl complexes that will damage DNA but aside from high valent ruthenium-oxo complexes[51-54] and the complexes $[P_p]^{4+}$ and $[MP_p]^{2+}$ reported by our group[15,19] all of these complexes require photoexcitation to cause DNA damage.[55-59] Excitation of the MLCT band leads to a long-lived triplet which can directly oxidize DNA or can activate dioxygen to form ROS.[60] These include even simple complexes such as $[Ru_b]^{2+}$ and $[Ru_p]^{2+}$.[61] Brewer and co-workers have shown that irradiation of the mixed-metal complexes, $[((bpy)_2Os(dpp))_2RhCl_2]^{5+}$ and $[((tpy)RuCl(dpp))_2RhCl_2]^{3+}$, leads to cleavage of DNA.[62,63] The system functions through the reactivity of an excited state previously unexplored. When irradiated with low energy visible light a Ru → Rh MMCT excited state is formed which brings about the photocleavage with or without molecular oxygen.

As reported by Janaratne et. al. complex $[P_p]^{4+}$ appears to be in a class by itself; in that it is not a potent oxidant nor does the reactivity of the complex towards DNA cleavage require light. It does require a reducing agent for activity but in this case activation of dioxygen to give ROS seems unlikely as the cleavage activity of this P_p^{4+}/reducing agent mixture occurs under anaerobic

conditions. In fact, the cleavage activity of this mixture is enhanced under anaerobic conditions, indicating a novel mechanism of action.

The unusual reactivity of $[P_p]^{4+}$ with DNA warranted further investigation to further probe the mechanism of action and to determine what are the essential components of this complex that are need for activity. For example, it appears that the tatpp unit is the essential pharmacophore as complexes with shorter, related tpphz and dppz ligands do not show any DNA cleaving activity with or without GSH. Of the three ligands, tatpp, tpphz and dppz, only tatpp is reduced at modest, biologically accessibly potentials suggesting that the redox chemistry of the tatpp ligand is essential for activity.[64] In this chapter, we have used a variety of radical scavengers to examine the mechanism of DNA cleavage as well as the use of EPR to identify radical species generated in solution. Furthermore, we have prepared and examined the monoruthanated complex, $[(phen)_2Ru(tatpp)]^{2+}$, $[MP_p]^{2+}$ and examined its reactivity to determine if two metals centers are needed for activity. As is shown in the latter chapters of this thesis, ruthenium(II) complexes containing the tatpp ligand show promising antineoplastic activity both in vitro and in vivo. The biological target of these ruthenium tatpp complexes is still undetermined; however given the high DNA binding affinity in vitro[18] and the DNA cleavage activity[19], we speculate that the anti-tumor activity is due to DNA cleavage.

2.3 Experimental

2.3.1 Chemicals

All reagents were purchased commercially and used without further purification unless noted. Millipore water was used to prepare all buffers. Supercoiled plasmid pUC18 DNA was purchased from Bayou Biolabs (New England). Agarose, ethidium bromide, glutathione (GSH), 2,2,6,6-Tetramethylpiperidine-1-oxyl (TEMPO) and Trizma base were purchased from Sigma Aldrich. DMSO was purchased from Alpha Aesar.

The complexes $[(phen)_2Ru(tatpp)Ru(phen)_2]^{4+}$, $[P_p]^{4+}$ [65] and $[(phen)_2Ru(H_2tatpp)Ru(phen)_2]^{4+}$, $[H_2P_p]^{4+}$ [66] were synthesized as described in the literature.

2.3.2 Instrumentation

^{1}H NMR spectra were obtained on JEOL Eclipse Plus 300 or 500 MHz Spectrometers. Spectra were referenced to tetramethlsilane (TMS) or residual solvent peaks from the deuterated solvent. UV-visible spectra were obtained on a Hewlett-Packard HP84535A spectrophotometer. Plasmid cleavage products were analyzed using an AlphaImage^{TM} 2200 gel analysis system and quantitated using a UVPGDS 8000 complete gel documentation and analysis system.

2.3.3 DNA Cleavage Assay by $[P_p]^{4+}$

A typical DNA cleavage experiment was carried out in a total volume of 20 μL of

7 mM sodium phosphate buffer (pH 7) containing 2 μL of supercoiled pUC18

DNA (1 μg/1 μL, 0.154 mM DNA base pairs). The concentration of and nature of

the complex added are given in the figure legends as well as the conditions and

time of reaction. The reaction was quenched by addition of 2 μL sodium acetate

(pH 5.2) and 80 μL ethanol which precipitated the DNA. The sample was

allowed to sit overnight at -20°C to complete the precipitation. The DNA was

pelleted by centrifugation at 13000 rpm for 15 minutes. The supernatant was

removed by decanting and the samples air-dried for 30 minutes before the DNA

was resuspended in a mixture of 65 μL deionized water, 40 μL of buffer I (40 mM

Tris-Cl, 1 mM EDTA at pH 8.0) and 12 μL of a loading buffer (30% glycerol in

water with 0.1% w/v bromophenol blue). Twenty microliters of this solution was

then loaded into a well on a 1 % agarose gel (horizontal slab configuration)

immersed in TAE buffer (40 mM Tris-acetate, 1 mM EDTA, pH 8). The gel was

made previously by dissolving 1 g agarose into 100 mL of hot TAE buffer

contained ethidium bromide (0.2 mM). The gel was electrophoresed at 80 V for

90 minutes. The DNA products were visualized by irradiation with ultra-violet

light and the image recorded using a UVPGDS 8000 gel analysis system.

Anaerobic conditions required the degassing of all the reagent solutions

including the DNA stock, which was done using five freeze-pump-thaw cycles

under N_2. The degassed reagents were taken into a N_2 glove box and all the

solutions were prepared inside it to minimize further contamination with oxygen. The assays were completed in the glove box and the reactions quenched by precipitating the DNA using 2 μL of degassed sodium acetate at pH 5.2 and 80 μL degassed ethanol under N_2 inside the glove box. This mixture was effective in removing at least some of the ruthenium complex which remains soluble while the DNA does not.

2.3.4 DNA Cleavage Reactions with added DMSO

DNA cleavage reactions with added DMSO were carried out in a total volume of 20 µL in 0.5 mL Eppendorf tubes which contained 6 µL of 7 mM Na_3PO_4 buffer medium (pH 7), 4 µL of $[P_p]^{4+}$ (0.0128mM), 4 µL of GSH (1.02 mM), 2 µL of plasmid pUC18 DNA (1 µg/1 µL, 0.154 mM DNA base pairs), and 4 µL of DMSO (1%, 3% or 5% DMSO). The 5% DMSO stock solution was prepared by dissolving 250 µL of DMSO in 750 µL of Millipore water. 1% and 3% solutions were prepared from serial dilutions of the 5 % stock solution. Solutions were left to incubate for 2 h at room temperature and then precipitated by adding 2 µL of 3 M sodium acetate (pH 5.2) and 80 µL of ethanol. The samples were then cooled at -20°C overnight. The precipitated DNA was then centrifuged at 13,000 rpm for 30 minutes followed by the removal of the ethanol solution from of the Eppendorfs. The samples were vacuum dried for 30 minutes and then resuspended in 30 µL storage buffer (40 mM Tris-Cl, 1 mM EDTA, pH 8.0) and 10 µL loading buffer (30% glycerol in distilled water with 0.1 % w/v bromophenol

blue). After that, 5 µL of each sample was loaded in a 1% agarose gel containing ethidium bromide (0.2 µL/1 mL) and subjected to electrophoresis at 70 V for 2 h using TAE buffer (40 mM Tris-acetate, 1 mM EDTA, pH 8.0). Bands were visualized by UV light and photographed with a UV illuminator.

2.3.5 DNA Cleavage Reactions with added TEMPO

In 0.5 mL Eppendorf tubes, 4 µL $[P_p]^{4+}$ (0.0128 mM), 4 µL of GSH (1.02 mM), 2 µL of plasmid pUC18 DNA (1 µg/1 µL, 0.154 mM DNA base pairs), and 4 µL of TEMPO (2 mM) were mixed thoroughly and made up to a final volume of 20 µL using 7 mM Na_3PO_4 buffer medium (pH 7.0), and then left to incubate for 2 h at room temperature. The samples were then subjected to subsequent precipitation and analysis steps similar to those described.

2.3.6 DNA Cleavage Assay by $[H_2P_p]^{4+}$

All experiment preparation was done in the glove box. In a typical experiment, 5 mg of $[H_2P_p]^{4+}$ was weighed out and dissolved in 1 mL of Millipore water. Of this solution, 20 µL pipetted out and mixed with 980 µL of H_2O to obtain a final concentration of 0.0256 mM. In a 0.5 mL Eppendorf, 4 µL of this solution was added to 2 µL of plasmid pUC18 DNA (1 µg/1 µL, 0.154 mM DNA base pairs) in 7 mM Na_3PO_4 buffer medium (pH 7.0) and left to incubate for 3 h. The solutions were then subjected to subsequent precipitation and analysis steps similar to those described.

2.3.7 EPR Experiment with $[H_2P_p]^{4+}$

We carried out EPR experiment at the same concentration as we carried out DNA cleavage experiment. 12.8µM $[H_2P_p]^{4+}$ was incubated with 0.154 mM DNA in the glove box so that the concentration is 12 bp/DNA. After certain period of time aliquots were withdrawn and frozen at -20^OC, thawed when we were about to start the EPR experiment.

2.4 Results and Discussion

2.4.1 DNA Cleavage Assay

Plasmid DNA (pUC 18- 2686 bp) exists in three different topological confirmations: supercoiled DNA (Form I), circular DNA (Form II) and linear DNA (Form III) which can be separated by agarose gel electrophoresis and visualized under UV light after staining the gel with ethidium bromide (Figure 2.2).
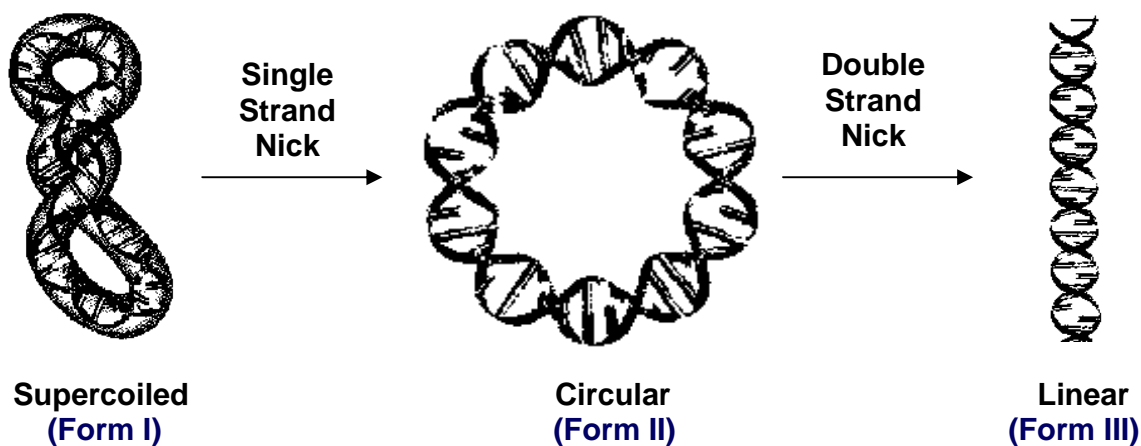
Figure 2.2: Topoisomers of plasmid DNA: Form I, II and III

2.4.2 DNA Cleavage Efficiency of $[P_p]^{4+}$

The initial studies into the cleavage activity were conducted by Dr. Thamara Janaratne in our group. She showed that the ability of $[P_p]^{4+}$ to cut DNA required addition of a reducing agent, e.g. glutathione (GSH), and is enhanced under anaerobic conditions compared to aerobic conditions, as shown in Figure 2.3. Fe-BLM was used as a positive control to show that the glove box was oxygen-free because while Fe-BLM can cause single strand (ss) nicks under anaerobic conditions, it required O_2 for double strand (ds) cleavage activity.[19]

Figure 2.3: DNA cleavage by $[P_p]^{4+}$

1 % agarose gel (negative image) stained with ethidium bromide of supercoiled pUC18 DNA (0.154 mM bp) cleavage products after incubation at 24 ^{0}C for 2 h with $[P_p]^{4+}$ or Fe-BLM complexes (12.8 μM) in a buffer of 0.5 mM GSH and 4 mM Na_3PO_4 (pH 7.0) under aerobic or anaerobic conditions (as indicated). Lanes M (marker lane of form I, II and III of pUC18 DNA), 1 (DNA without GSH), 2 (DNA plus GSH) and 3 (DNA plus P_p^{4+}) served as controls. Lane 4 and 5 are (DNA plus P_p^{4+} with GSH) under aerobic and anaerobic conditions respectively. Lane 6 and 7 are (DNA plus Fe-BLM) and served as positive controls.

As seen in lane 3, $[P_p]^{4+}$ alone does not cause appreciable DNA cleavage; however, the addition of a GSH leads to some ss cleavage activity (lanes 4 and 5). When $[O_2]$ is removed this mixture is more effective at DNA ss cleavage as

25

can be seen by comparing lanes 4 vs. 5. Yields of cleavage products (forms II +

III) under aerobic and anaerobic conditions were found to be 50 % and 87 %,

respectively.[67] The appearance of linear DNA in lane 5 appears to result from

sequential single-strand (ss) cuts, not double-strand (ds) cleavage; thus, the

overall cleavage activity is ss-scission.

2.4.3 Identification of the Species Responsible for DNA Damage

The redox chemistry of complex $[P_p]^{4+}$ has been extensively studied and it is

known that $[P_p]^{4+}$ can undergo multiple reductions and protonations centered on

the planar tatpp bridging ligand.[66, 68] Changes in redox and/or protonation state

of $[P_p]^{4+}$ lead to easily discernable changes in the visible absorption spectrum

which allows us to readily identify a particular species from a simple visible

absorption spectrum.

Three complexes are possible at pH 7 in the presence of GSH; they are

$[P_p]^{4+}$, the radical species $[P_p]^{3+}$, and the doubly-reduced, doubly-protonated

complex $[H_2P_p]^{4+}$. We prepared these complexes and examined their ability to

cleave DNA under anaerobic conditions without added reductant (i.e. GSH). The

data from this experiment is shown in the resulting gel in Figure 2.4
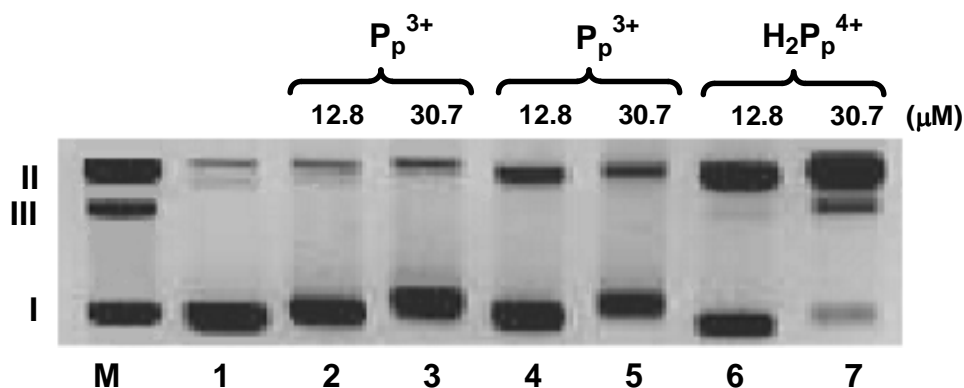
Figure 2.4: DNA Cleavage by $[P_p]^{4+}$, $[P_p]^{3+}$ and $[H_2P_p]^{4+}$

1% agarose gel (negative image) stained with ethidium bromide of supercoiled pUC18 DNA (0.154 mM bp) cleavage products after incubation at 24 ^{0}C for 3 h with different concentrations of $[P_p]^{4+}$, $[P_p]^{3+}$ and $[H_2P_p]^{4+}$ in a buffer of 4 mM Na_3PO_4 (pH 7.0) under anaerobic conditions. Lanes M (marker lane of form I, II and III pUC18 DNA), and 1 (supercoiled DNA) served as controls. Lane 2 (12.8 μM P_p^{4+}, 0.083 complex/DNA$_{bp}$ ratio), lane 3 (30.7 μM P_p^{4+}, 0.20 complex/DNA$_{bp}$ ratio), lane 4 (12.8 μM P_p^{3+}, 0.083 complex/DNA$_{bp}$ ratio), lane 5 (30.7 μM P_p^{3+}, 0.083 complex/DNA$_{bp}$ ratio), lane 6 (12.8 μM $H_2P_p^{4+}$, 0.083 complex/DNA$_{bp}$ ratio), lane 7 (30.7 μM $H_2P_p^{4+}$, 0.20 complex/DNA$_{bp}$ ratio).

As seen in lanes 2 and 3, $[P_p]^{4+}$ shows no significant damage to the DNA. The monoreduced complex $[P_p]^{3+}$ shows slightly more cleavage (lanes 4 and 5) than $[P_p]^{4+}$ but only marginally so. Interestingly, the doubly-reduced, doubly-protonated complex $[H_2P_p]^{4+}$ causes extensive ss cleavage (lanes 6 and 7) with almost full conversion to circular DNA observed with 0.0307 mM $[H_2P_p]^{4+}$ (lane 7). From this data, we can surmise that the active DNA cleavage agent is $[H_2P_p]^{4+}$ and the role of GSH is simply to reduce $[P_p]^{4+}$ to $[H_2P_p]^{4+}$, in situ. The conclusion is supported by the changes in the absorption spectrum of $[P_p]^{4+}$ upon addition of GSH. The resulting spectrum matches that of $[H_2P_p]^{4+}$ prepared by other methods. There is one other important conclusion that we learned from this study. Glutathyl radicals could have been the active DNA cleavage agent in the

27

solutions containing both $[P_p]^{4+}$ and GSH. In that case, $[P_p]^{4+}$ would 'activate' GSH by one electron oxidation. The observation that $[H_2P_p]^{4+}$ is capable of DNA cleavage in the absence of GSH shows this is not the case.

2.4.4 Addition of Oxygen-Radical Scavengers: Are Reactive Oxygen Species Involved in the DNA Cleavage?

DMSO is effective in scavenging oxygen-based radicals in solution.[69,70] The gel shown in Figure 2.5 shows the effect of added DMSO on the cleavage activity of $[P_p]^{4+}$ and GSH, in this case under aerobic conditions. As seen in lane 4, the combination of $[P_p]^{4+}$ and GSH in air gives a reasonable amount of ss cleavage. Lanes 5, 6 and 7 contain 1%, 3% and 5% DMSO by volume in the cleavage medium yet show no attenuation of the ss cleavage activity, whereas normally this much DMSO would attenuate the cleavage activity if ROS were involved. As this experiment was done in the presence of $[O_2]$ is even more informative as the potential for forming ROS was clearly present, yet does not occur to any significant extent.

Figure 2.5: Effect of DMSO on DNA cleavage by $[P_p]^{4+}$ under aerobic conditions

Agarose gel (1%) stained with ethidium bromide of supercoiled pUC18 DNA (0.154 mM) cleavage products after incubation at 25 $^\circ$C for 2 h with $[P_p]^{4+}$, GSH and DMSO in 7 mM Na_3PO_4 buffer (pH 7.0) under aerobic conditions. Lane 1: DNA control ; Lane 2: DNA plus GSH (0.513 mM); Lane 3: DNA plus P_p^{4+} (0.0128 mM); Lane 4: DNA plus GSH (0.513 mM) plus P_p^{4+}(0.0128 mM); Lane 5: DNA, GSH (0.513 mM), P_p^{4+}(0.0128 mM) plus 1% DMSO; Lane 6: DNA, GSH (0.513 mM), P_p^{4+}(0.0128 mM) plus 3% DMSO; Lane 7: DNA, GSH (0.513 mM), P_p^{4+}(0.0128 mM) plus 5% DMSO.

We repeated the same experiment under anaerobic conditions and observed similar results as seen in Figure 2.6. The addition of up to 5% DMSO had no measurable effect of the cleavage activity of P_p^{4+}-GSH-DNA mixture. It is clear however that the overall cleavage activity is better under anaerobic conditions compared to aerobic conditions, as expected. The increased DNA cleavage in this situation suggests that $[O_2]$ does play a role in the chemistry of this here; however, this role is a scavenging role. As the presence of $[O_2]$ attenuates the cleavage activity of a mixture of P_p^{4+}-GSH, we speculate that is does so by reoxidizing $[H_2P_p]^{4+}$ formed by reduction of $[P_p]^{4+}$.

29
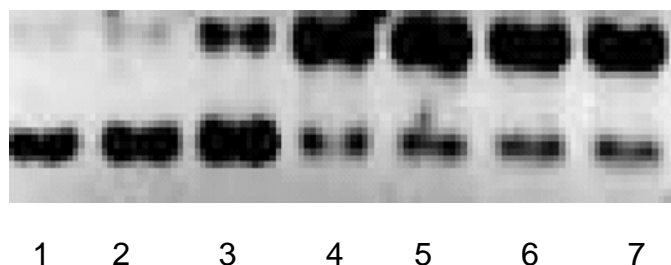
Figure 2.6: Effect of DMSO on DNA cleavage by $[P_p]^{4+}$ under anaerobic conditions

Agarose gel (1%) stained with ethidium bromide of supercoiled pUC18 DNA (0.154 mM) cleavage products after incubation at 25 $^\circ$C for 2 h with $[P_p]^{4+}$, GSH and DMSO in 7 mM Na_3PO_4 buffer (pH 7.0) under anaerobic conditions. Lane 1: DNA control; Lane 2: DNA plus GSH (0.513 mM); Lane 3: DNA plus P_p^{4+} (0.0128 mM); Lane 4: DNA,GSH (0.513 mM) plus P_p^{4+}(0.0128 mM); Lane 5: DNA, GSH (0.513 mM), P_p^{4+}(0.0128 mM) plus 1% DMSO; Lane 6: DNA, GSH (0.513 mM), P_p^{4+}(0.0128 mM) plus 3% DMSO; Lane 7: DNA, GSH (0.513 mM), P_p^{4+}(0.0128 mM) plus 5% DMSO.

2.4.5 Addition of Carbon-Radical Scavengers: Is a Carbon-Centered Radical Involved in the Cleavage Mechanism?

One possible mechanism for DNA cleavage under anaerobic conditions is through formation of carbon-centered radical species. In order to investigate the potential role of carbon radicals in cleavage activity of $[P_p]^{4+}$, we examined the cleavage activity in the presence of 2,2,6,6-tetramethylpipiridine-1-oxyl (TEMPO) which is a nitroxide radical species that effectively traps carbon and metal-centered radicals.[71]

Figure 2.7 shows the DNA cleavage activity of $[P_p]^{4+}$ and GSH in the presence 2 mM TEMPO (lanes 6 (aerobic) and 7(anaerobic)) and in its absence (lanes 4 (aerobic) and 5 (anaerobic)). As seen in the lanes 6 and 7, TEMPO quenches the cleavage activity of this complex in the presence or absence of $[O_2]$, showing clearly that a carbon-centered radical is involved in the chemistry here. ,

30

Figure 2.7: DNA cleavage activity of $[P_p]^{4+}$ in presence of TEMPO

Agarose gel (1%) stained with ethidium bromide of supercoiled pUC18 DNA (0.154 mM) cleavage products after incubation at 25°C for 2 h with $[P_p]^{4+}$, GSH and TEMPO in 7 mM Na_3PO_4 buffer (pH 7.0) under aerobic and anaerobic conditions. Lane 1: DNA control; Lane 2: DNA plus GSH (0.513 mM); Lane 3: DNA plus P^{4+} (0.0128 mM); Lane 4: DNA, GSH (0.513 mM) plus P^{4+}(0.0128 mM); Lane 5: DNA, GSH (0.513 mM) plus P^{4+}(0.0128 mM) under anaerobic conditions; Lane 6: DNA, GSH (0.513 mM), P^{4+}(0.0128 mM) plus TEMPO (2.04 mM); Lane 7: DNA, P^{4+}(0.0128 mM) plus TEMPO (2.04 mM) under anaerobic conditions .

2.4.6 Effect of Radical Scavengers on the DNA Cleavage Activity of $[H_2P_p]^{4+}$

The experiments with addition of DMSO and TEMPO were repeated with $[H_2P_p]^{4+}$ under anaerobic conditions. In this experiment, no GSH is needed and therefore the results are easier to interpret. The data is shown in Figure 2.8. Added DMSO (lane 4) has no effect on the cleavage activity whereas added TEMPO (lane 5) largely shuts down the cleavage activity. The last lane (lane 6) shows that added EDTA also has no effect on the cleavage activity. This was done to demonstrate that any trace metal ions that may be present are not responsible for the observed activity. EDTA effectively complexes trace metal ions (especially Cu^{2+}) and would be expected to attenuate their activity. As no difference is seen in the cleavage activity, trace metals can be ruled out.
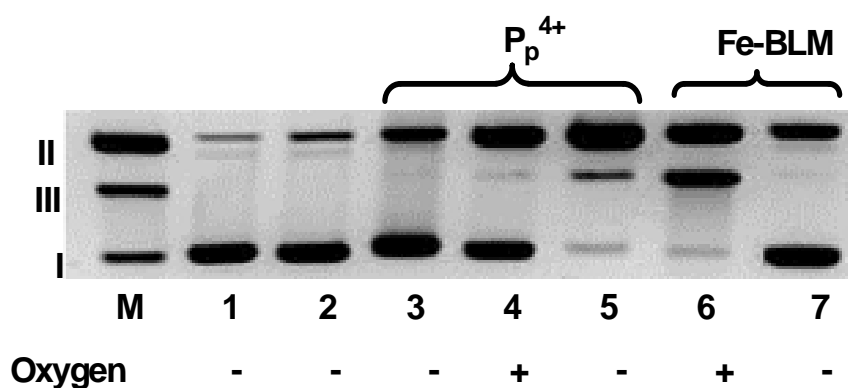
31
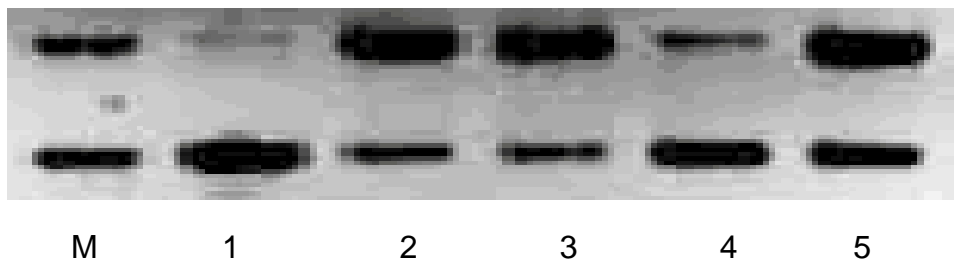
Figure 2.8: DNA cleavage activity of $[H_2P_p]^{4+}$

Agarose gel (1%) stained with ethidium bromide of supercoiled pUC18 DNA (0.154 mM) cleavage products after incubation at 25 ^{o}C for 2 h with $[H_2P_p]^{4+}$ in 7 mM Na_3PO_4 buffer (pH 7.0). Lane 1: Marker lane; Lane 1: DNA control under anaerobic conditions; Lane 2: H_2P^{4+} (0.0256 mM) plus DNA; Lane 3: DNA, H_2P^{4+} (0.0256 mM) plus 5% DMSO; Lane 4: DNA, H_2P^{4+} (0.0256mM) plus TEMPO (1.02 mM); Lane 5: DNA, H_2P^{4+} (0.0256 mM) plus EDTA (1.02 mM). All reactions were carried out under anaerobic conditions.

The quenching by TEMPO seen in Lane 4 again supports the role of a carbon-based radical in the DNA cleavage and the absence of GSH shows that the radical is on the $[H_2P_p]^{4+}$ complex.

EPR experiments were used to see if the radical species could be observed spectroscopicaly. As shown in Figure 2.9, solutions of both $[H_2P_p]^{4+}$ and DNA alone did not show an EPR signal. However, when $[H_2P_p]^{4+}$ is incubated with DNA at 25°C for 1-2 hour and then frozen in liquid N_2, a g signal, characteristic of a carbon-based radical species, is observed (Figure 2.9)
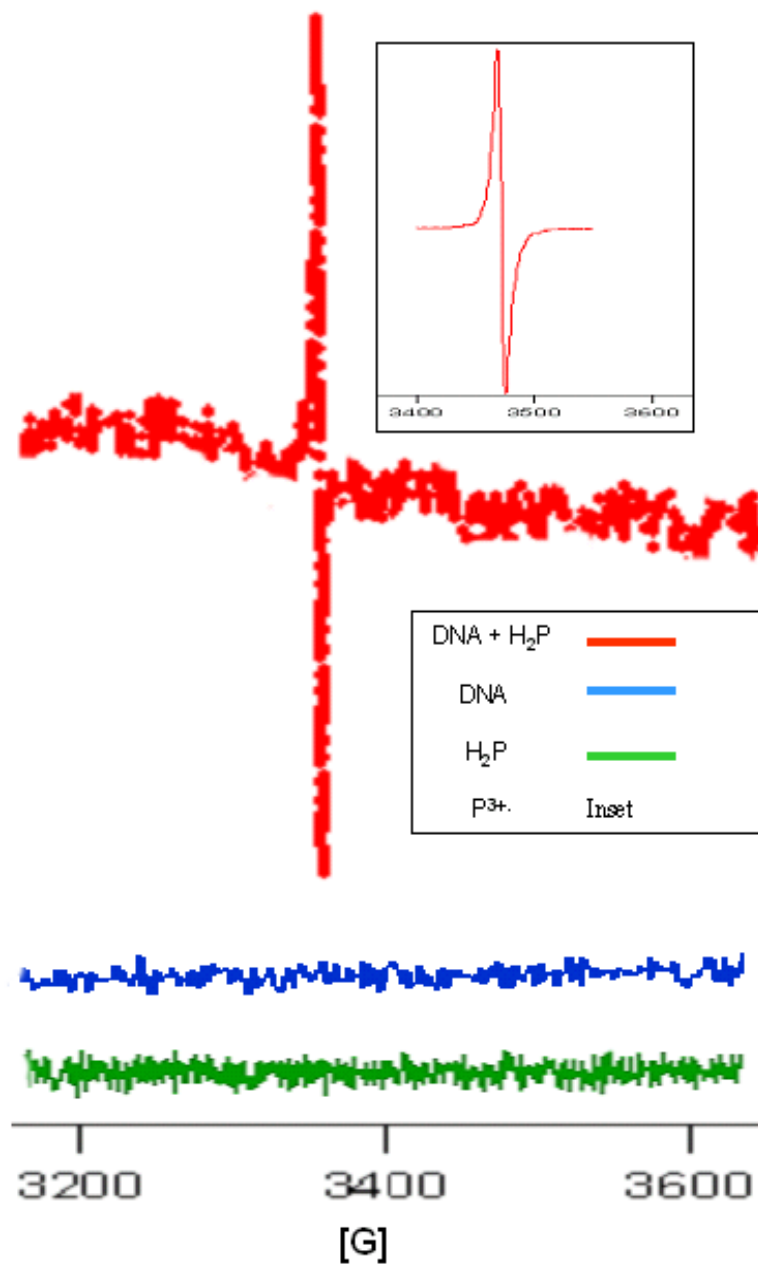
Figure 2.9: EPR spectra of $[H_2P_p]^{4+}$ in presence of DNA

$(H_2P_p^{4+}= 12.8 \ \mu M, DNA= 0.154 \ mM, pH= 7.4)$

It has been shown by NMR studies that $[H_2P_p]^{4+}$ is diamagnetic which is consistent with the EPR spectrum of $[H_2P_p]^{4+}$ alone. We suspect that the radical may be $[P_p]^{3+}$ (Inset- Figure 2.9) which is somehow generated upon $[H_2P_p]^{4+}$ binding DNA via a one electron oxidation. When we varied the incubation time in which DNA and $[H_2P_p]^{4+}$ were mixed, we observed little difference in the intensity of the EPR signal after the first 10 min, suggesting that the radical formed is quite stable once formed which rules out DNA-based carbon radical species as such species would be expected to be unstable and short lived. If $[P_p]^{3+}$ is being generated in situ, then this species when bound via intercalation would be in an optimal position to react with the DNA. It is interesting to note that the product of an H-atom abstraction process by $[P_p]^{3+}$ would be $[H_2P_p]^{4+}$ at pH 7, suggesting the cleavage activity could be catalytic. The question still remains as to how $[P_p]^{3+}$ is generated in situ as this requires something to oxidize $[H_2P_p]^{4+}$ and DNA is a poor oxidant.

2.4.7 Role of Second Metal Ion in DNA Cleavage

As indicated in the previous sections, the tatpp bridging ligand is the site of the relevant redox and protonation chemistry and it is the presumed active unit for DNA cleavage. This ligand, by itself, is insoluble in most common solvents including water and coordination of the $[Ru(phen)_2]^{2+}$ units acts to solubilize it and the cationic charge of the complex is no doubt an important factor in the observed DNA binding affinity. That said, the role of the Ru(II) ions in the

34

cleavage mechanism is not clear, nor is it certain that tatpp is the chemically active nuclease. We wished to determine if one or two Ru(II) ions were required for the nuclease activity and to address this issue, we prepared the mono-ruthenium tatpp complex, $[Ru(phen)_2tatpp]^{2+}$, $[MP_p]^{2+}$ (Figure 2.10). The active nuclease in the DNA cleavage is the central ligand, tatpp, so we decided to investigate the role of ligand and the very first steps towards it was removing one ruthenium center and see the effect on DNA Cleavage.
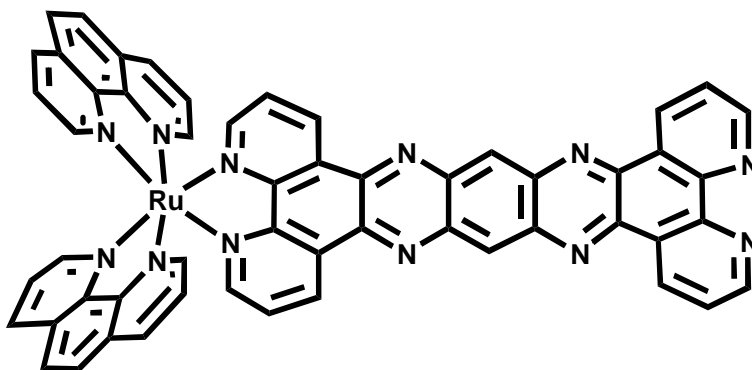
Figure 2.10: Mononuclear Ru(II) polypyridyl complex, $[(phen)_2Ru(tatpp)]^{2+}$, $[MP_p]^{2+}$

2.4.7.1 DNA Cleavage with $[MP_p]^{2+}$ under Aerobic Conditions

DNA cleavage activity was observed for the complex $[MP_p]^{2+}$ under aerobic conditions. Figure 2.11 shows the same.
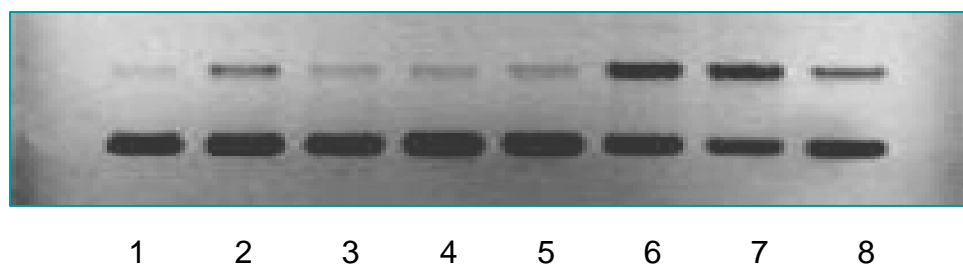
Figure 2.11: DNA cleavage with $[MP_p]^{2+}$ under aerobic conditions

Agarose gel (1%) stained with ethidium bromide of supercoiled pUC18 DNA (0.154 mM) cleavage products after incubation at 25 °C for 2 h with $[MP_p]^{2+}$ in 7 mM Na_3PO_4 buffer (pH 7.0). Lane 1: DNA control ; Lane 2: MP^{2+} (0.0256 mM) plus DNA; Lane 3: DNA plus GSH; Lane 4: DNA plus 5% DMSO; Lane 5: DNA plus TEMPO (1.02 mM); Lane 6: MP^{2+} (0.0256 mM) plus GSH plus DNA; Lane 7: MP^{2+} (0.0256 mM) plus GSH plus DMSO and Lane 8: MP^{2+} (0.0256 mM) plus GSH plus TEMPO. All reactions were carried out under aerobic conditions.

We saw substantial DNA cleavage activity under aerobic conditions (lane 6) that was not quenched even in the presence of 5% DMSO as seen in Lane 7. TEMPO inhibited the cleavage activity (lane 6 & 8). For a better understanding of the cleavage activity the reaction was carried out under anaerobic conditions, as we did for $[P_p]^{4+}$.

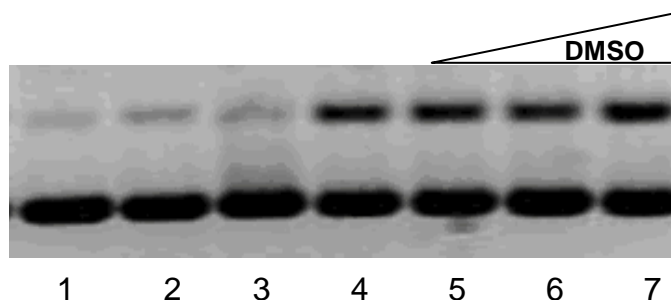## 2.4.7.2 DNA Cleavage with $[MP_p]^{2+}$ under Anaerobic Conditions
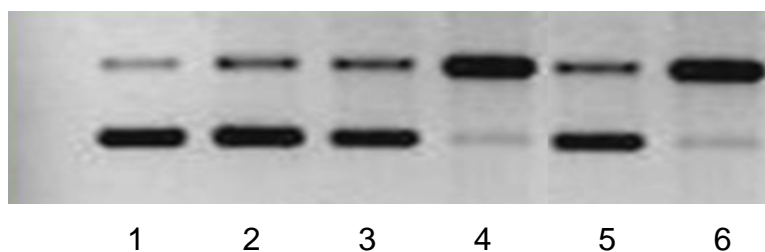
Figure 2.12: DNA cleavage with $[MP_p]^{2+}$ under anaerobic conditions

Agarose gel (1%) stained with ethidium bromide of supercoiled pUC18 DNA (0.154 mM) cleavage products after incubation at 25 °C for 2 h with $[MP_p]^{2+}$ in 7 mM Na_3PO_4 buffer (pH 7.0). Lane 1: DNA control ; Lane 2: MP^{2+} (0.0256 mM) plus DNA; Lane 3: DNA plus GSH; Lane 4: DNA plus MP^{2+} (0.0256 mM) plus GSH ; Lane 5: MP^{2+} (0.0256 mM) plus GSH plus TEMPO and Lane 6: MP^{2+} (0.0256 mM) plus GSH plus 5% DMSO. All reactions were carried out under aerobic conditions.

36

We observed DNA cleavage activity with $[MP_p]^{2+}$ under anaerobic conditions, and this was comparable to $[P_p]^{4+}$ where there was a complete cleavage in presence of GSH (Lane 4); again the activity was inhibited in presence of TEMPO but not in presence of DMSO, suggesting the involvement of carbon centered radical in the cleavage.

The absorption spectra of $[MP_p]^{2+}$ in water with 1mM GSH is shown in Figure 2.13. As can be seen the reduced complex, formulated as $[H_2MP_p]^{2+}$ show a strong broad absorption at ~580 nm which is characteristic of the doubly reduced, doubly protonated tatpp unit $[H_2tatpp]$. The fact that DNA cleavage is only observed when the $[H_2tatpp]$ unit is present allows us to definitively assign this species as the active nuclease but the question remains as to how exactly this unit reacts with the DNA.
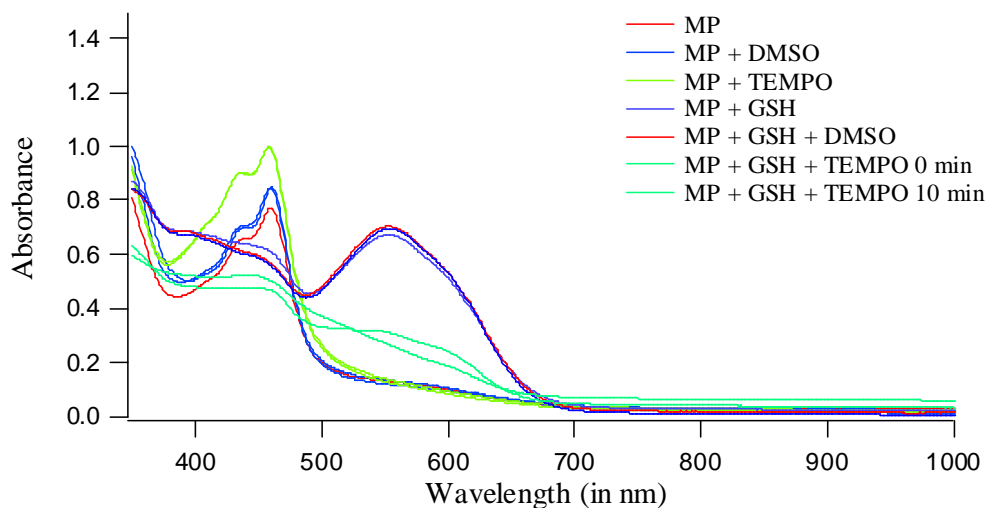
Figure 2.13: Changes on UV- Visible spectrum of $[MP_p]^{2+}$ with addition of DMSO and TEMPO

37

Addition of DMSO did not result in any change in spectrum. TEMPO was able to quench the $[H_2MP_p]^{2+}$ formation, a result consistent with the observed inhibition of DNA cleavage upon addition of TEMPO. No other active species was observed.

2.4.8 Reactive Species for DNA Damage is $[H_2MP_p]^{2+}$

In order to determine whether the interaction of GSH with $[MP_p]^{2+}$ is inhibited by the presence of DNA due to intercalation, we tested whether incubation of this compound with DNA prior to addition of GSH will reduce DNA-cleavage. Thus, the effect of the order of addition of GSH and DNA were compared.
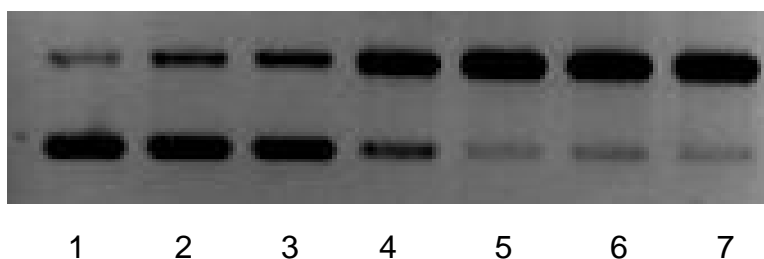
Figure 2.14: Effect of order of addition of GSH to the DNA cleavage activity of $[MP_p]^{2+}$

Agarose gel (1%) stained with ethidium bromide of supercoiled pUC18 DNA (0.154 mM) cleavage products after incubation at 25 ^{o}C for 2 h with $[MP_p]^{2+}$ in 7 mM Na_3PO_4 buffer (pH 7.0). Lane 1: DNA control; Lane 2: MP_p^{2+} (0.0256 mM) plus DNA; Lane 3: DNA plus GSH (2.0 mM); Lane 4: GSH (2.0 mM) plus MP_p^{2+} (0.0256 mM) then DNA; Lane 5: MP_p^{2+} (0.0256 mM) plus GSH (2.0 mM) then DNA; Lane 6: MP_p^{2+} (0.0256 mM) plus DNA then GSH (2.0 mM) and Lane 7: GSH (2.0 mM) plus DNA then MP_p^{2+} (0.0256 mM). All reactions were carried out under anaerobic conditions.

As we see in Figure 2.14 changing the order of addition of GSH to generate $[H_2MP_p]^{2+}$ does not change the DNA cleavage activity. If we compare lanes 4-7, in lane 4 and 5 we made $[H_2MP_p]^{2+}$ before introducing DNA in the

38

reaction mixture thus $[H_2MP_p]^{2+}$ is the species which intercalates into DNA. Lane

6 was $[MP_p]^{2+}$ and DNA added before introducing GSH thereby $[MP_p]^{2+}$ is the

species which interacts with DNA. Lane 7 was incubation of GSH and DNA thus

making the atmosphere reducing in nature prior to the $[MP_p]^{2+}$. As we see in all

the lanes, addition of $[MP_p]^{2+}$ does not influence the cleavage.

To ensure that the observed cleavage was due to the formation of $[H_2MP_p]^{2+}$

rather than other reduced species such as $[MP_p]^+$, which could also cause the

observed DNA damage. TEOA (triethanolamine), a 1-electron donor was added

to determine whether DNA cleavage would be reduced by formation of $[MP_p]^+$

rather than $[H_2MP_p]^{2+}$.


```
  1     2     3     4     5     6     7
```
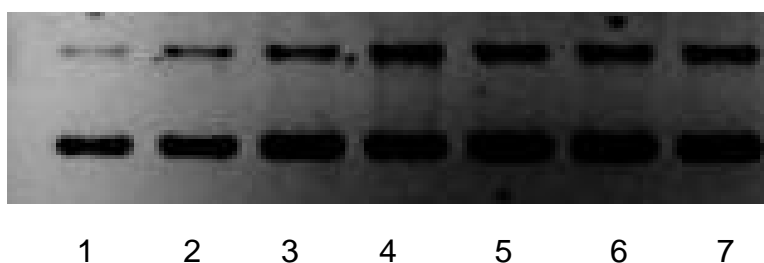
Figure 2.15: Effect of order of addition of TEOA to the DNA cleavage activity of $[MP_p]^{2+}$
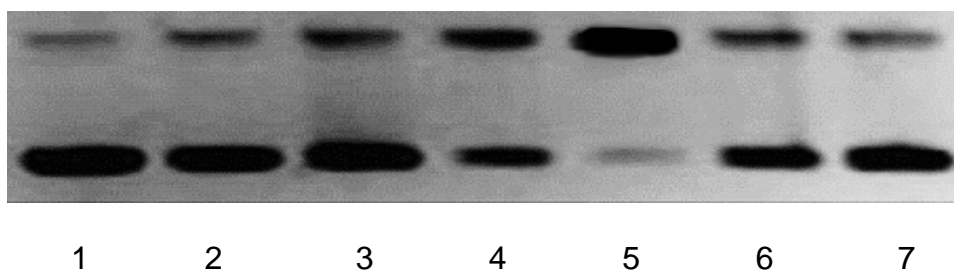
Agarose gel (1%) stained with ethidium bromide of supercoiled pUC18 DNA (0.154 mM) cleavage
products after incubation at 25 ^{o}C for 2 h with $[MP_p]^{2+}$ in 7 mM Na_3PO_4 buffer (pH 7.0). Lane 1:
DNA control; Lane 2: MP_p^{2+} (0.0256 mM) plus DNA; Lane 3: DNA plus TEOA (2.0 mM); Lane 4:
TEOA (2.0 mM) plus MP_p^{2+} (0.0256 mM) then DNA; Lane 5: MP_p^{2+} (0.0256 mM) plus TEOA (2.0
mM) then DNA; Lane 6: MP_p^{2+} (0.0256 mM) plus DNA then TEOA (2.0 mM) and Lane 7: TEOA
(2.0 mM) plus DNA then MP_p^{2+} (0.0256 mM). All reactions were carried out under anaerobic
conditions.

As we see in Figure 2.15 changing the order of addition of TEOA to

generate $[MP_p]^+$ does not change the DNA cleavage activity considerably. If we

compare lanes 4-7 of Figures 2.14 and 2.15 all the lanes have same amount of

$[MP_p]^{2+}$, yet DNA cleavage ability is seen more when the complex is incubated with GSH as compared to TEOA. These result rule out a significant role of $[MP_p]^+$ in DNA cleavage, and supports the assertion that formation of the $[H_2MP_p]^{2+}$ species is necessary for the observed DNA cleavage under present conditions.

2.4.9 Establishing a Potential Mechanism for DNA Cleavage

Our working hypothesis on the mechanism of DNA cleavage by $[H_2P_p]^{4+}$ and $[H_2MP_p]^{2+}$ is that both are oxidized by one electron in situ to form the radical species, $[P_p]^{3+}$ and $[MP_p]^+$, respectively. These radical species are expected to be reasonably stable but still reactive and capable of damaging DNA through either adducts formation or H-atom abstraction. Experiments in which $[P_p]^{3+}$ was directly mixed with DNA under anaerobic conditions (see Figure 2.6) did show some cleavage activity, however the activity was considerably less than for $[H_2P_p]^{4+}$ under the same conditions. One explanation for this anomaly would be in the preparation and isolation of $[P_p]^{3+}$. Reduction of $[P_p]^{4+}$ by excess triethylamine (TEA) in MeCN leads to the one-electron reduced product $[P_p]^{3+}$. When concentrated and precipitated to remove the excess TEA it is possible that a significant portion of the radical $[P_p]^{3+}$ dimerizes as shown in Figure 2.16 to form $[P_p]_2^{6+}$. This dimer of dimers is diamagnetic and would have a difficult time intercalating into the DNA and thus could explain the relatively poor cleavage activity of "$[P_p]^{3+}$". Reduction of $[P_p]^{4+}$ by two electrons (plus two protons) forms

$[H_2P_p]^{4+}$ which is able to intercalate. Once intercalated into DNA, a one-electron oxidation of $[H_2P_p]^{4+}$ would form a reactive carbon radical species, $[P_p]^{3+}$, that would be unable to dimerize as before and would also be in an optimal position for the radical to attack the DNA duplex. As mentioned earlier, we believe that $[P_p]^{3+}$ is a radical which is capable of abstracting hydrogen from the sugar moiety in DNA or of forming a radical-DNA adduct.
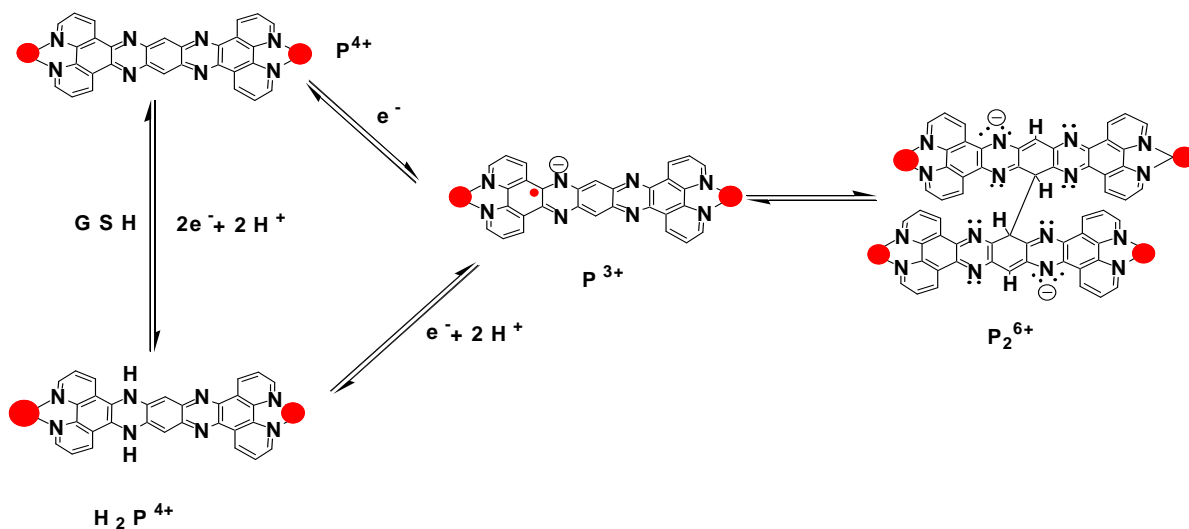
Figure 2.16: Postulated mechanism of DNA cleavage by $[P_p]^{3+}$ species

Another reason to suspect the radical species $[P_p]^{3+}$ and $[MP_p]^+$ is that dihydropyrazines have been reported to cleavage vis a similar mechanism involving the one-electron oxidized radical. Yamaguchi and co-workers have reported that dihydropyrazines are able to cause DNA cleavage by two apparent mechanisms.[72-80] One mechanism is via the activation of $[O_2]$ to form ROS and does not appear to be relevant here. They also reported that an oxygen-

41

independent mechanism involving a carbon radical species is also responsible for cleaving the DNA. They postulated that Cu^{2+} in their experiments was oxidizing the dihydropyrazine function to form a radical species as shown in Figure 2.17. This radical species was attributed to causing some of the observed DNA cleavage, the rest was attributed to ROS. As their experiments were done in the presence of $[O_2]$, the Cu^{2+} was regenerated by oxidation of the Cu^+ species. Clearly, the dihydropyrazine functions in $[H_2P_p]^{4+}$ and $[H_2MP_p]^{2+}$, are related to these compounds and a similar mechanism could be at work here, albeit without the Cu^{2+}.   Interestingly, we are able to observe DNA cleavage at much lower doses than reported by Yamaguchi which is likely a result of the higher DNA binding affinity that would be expected for our cationic, metallointercalators.
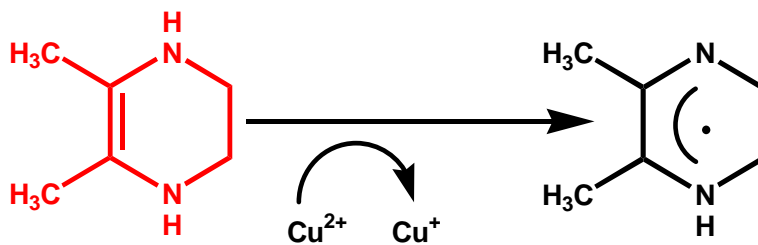
Figure 2.17: Dihydropyrazine as the structural unit

2.4.10 Conclusions

We have discovered the doubly-reduced, doubly-protonated $[H_2P_p]^{4+}$ is a potent DNA cleaving agent and that its activity is potentiated under hypoxic conditions.

42

The active nuclease, formulated as $[H_2P_p]^{4+}$, can be generated in situ via the reduction of $[P_p]^{4+}$ with common biologically common reducing agents, such as GSH. The difference in the nuclease activity of $[P_p]^{4+}$ under aerobic vs. anaerobic conditions can be understood as a shift in the $[H_2P_p]^{4+}$ as dictated by the $[O_2]$. At low $[O_2]$, the dominant solution species is $[H_2P_p]^{4+}$ whereas at normal (aerobic) $[O_2]$ some of the $[H_2P_p]^{4+}$ is being oxidized to $[P_p]^{4+}$ and presumably then re-reduced by the excess GSH (or other reducing agent) present. Thus the steady-state concentration of $[H_2P_p]^{4+}$ is less under aerobic conditions. We speculate that $[H_2P_p]^{4+}$ may be catalytic in its nuclease activity and the presence of excess reducing agents act to ensure $[H_2P_p]^{4+}$ is regenerated in solution.
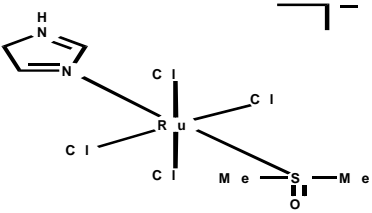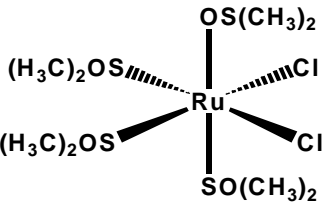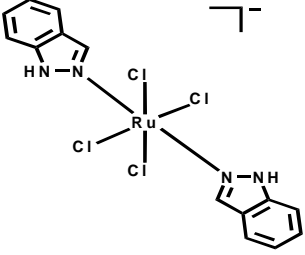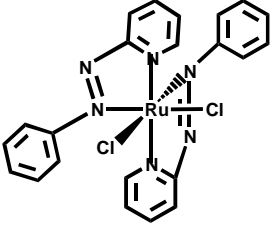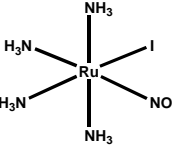
DNA cleavage studies on $[P_p]^{4+}$ and $[H_2P_p]^{4+}$ using plasmid pUC 18 DNA in the presence of different radical scavengers and complexing agents confirm the role of carbon-based radicals in DNA damage. EPR Studies reveal that a stable radical species forms upon incubation of $[H_2P_p]^{4+}$ and DNA. We postulate that $[H_2P_p]^{4+}$ is reduced in situ to form $[P_p]^{3+}$ and it is this species that goes on to cleave the DNA through a pathway that has yet to be fully elucidated. However, this mechanism is not completely consistent with the DNA cleavage observed when $[MP_p]^{2+}$ is incubated with TEOA as the singly-reduced complex $[MP_p]^{+}$ should show the same cleavage activity or better than the doubly-reduced, doubly-protonated $[H_2P_p]^{4+}$.

CHAPTER 3

STRUCTURE-ACTIVITY STUDIES OF RUTHENIUM(II) POLYPYRIDYL COMPLEXES BASED ON CYTOTOXICITY

3.1 Introduction

The use of transition metal complexes as therapeutic agents for cancer treatment started with the discovery of cisplatin.[81] This complex has become one of the most successful anti-cancer drugs of all time and it is known to initiate apoptosis by the formation of DNA inter- and intra-strand crosslinks.[82] Despite an exhaustive search for derivatives with lower overall toxicity, only a few, such as carboplatin[83] and oxaliplatin,[84] are currently in clinical use. Despite this limited success in the clinic, there has been an extensive amount of research into the cytotoxicity of metal complexes with respect to their anti-proliferative activity towards various tumor cells lines. Next to platinum complexes, ruthenium complexes are among the best studied, in part, due to their similar substitution kinetics relative to Pt(II).[85-87] A number of complexes, such as those listed in Table 3.1[88] have shown good cytotoxicity towards cancer cells in vitro and in vivo. The common feature of these complexes is the presence of labile ligands which are postulated to be involved in the complexes biological mechanism of action.

44

Table 3.1: Some substitutionally labile Ru(II) complexes[88]

Complex	Structure	MTD (mg/kg)- mice
Na[trans-RuCl$_4$(DMSO)Im] (NAMI-A)		40
[Ru(II)(DMSO)$_4$Cl$_2$]		565
Hind trans-[RuCl$_4$(ind)$_2$] (KP1019)		91
[Ru(azpy)$_2$Cl$_2$]		80
cis-[RuI(NO)(NH$_3$)$_4$]I$_2$		25

Another common class of ruthenium complexes that has enjoyed extensive attention with respect to their interactions with biological systems are the substitutionally inert polypyridyl complexes, such as $[Ru(phen)_3]^{2+}$, $[Ru_p]^{2+}$, $[Ru(bpy)_3]^{2+}$, $[Ru_b]^{2+}$ and $[Ru(phen)_2(dppz)]^{2+}$ (Figure 3.1)

$[Ru(phen)_3]^{2+}$, **Ru$_p$** $[Ru(bpy)_3]^{2+}$, **Ru$_b$** $[(phen)_2Ru(dppz)]^{2+}$
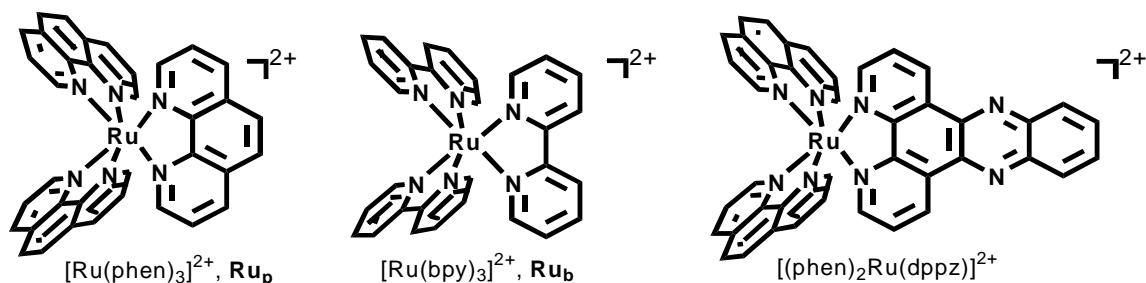
Figure 3.1: Substitutionally inert Ru(II) polypyridyl complexes

These cationic complexes are known to bind DNA electrostatically and if the ligands are large planar aromatic ligands, to also bind via intercalation, as is the case with $[Ru(phen)_2(dppz)]^{2+}$.[89] These complexes are chiral and exist either in a right-handed helical arrangement ($\Delta-$) or a left-handed helical arrangement ($\Lambda-$) and their chirality often influences their observed biological activity. For example, the binding constant for $\Delta-$ and $\Lambda-$ enatiomers of $[Ru(phen)_2(dppz)]^{2+}$ with $\beta-$DNA show a two-fold difference with the right-handed enantiomer, $\Delta-$ $[Ru(phen)_2dppz]^{2+}$ binding more tightly. This is thought to be due to a better fit when bound in the major groove of the right-handed double helix. The binding constant for the two enantiomers are: 3.2×10^6 M^{-1} for $\Delta-$ enantiomer and 1.7×10^6 M^{-1} for the $\Lambda-$ enantiomer.[12, 13]

In another example of their biological activity, the two enantiomers of $[Ru_p]^{2+}$ show different inhibitory activity for acetylcholine esterase (AChE), with $\Delta-$ being a better inhibitor than $\Lambda-$. Identical doses of the two show 90% inhibition for the $\Delta-$ enantiomer compared to 20% inhibition for the $\Lambda-$ enantiomer.[10,9]

Despite their interesting biological activity, these cationic complexes were generally considered poor candidates for drugs because of the acute toxicity seen in mice at relatively low doses for $[Ru_p]^{2+}$.[8] The mice were observed to have seizures seconds after i.p. injection of the complex and subsequently die in minutes. These symptoms suggest the complex is acting as a neurotoxin which is consistent with their inhibitory activity for AChE (a central enzyme in synaptic nerve function). The effect of chirality on AChE inhibition ($\Delta-$ more inhibitory than $\Lambda-$ enantiomer) is mirrored in the lethality of the two enantiomers with minimum lethal doses of 18.4 mg/kg and 9.2 mg/kg for $\Delta-[Ru_p]^{2+}$ and $\Lambda- [Ru_b]^{2+}$, respectively.[8]

While the apparent neurotoxicity was discouraging, a number of these cationic complexes have shown promising cytotoxicity against cancer cell lines in vitro,[90] and for inhibiting HIV activity in H9 lymphocytes. For example, Ru(II) polypyridyl complexes in which one of the ancillary ligands is nmit, icpl or aze (Figure 3.2) have been synthesized and tested for their anti-tumor activity[91]. Ru(II) polypyridyl complexes containing 3-hydroxyflavone derivatives have been screened for cytotoxic activity against 11 tumor cell lines.[92]
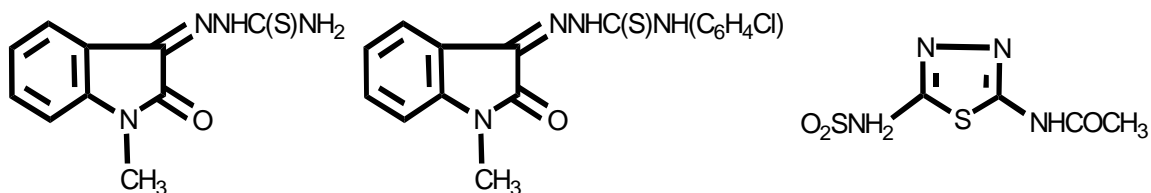
Figure 3.2: Ligands a) nmit b) icpl and c) aze

In this lab, Janaratne and coworkers established that dinuclear ruthenium polypyridyl complexes containing the tatpp and tpphz ligands shown in Figure 3.3 showed good cytotoxicity towards NSCLC H358 and H226 cancer cells.[15] In general, complexes containing the longer tatpp ligand exhibited lower IC_{50} values relative to those containing the tpphz ligand, which was postulated to be related to the redox activity of the tatpp ligand. The tatpp ligand is easily reduced at modest biological potentials whereas reduction of tpphz requires potentials not accessible by common biological reductants (e.g. glutathione). This preliminary study was limited to diastereotopic mixtures of the dinuclear complexes, $[Z_p]^{4+}$ and $[P_p]^{4+}$.
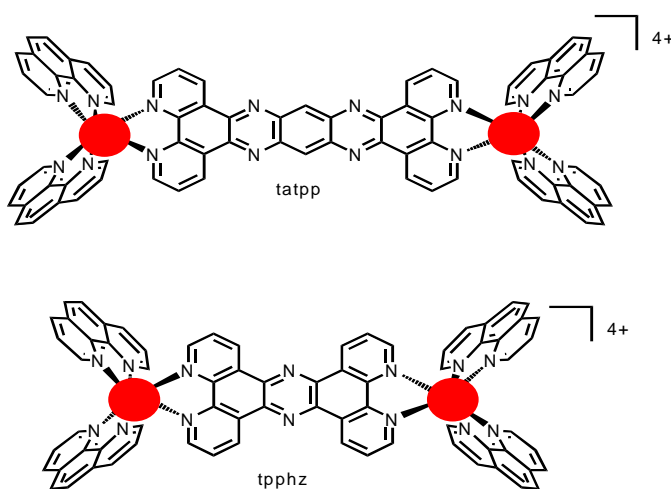
Figure 3.3: Structures of the Ru(II) polypyridyl complexes $[P_p]^{4+}$ (top) and $[Z_p]^{4+}$ (bottom)

In this work, we present a systematic structure-activity study which evaluated the role of the following factors in the cytotoxicity of this class of compounds: tpphz versus tatpp, the number of metal ions in the complex (one or two), the nature of the peripheral ligands (bpy vs. phen) and absolute stereochemistry (diastereomers and enantiomers). To be complete, the simple homoleptic complexes $[Ru_p]^{2+}$ and $[Ru_b]^{2+}$ were included in the study to serve as controls.

The specific complexes examined in this study are listed in Table 3.2 along with our shorthand notation for each complex.

Table 3.2: List of complexes tested for their cytotoxicity

Complex	Stereoisomers examined	Abbreviation
$[Ru(phen)_3]^{2+}$	rac–$[Ru(phen)_3]^{2+}$	rac–$[Ru_p]^{2+}$
	Δ–$[Ru(phen)_3]^{2+}$	Δ–$[Ru_p]^{2+}$
	Λ–$[Ru(phen)_3]^{2+}$	Λ–$[Ru_p]^{2+}$
$[Ru(phen)_2(tpphz)]^{2+}$	rac–$[Ru(phen)_2(tpphz)]^{2+}$	rac–$[MZ_p]^{2+}$
	Δ–$[Ru(phen)_2(tpphz)]^{2+}$	Δ–$[MZ_p]^{2+}$
	Λ–$[Ru(phen)_2(tpphz)]^{2+}$	Λ–$[MZ_p]^{2+}$
$[Ru(phen)_2(tatpp)]^{2+}$	rac–$[Ru(phen)_2(tatpp)]^{2+}$	rac–$[MP_p]^{2+}$
	Δ–$[Ru(phen)_2(tatpp)]^{2+}$	Δ–$[MP_p]^{2+}$
	Λ–$[Ru(phen)_2(tatpp)]^{2+}$	Λ–$[MP_p]^{2+}$

Table 3.2- Continued

[(phen)$_2$Ru(tpphz)(phen)$_2$]$^{4+}$	mix–[(phen)$_2$Ru(tpphz)(phen)$_2$]$^{4+}$	mix–[Z$_p$]$^{4+}$
	ΔΔ–[(phen)$_2$Ru(tpphz)(phen)$_2$]$^{4+}$	ΔΔ–[Z$_p$]$^{4+}$
	ΛΛ–[(phen)$_2$Ru(tpphz)(phen)$_2$]$^{4+}$	ΛΛ–[Z$_p$]$^{4+}$
	ΔΛ–[(phen)$_2$Ru(tpphz)(phen)$_2$]$^{4+}$	ΔΛ–[Z$_p$]$^{4+}$
[(phen)$_2$Ru(tatpp)(phen)$_2$]$^{4+}$	mix–[(phen)$_2$Ru(tatpp)(phen)$_2$]$^{4+}$	mix–[P$_p$]$^{4+}$
	ΔΔ–[(phen)$_2$Ru(tatpp)(phen)$_2$]$^{4+}$	ΔΔ–[P$_p$]$^{4+}$
	ΛΛ–[(phen)$_2$Ru(tatpp)(phen)$_2$]$^{4+}$	ΛΛ–[P$_p$]$^{4+}$
	ΔΛ–[(phen)$_2$Ru(tatpp)(phen)$_2$]$^{4+}$	ΔΛ–[P$_p$]$^{4+}$
[Ru(bpy)$_3$]$^{2+}$	rac–[Ru(bpy)$_3$]$^{2+}$	rac–[Ru$_b$]$^{2+}$
[(bpy)$_2$Ru(tpphz)(bpy)$_2$]$^{4+}$	mix–[(bpy)$_2$Ru(tpphz)(bpy)$_2$]$^{4+}$	mix–[Z$_b$]$^{4+}$
[(bpy)$_2$Ru(tatpp)(bpy)$_2$]$^{4+}$	mix–[(bpy)$_2$Ru(tatpp)(bpy)$_2$]$^{4+}$	mix–[P$_b$]$^{4+}$

The most cytotoxic complexes were then examined for cytotoxicity against two normal cell lines (HUVEC and HAVSMC) to determine if the complexes were selective for malignant cells.

Complexes containing two chiral centers (e.g. [P$_p$]$^{4+}$ and [Z$_p$]$^{4+}$) were first tested without regard to the stereochemistry at each metal center, meaning that the compound tested were a statistical mixture of the ΔΔ–, ΛΛ– and ΔΛ– diastereomers and enantiomers. When this mixture was used, we refer to it as mix–[P$_p$]$^{4+}$ or mix–[Z$_p$]$^{4+}$ for simplicity. When complexes containing just one metal

center were examined, the stereochemical composition of the compound is indicated by either rac– for a racemate or Δ– or Λ– for the two enantiomeric forms.

Table 3.2 thus lists a total of 20 compounds that were tested at various stages and are comprised of either stereochemical mixtures (rac or mix) or enantiopure compounds. The analogous compounds with bpy terminal ligands $[Ru_b]^{2+}$, $[P_b]^{4+}$ and $[Z_b]^{4+}$ were only prepared in racemic (Δ– or Λ–) or mixture ($\Delta\Delta$–, $\Lambda\Lambda$– or $\Delta\Lambda$–) form as the data did not warrant further studies (vide infra).

Figure 3.4 and 3.5 shows the basic chemical structure of the mononuclear and dinuclear complexes. All these complexes were used as chloride salts for ease of solubility in water.

$[Ruphen)_3]^{2+}$, Ru_p

$[(phen)_2Ru(tpphz)]^{2+}$, $MZ_p{}^{2+}$

$[Ru(bpy)_3]^{2+}$, Ru_b

$[(phen)_2Ru(tatpp)]^{2+}$, $MP_p{}^{2+}$
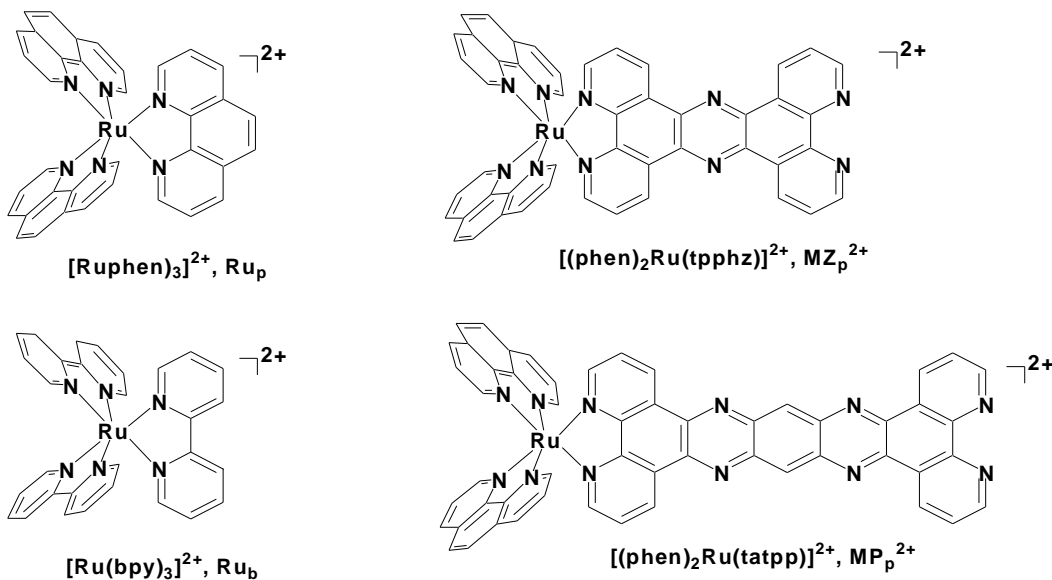
Figure 3.4: Mononuclear Ru(II) polypyridyl complexes

[(phen)₂Ru(tpphz)Ru(phen)₂]⁴⁺, Zₚ⁴⁺

[(bpy)₂Ru(tpphz)Ru(bpy)₂]⁴⁺, Zᵦ⁴⁺

[(phen)₂Ru(tatpp)Ru(phen)₂]⁴⁺, Pₚ⁴⁺

[(bpy)₂Ru(tatpp)Ru(bpy)₂]⁴⁺, Pᵦ⁴⁺
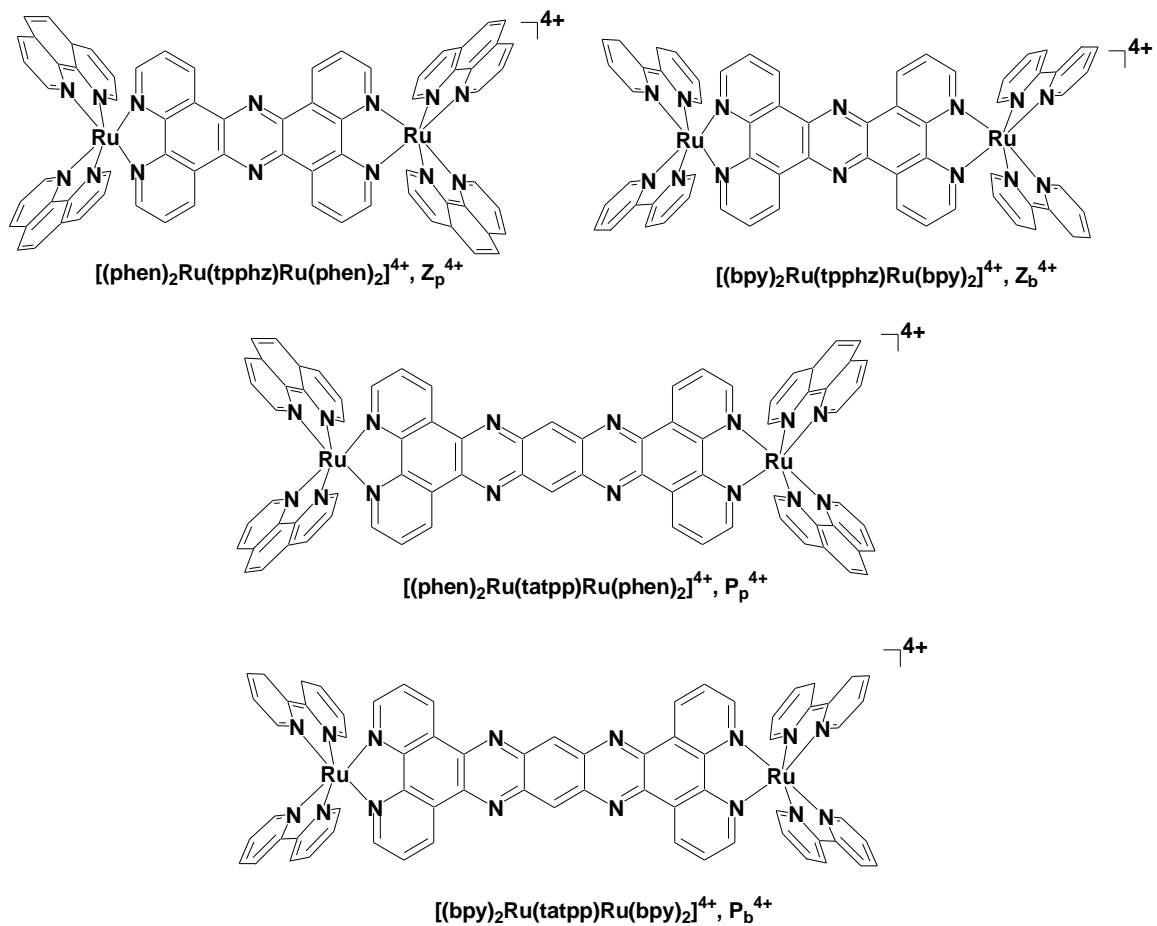
Figure 3.5: Dinuclear Ru(II) polypyridyl complexes

Methods to prepare these complexes in diastereomerally pure and enantiomerally pure have previously been developed in this lab[65,93-95] and were used here.

3.2 Experimental Section

3.2.1 Experimental- Synthesis

3.2.1.1 Instrumentation

^{1}H NMR spectra were obtained on either a JEOL Eclipse Plus 500 or 300 MHz spectrometer using either CD_3CN and d^6-DMSO as the solvent. Chemical shifts were given in ppm relative to tetramethylsilane (TMS). UV-visible spectra were obtained on a Hewlett-Packard HP8453A spectrophotometer. Elemental analyses were performed using a Perkin-Elmer model 2400 CHN analyzer. Mass spectra measurements were carried out using an LCQ Deca XP ion trap mass spectrometer (Thermo Electron Corp., West Palm Beach, FL) equipped with an electrospray ion source. Circular Dichroism (CD) spectra were recorded on a Jasco 710 spectrophotometer in CH_3CN. The chromatographic system was a HP (Agilent Technologies, Palo Alto, CA, USA) 1050 system with a UV detector, an autosampler and Chemstation software. The determination of diastereomeric and enantiomeric purity was done by HPLC using chiral stationary phases as described in the literature[96,97]

3.2.1.2 Chemicals

The compounds 1,10-phenanthroline (phen), 2,2'-bipyridyl (bpy), arsenic(III) oxide, L(+)- and D(-)-tartaric acid, tetra-n-butylammonium chloride hydrate were purchased from Alfa Aesar and ruthenium(III) chloride trihydrate was purchased from Pressure Chemical Company and used without further purification.

Palladium on carbon (Pd/C, 10%) was purchased from Sigma-Aldrich. All

organic solvents were of reagent grade and used as received. Sodium arsenyl

(+) tartrate and sodium arsenyl (-) tartrate were synthesized according to the

literature.[98] [Ru(phen)$_2$phendione]Cl$_2$ was prepared from the reaction of

Ru(phen)$_2$Cl$_2$ and 1,10-phenanthroline-5,6-dione and then resolved into $\Delta-$ and

$\Lambda-$ stereoisomers using previously published procedures.[93,94] $\Delta-$[MZ$_p$]$^{2+}$ and

$\Lambda-$[MZ$_p$]$^{2+}$ compound were synthesized in a similar manner as reported for

racemic complex in the literature except that chiral starting materials were

used.[99,100] Synthesis of $\Delta\Delta-$, $\Lambda\Lambda-$ and $\Delta\Lambda-$[Z$_p$]$^{4+}$ followed the literature

procedures reported by this lab. Synthesis of $\Delta\Delta-$, $\Lambda\Lambda-$ and $\Delta\Lambda-$[P$_p$]$^{4+}$ also

followed literature procedure from this lab.[101]

3.2.2 Synthesis

3.2.2.1 Synthesis of $\Delta-$[(phen)$_2$Ru(tatpp)]$^{2+}$, $\Delta-$[MP$_p$]$^{2+}$

11,12-diaminodipyridophenazine, dadppz (0.18 g , 0.05 mmol) was dissolved in

a 40 mL mixture of glacial acetic acid and absolute ethanol (1:1 ratio) in a 100

mL round bottomed flask. A solution of $\Delta-$ [Ru(phen)$_2$1,10-phenanthroline-5,6-

dione](PF$_6$)$_2$ (0.45 g, 0.05 mmol) in 20 mL dry acetonitrile was slowly poured into

the same flask. The solution was purged with nitrogen gas for 10 min and then

heated to reflux for 12 h under a nitrogen atmosphere. The hot solution was

filtered through a medium porosity glass frit and the solvent volume was reduced

by 50 % on a rotary evaporator. The product was then precipitated by slow

addition of a concentrated aqueous solution of NH_4PF_6 until no further precipitation occurred. The solution was filtered and the precipitate washed with water and dried under vacuum at 60 ^oC to afford the compound in 60% yield. The $\Lambda-$ isomer of the compound was prepared in a similar fashion by taking $\Lambda-$ [Ru(phen)$_2$(1,10-phenanthroline-5,6-dione)]Cl$_2$ as the starting material.

3.2.2.2 Synthesis of $\Delta\Delta-$[(phen)$_2$Ru(tatpp)Ru(phen)$_2$]$^{4+}$, $\Delta\Delta-$[P$_p$]$^{4+}$

$\Delta-$[Ru(phen)$_2$(phendione)](PF$_6$)$_2$ (20 mg, 0.02 mmol) and

$\Delta-$[Ru(phen)$_2$(dadppz)](PF$_6$)$_2$ (20 mg, 0.02 mmol) were dissolved in 10:10:1

mixture of water, acetonitrile and acetic acid and refluxed for 24 hours under

N_2(g). The acetonitrile was removed under reduce pressure and 20 mg of

NH_4PF_6 dissolved in water (5 mL) was added to the remaining solution to obtain

a precipitate which was filtered. The crude product was dissolved in 2 mL of

acetonitrile and precipitated by the addition of 5 mL 10% ethanolic water

containing 20 mg of NH_4PF_6. The product was filtered dried and further purified

by dissolving in acetonitrile and precipitating by addition of diethyl ether.

The $\Lambda\Lambda-$ isomer was obtained in the same way by using

$\Lambda-$[Ru(phen)$_2$(phendione)](PF$_6$)$_2$ and $\Lambda-$[Ru(phen)$_2$(dadppz)](PF$_6$)$_2$ as the

starting materials.

The meso diastereoisomer $\Delta\Lambda-$ stereoisomer was obtained in the same way by

using $\Delta-$[Ru(phen)$_2$(phendione)](PF$_6$)$_2$ and $\Lambda-$[Ru(phen)$_2$(dadppz)](PF$_6$)$_2$ as the

starting materials.

3.3 Experimental- Cytotoxicity

3.3.1 Reagents

RPMI-1640 and DMEM medium, PBS, penicillin/streptomycin solution (P/S), fetal bovine serum (FBS), trypsin-EDTA and trypan blue were purchased from Life Sciences Technologies, Inc., Grand Island, NY. DMSO and 3-(4,5-dimethylthiazol-2-yl)-2,5-diphenyltetrazolium bromide (MTT) were obtained from Sigma.

3.3.2 Cell Lines and Cultures

The cell lines non-small cell lung cancer (NSCLC) lines H358 (bronchioalveolar), H226 (squamous cell carcinoma), B-16 mouse skin melanoma and human aortic vascular smooth muscle (HAVSMC) were kindly donated by Dr. Sanjay Awasthi. The cryopreserved primary culture of HUVEC was purchased from Lonza Walkersville, Inc. Maryland, USA. The experiments with human cervical carcinoma cells (HeLa) cells were performed in collaboration with Dr. Alakananda Basu at the University of North Texas Health Science Center, Fort Worth.

The NSCLC cells were cultured in RPMI 1640 medium supplemented with 10% (v/v) heat-inactivated Fetal Bovine Serum (FBS), 1% (v/v) Penicillin/Streptomycin solution (P/S), 2 mmol/L L-glutamine, 10 mmol/L HEPES, 1 mmol/L sodium pyruvate, 4.5 g/L glucose, and 1.5 g/L sodium bicarbonate.

HAVSMC cells were cultured in DMEM medium supplemented with 10% (v/v) FBS and 1% (v/v) P/S solution and the primary culture of HUVEC cells in EGM medium supplemented with BBE (Bovine Brain Extract), heparin, hEGF, Hydrocortisone, GA-1000 (Gentamicin, Amphotericin B) and FBS 10 ml. All the cells were cultured at 37℃ in a humidified atmosphere of 5% CO_2.

Human cervical carcinoma (HeLa) cells were maintained as monolayer cultures in Dulbecco's modified minimal essential medium (GIBCO) supplemented with 2 mM L- glutamine, 10% fetal bovine serum (HyClone, Logan, UT), 25mM HEPES buffer (pH 7.4), penicillin (100 units/mL) and streptomycin (100 μg/mL) and kept in a humidified incubator at 37^OC with 5% CO_2.

3.3.3 Drug Sensitivity Assay

Cell density measurements were done using a hemocytometer to count dye-excluding cells resistant to staining with trypan blue. Approximately 2×10^4 cells were plated into each well of a 96-well flat-bottomed microtiter plate 24 hours prior to addition of medium containing varying concentrations of ruthenium polypyridyl complexes. After 96-hour incubation, 20 μL of 5mg/mL 3-(4,5-dimethylthiazol-2-yl)-2,5-diphenyltetrazolium bromide (MTT) was introduced to each well and incubated for 2 hour at room temperature as previously described[102] with eight replicate wells per measurement, and three separate experiments to determine IC_{50} of the drug, which is defined as the concentration that reduced formazan formation by 50%. Finally, the plates were centrifuged

and medium was decanted. Cells were subsequently dissolved in 100 µL DMSO

with gentle shaking for 2 hour at room temperature. Measured absorbance

values were directly linked with a spreadsheet for calculation of IC_{50}.

3.4 Results and Discussion

3.4.1 Synthesis

The preparation of the enantiopure complexes shown in Table 3.2 required

stereospecific synthetic methods Our lab have previously shown that enantiopure

monomeric complexes of the type, $\Delta-$ or $\Lambda-[Ru(phen)_2(phendione)]^{2+}$ and

$\Delta-$or $\Lambda-[Ru(phen)_2(phendiamine)]^{2+}$, can undergo facile and high yield

condensation reactions to form the dimeric tpphz complexes. This approach

guarantees retention of stereochemistry at the metal centers as it does not

involve making or breaking bonds at the metal stereocenter in contrast to the

ligand displacement approach. Resolution and synthesis of the chiral starting

complexes is a relatively simple process, the most common procedure being

resolution by diastereoselective precipitation upon addition of chiral anions. For

example, addition of sodium arsenyl L(+)tartrate to a racemic mixture of

$[Ru(phen)_3]^{2+}$ in solution, selectively precipitates out the [Ru][As]. The

diastereomeric and enantiomeric purity of the various complexes in this study

were determined using chiral HPLC in collaboration with with he laboratory of

Prof. Daniel Armstrong at UTA. Table 3.3 summarizes these results and shows

that most complexes were prepared with excellent diastereomeric and

enantiomeric purity.

Table 3.3: Enantiopurity of Ru(II) complexes

Complex	Stereoisomers	% Purity
$\Delta-[Ru(phen)_2(tatpp)]^{2+}$	$\Delta-[MP_p]^{2+}$	98.6
$\Lambda-[Ru(phen)_2(tatpp)]^{2+}$	$\Lambda-[MP_p]^{2+}$	99.2
$\Delta\Delta-[(phen)_2Ru(tatpp)(phen)_2]^{4+}$	$\Delta\Delta-[P_p]^{4+}$	97.6
$\Lambda\Lambda-[(phen)_2Ru(tatpp)(phen)_2]^{4+}$	$\Lambda\Lambda-[P_p]^{4+}$	98.2
$\Delta\Lambda-[(phen)_2Ru(tatpp)(phen)_2]^{4+}$	$\Delta\Lambda-[P_p]^{4+}$	n.d.

3.4.2 Cytotoxicity in Cancer Cells

The structure-activity study describe herein evaluated the role of the following

factors in the cytotoxicity of this class of compounds: tpphz versus tatpp, the

number of metal ions in the complex (one or two), the nature of the peripheral

ligands (bpy vs. phen), and the absolute stereochemistry of the complexes

(diastereomers and enantiomers).

3.4.2.1 Cytotoxicity of Ru(II) Complexes- phen vs. bpy

The first structure-activity relationship investigated examined the role of the

peripheral ligand in the cytotoxicity of the complexes. While these peripheral

ligands seem unlikely to dramatically change the basic chemistry of the

complexes involved, their biological activity can be dramatically different. In a

cytotoxicity study by Liu et al., the two complexes shown in Figure 3.6 were compared. These racemic compounds differ only in the phen vs. bpy. As seen from the data in Table 3.4, the bpy complexes were 10 times more cytotoxic than the relate phenanthroline analogues.
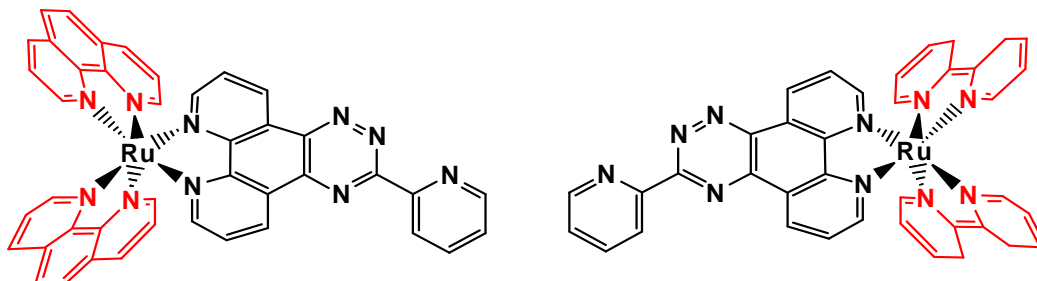
Figure 3.6: IC_{50} for the complexes: $[Ru(phen)_2(pytp)]^{2+}$ and $[Ru(bpy)_2(pytp)]^{2+}$

Table 3.4: Comparison of cytotoxicity of phen vs. bpy complexes

Complexes	IC_{50} (µM)			
	HL-60	BEL-7402	KB	HeLa
$[Ru(bpy)_2(pytp)]^{2+}$	65.4	9.6	14.6	6.8
$[Ru(phen)_2(pytp)]^{2+}$	98.6	>100	>100	>100

We decided to examine this factor in our complexes first so as to minimize the number of total compounds that would be needed to be prepared in enantiopure form, assuming that one or the other would be more active biologically. The data collected in Table 3.5 compares the cytotoxicity of the

phen and bpy analogues (all in either racemic or mix form) for the ruthenium(II)

complexes.

Table 3.5: IC$_{50}$ of phen vs. bpy Ru(II) complexes (H358 and H226)

	phen			Bpy		
	$[Ru_p]^{2+}$	$[Z_p]^{4+}$	$[P_p]^{4+}$	$[Ru_b]^{2+}$	$[Z_b]^{4+}$	$[P_b]^{4+}$
H358	86.7 ± 4.1	41.8 ± 2.7	15.2 ± 1.8	208.8±15.6	125.7 ± 9.4	47.9 ± 3.8
H226	92.8 ± 5.7	51.1 ± 3.4	16.2 ± 1.9	198.5±14.8	101.4 ± 7.6	37.3 ± 2.8

As can be seen, complexes containing phen ligand are always 2 to 3

times more cytotoxic than the analogous compounds with bpy ligands. This is in

contrast to the results found by Liu et. al. The data in Table 3.5 also shows that

the complexes containing the longer tatpp ligand are the most cytotoxic in the

group, followed by the tpphz complexes, and finally the simple homoleptic

complexes which are the least cytotoxic. As a result of this data, all further

studies were done with phen as our ancillary ligand.

3.4.2.2 Cytotoxicity of Ru(II) Complexes- monomers vs. dimers

The need for two metal centers in complex $[Z_p]^{4+}$ and $[P_p]^{4+}$ was examined by

preparing the monomeric complexes $[MZ_p]^{2+}$ and $[MP_p]^{2+}$ and comparing

cytotoxicity. As seen in Figure 3.7, the presence or the extra metal center in

$[Z_p]^{4+}$ and $[P_p]^{4+}$ has little benefit by this measure. Assuming that the complexes

may have some animal toxicity, we presume that complexes with lesser amounts of heavy metals in them may be more desirable.

As will be shown later in this chapter, both $[MP_p]^{2+}$ and $[P_p]^{4+}$ were submitted for testing to the NCI, (Developmental Therapeutics Program- 60 cell line panel) and the data from these tests reveal $[MP_p]^{2+}$ to be more broadly active. Surprisingly, another screen of the two complexes, $\Delta-[MP_p^{2+}]$ and $\Delta\Delta-[P_p^{4+}]$ against cis-platin resistant cells showed that the dimer $\Delta\Delta-[P_p^{4+}]$ was the more cytotoxic of the two, suggesting both compounds may have unique desirable activity in certain circumstances.
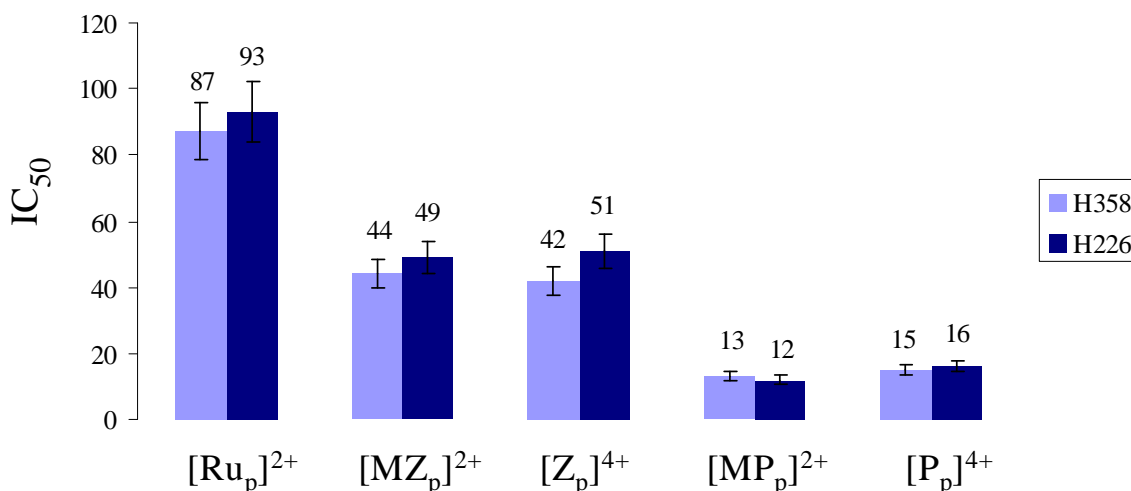
Figure 3.7: IC$_{50}$ of rac/mix- Ru(II) complexes- monomer vs. dimer

The data from Figure 3.7 again shows enhanced cytotoxicity for the tpphz and tatpp complexes over the simple $[Ru_p]^{2+}$ and $[Ru_b]^{2+}$ complexes. The tatpp and tpphz complexes are both known to bind DNA via electrostatics and intercalation[18] compared to $[Ru_p]^{2+}$ and $[Ru_b]^{2+}$ which only bind via

electrostatics.[103] This extra mode of binding increases the binding affinity by at least three orders of magnitude and may be the reason for the enhanced cytotoxicity. Using fluorescence microscopy, Barton and coworkers have shown that the related complex, $[Ru(DIP)_2(dppz)]^{2+}$, is able to penetrate both the cell and nuclear membrane in HeLa cells[104] and can thus directly interact with cellular DNA.

The greater cytotoxicity of tatpp complexes compared to tpphz complexes is postulated to be due to the redox activity of the tatpp ligand at modest, biologically accessible potentials. Table 3.6 shows the ligand-based reduction and metal-based oxidation potentials for a number of the complexes under study, in both water and MeCN. For both the tatpp[105] and tpphz[106] based complexes, the first reduction processes (E_{red1}) seen in MeCN are assigned to a one-electron tatpp or tpphz-based reduction. As can be seen, the tatpp complexes are generally the easiest to reduce. A comparison of the tatpp and tpphz dimers ($[Z_p]^{4+}$ and $[P_p]^{4+}$) shows that the tatpp complex is reduced at a potential 470 mV more positive than the tpphz dimer. A similar comparison for the monomers ($[MZ_p]^{2+}$ and $[MP_p]^{2+}$) reveal the tatpp complex is reduced at a potential 350 mV more positive than the tpphz complex. The absolute value of the reduction potential shows that the tatpp complexes can be reduced in situ by common cellular reductants, such as glutathione.

Table 3.6: Half wave potentials for the oxidation, E_{ox}, and the reduction, E_{red} of the Ru(II) polypyridyl complexes

Complex	E_{ox}	E_{red1}	E_{red2}
$[MZ_b]^{2+}$	1.33	-0.87	-1.33
$[Z_b]^{4+}$	1.34	-0.71	-1.31
$[MP_b]^{2+}$	1.31	-0.52	-0.90
$[P_b]^{4+}$	1.35	-0.24	-0.74

T
tpphz- oxidation potentials are given vs. SCE in CH_3CN and reduction potentials are given vs. SCE in DMF. tatpp- oxidation and reduction potentials are given vs. SCE in CH_3CN.

Janaratne and coworkers showed that GSH could reduce $[P_p]^{4+}$ in aqueous solution to form the doubly-reduced, doubly protonated complex, $[(phen)_2Ru(H_2tatpp)Ru(phen)_2]^{4+}$, $[H_2P_p]^{4+}$.[67] Both the reductions and protonations are known to be localized on the tatpp ligand and the reduction results in the initially orange complex turning green in solution. Similar incubation of $[Z_p]^{4+}$ with GSH does not result in any detectable reduction.

3.4.2.3 Cytotoxicity of Ru(II) Complexes- Chirality

As previously noted, these complexes contain chiral centers and the absolute stereochemistry can have an important and noticeable effect on their biological activity. This stereochemistry could potentially affect numerous important biological processes including: DNA binding and affinity, membrane transport, biodistribution and toxicity.

64

We first examined the effect of chirality on the cytotoxicity of $[Ru_p]^{2+}$ and its enantiomers $\Delta-$ and $\Lambda-$. As shown in Table 3.7 the $\Delta-$ enantiomer is approximated twice as cytotoxic as the $\Lambda-$ enantiomer. The racemate appears to be a weighted average of the toxicity of the two enantiomers.

Table 3.7: IC_{50} of stereoisomers of $[Ru_p]^{2+}$

Cell lines	rac–$[Ru_p]^{2+}$	Δ–$[Ru_p]^{2+}$	Λ–$[Ru_p]^{2+}$
H358	86.7 ± 4.1	64.8 ± 4.2	93.6 ± 6.3
H226	92.8 ± 5.7	61.4 ± 4.7	115.8 ± 6.9

Next, we examined the effect of stereochemistry on the monomeric complexes of tpphz and tatpp. As seen in Figure 3.8, the $\Delta-$ enantiomer is more cytotoxic in both cases; however the difference between enantiomers is not very pronounced with the $[MP_p]^{2+}$ complexes. Consistent with our previous studies, the tatpp complexes remain the most cytotoxic.
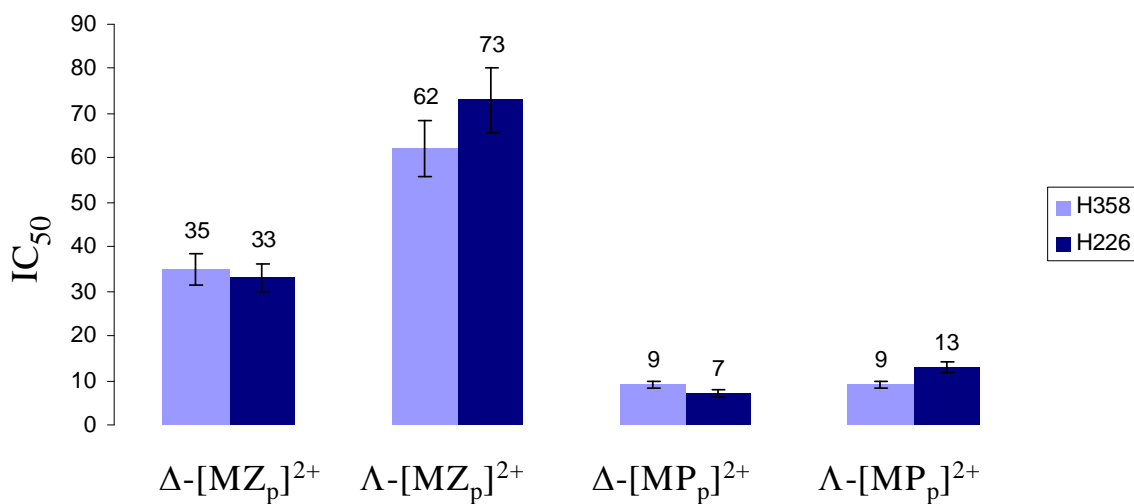
Figure 3.8: IC$_{50}$ of $\square$– vs. $\square$– enantiomers of complexes [MZ$_p$]$^{2+}$ and [MP$_p$]$^{2+}$

The stereochemistry of the dinuclear complexes is more complicated because each complex contains two chiral centers. Each dimer consists of a mixture of a pair of enantiomers, $\Delta\Delta$–, $\Lambda\Lambda$– and the meso diastereomer, $\Delta\Lambda$-. The cytotoxicity of each of these three stereoisomers for [Z$_p$]$^{4+}$ and [P$_p$]$^{4+}$ was examined and the data is shown in Figures 3.9 and 3.10, respectively.
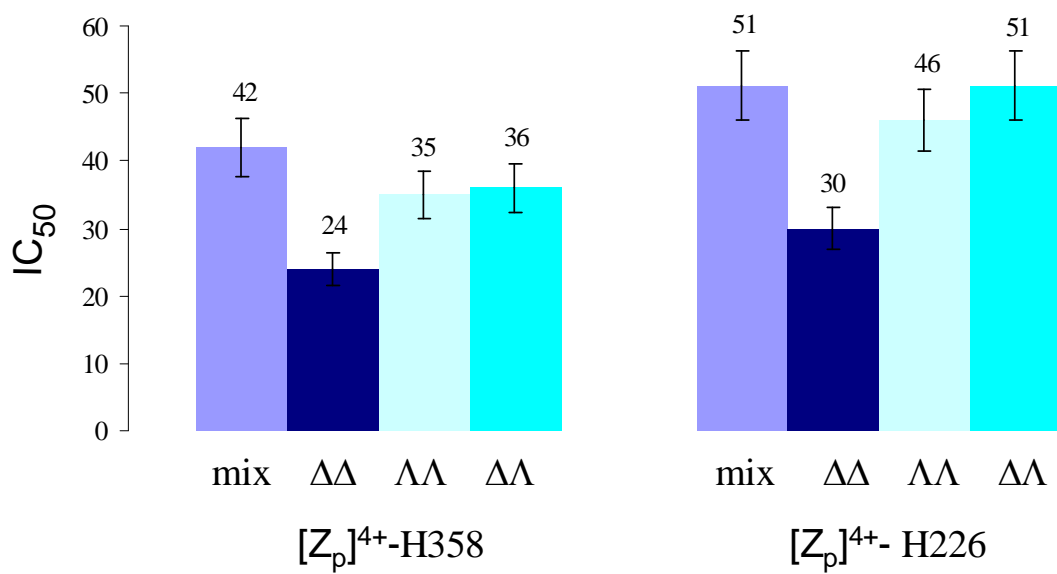
Figure 3.9: Effect of stereochemistry in complex $[Z_p]^{4+}$
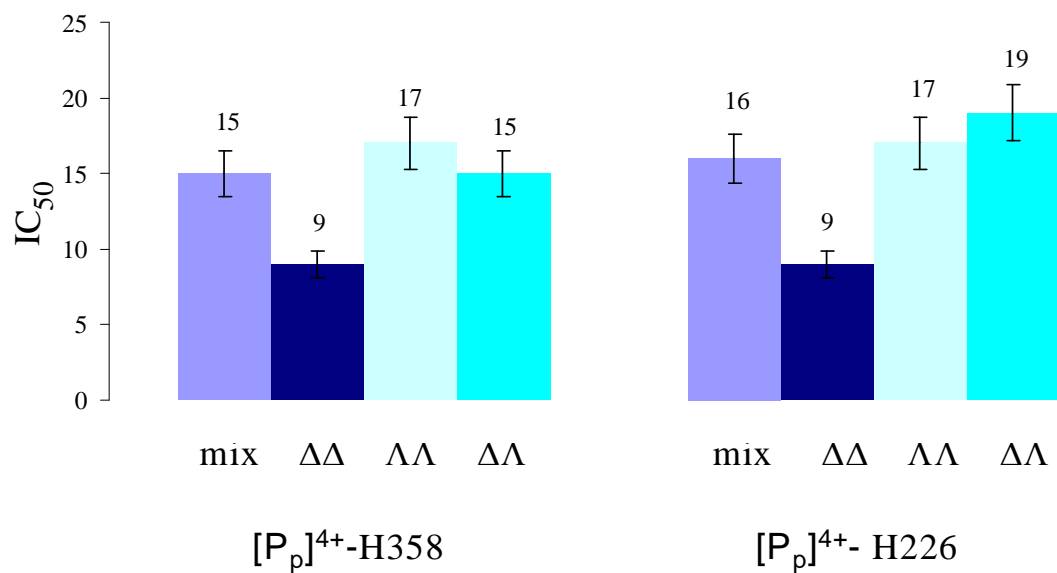
Figure 3.10: Effect of stereochemistry in complex $[P_p]^{4+}$

As seen with the monomeric complexes, the $\Delta\Delta-$ stereoisomers are the most potent for both $[Z_p]^{4+}$ and $[P_p]^{4+}$. Surprisingly, the $\Lambda\Lambda-$ stereoisomer is not the most toxic and has roughly the same toxicity as the $\Delta\Lambda-$ stereoisomer for both $[Z_p]^{4+}$ and $[P_p]^{4+}$. The advantage of having both chiral centers $\Delta-$ is more noticeable for the $[P_p]^{4+}$ complexes with an approximate two-fold enhancement compared to the ~1.5-fold increase for the $[Z_p]^{4+}$ complexes. Surprisingly, the statistical mixture of stereoisomers in mix-$[Z_p{}^{4+}]$ gives an IC_{50} value higher than expected for a weighted average of the three component stereoisomers. The data is similarly skewed for mix$-[P_p{}^{4+}]$ however the difference is less significant. At present we have no explanation for this result.

The tatpp complexes remain the most cytotoxic overall and comparing $\Delta\Delta-[P_p]^{4+}$ with $\Delta-[MP_p]^{2+}$, we observe that the monomeric and dimeric complexes have virtually identical activity in this assay. This is a little surprising in that the two complexes are expected to have significantly different DNA binding affinities. Ruthenium metallointercalators with an overall charge of +2 typically have binding constants on the order of 10^6 M^{-1} whereas the binding affinity of mix$-[P_p]^{4+}$ is 1.1×10^8 M^{-1}. Thus it is apparent that the DNA binding affinity is not a determining factor in the cytotoxicity, assuming a minimum binding constant on the order of 10^6 M^{-1}. Of course, it is possible that DNA is not the cellular target, or at least the main cellular target.

3.4.3 Cytotoxicity in Normal Cells

In the development of any anti-cancer drug it is imperitive that the drug be less cytotoxic towards normal, healthy cells and at least partially selective for cancer cells.   In order to test the drug potential of our two most cytotoxic compounds, $\Delta-[MP_p]^{2+}$ and $\Delta\Delta-[P_p]^{4+}$, we treated two normal cell lines with these two compounds. Human Aorta Vascular Smooth Muscle Cells (HAVSMC) and Human Umbilical Vein Endothelial cells (HUVEC) are easily grown and commonly used cells lines for drug testing.
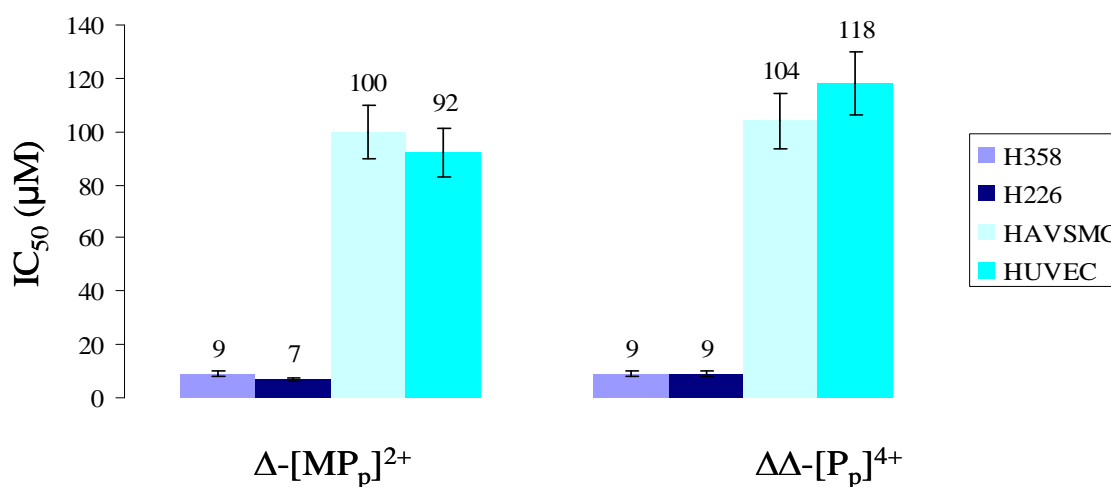
Figure 3.11: Cytotoxicity of $\Delta-[MP_p]^{2}]$ and $\Delta\Delta-[P_p]^{4+}$ towards cancerous and normal human cells lines

The data collected from this study are shown graphically in Figure 3.11. The cytotoxicity of $\Delta-[MP_p]^{2+}$ and $\Delta\Delta-[P_p]^{4+}$ towards cancer cell lines, H358 and H226, and normal cells lines, HUVEC and HAVSMC, are displayed.   As can be seen, the complexes are considerably less cytotoxic towards the normal cell

lines. A therapeutic window can now be defined as the drug concentrations above those needed for good cytotoxicity towards cancer cell lines yet below those concentrations which will significantly affect the normal cells. In this case, the IC_{50} of $\Delta\Delta-[P_p]^{4+}$ in H358 cancer cells is 9.5 μM while the IC_{50} of the same complex in HUVEC is 118.0 μM, revealing a large therapeutic window. The data for $\Delta-[MP_p]^{2+}$ shows a similarly large therapeutic window.

Table 3.8: IC_{50} of Ru(II) complexes in normal cells

Compound Name	Cell Line	IC_{50} μM			
		rac/mix	$\Delta/\Delta\Delta$	$\Lambda/\Lambda\Lambda$	Meso
$\Delta-[MP_p]^{2+}$	HAVSMC	99.4±7.0	100.3±6.0	91.2±5.1	N/A
	HUVEC	93.9±5.4	91.6±4.7	104.4±5.5	N/A
$\Delta\Delta-[P_p]^{4+}$	HAVSMC	133.3±10.6	104.5±6.8	124.9±7.6	116.2±6.7
	HUVEC	132.5±8.7	118.0±7.0	127.3±8.6	135.9±10.4

An examination of the cytotoxicity of the various stereoisomers of $\Delta-[MP_p]^{2+}$ and $\Delta\Delta-[P_p]^{4+}$ towards normal cells revealed little differences between stereoisomers, as shown in Table 3.8. These results suggest the stereochemistry may be an important factor in their ability to cross the cell and nuclear membrane in cancerous cells. Normal cells with presumably better

70

transport regulations are better able to prevent these drugs from building-up inside the cell.

3.4.4 Cytotoxicity in B-16 Mouse Melanoma Cells

A syngeneic mouse model is an in vivo tumor model in which mouse cancer cells are given to a mouse to induce a tumor. Preliminary studies on tumor regression upon treatment with mix–$[P_p]^{4+}$ in a syngeneic mouse melanoma (B-16) model showed some tumor growth inhibition. The cytotoxicity of the various ruthenium complexes with this cell line had not been established and therefore was examined here. The data from this study are shown below in Figure 3.12.
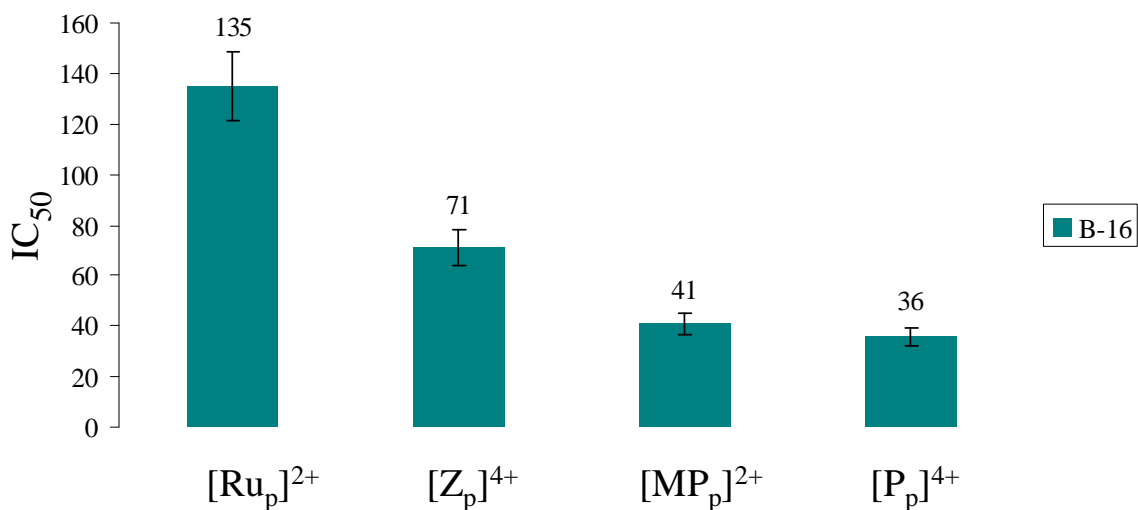
Figure 3.12: IC$_{50}$ of Ru(II) complex in syngeneic mouse melanoma model B-16 melanoma cells

As with the other cancer cell lines, rac–$[MP_p]^{2+}$ and mix–$[P_p]^{4+}$ are the most cytotoxic, however the IC_{50} values are approximately three times higher than was observed with human lung cancer cell lines, H226 and H358. The B16 melanoma cell line is known to be a particularly difficult and resistant cancer to treat in vivo which may explain, in part, the higher IC_{50} values seen here.

3.5 Comparative in-vitro Cytotoxicity with HeLa and Cisplatin Resistant HeLa Cells

Cisplatin is among the most effective drugs for treatment of solid tumors, including ovarian, testicular, small cell lung and cervical carcinomas.[107] The success of cisplatin is, however, often compromised by the development of drug resistance.[108] Drugs which can not only act on parental or cisplatin sensitive cancer cells but also are active against cisplatin resistance cells are needed for the treatment of cancers where cisplatin is no longer effective alone. In a collaborative effort with Dr. Alakananda Basu at University of North Texas Health Science Center, Fort Worth, we screened Δ–$[MP_p]^{2+}$ and $\Delta\Delta$–$[P_p]^{4+}$ for activity against both HeLa cells and cisplatin resistant HeLa cells (HeLa/CP).

The HeLa/CP cells were developed by exposing the parental HeLa cells with escalating concentrations of cisplatin for several months, starting with concentrations of cisplatin that caused 10% cell death.[109] The IC_{50} values of the parental and cisplatin resistant cells are known to differ by approximately a 5-fold difference.[110] In this study, the difference in the IC_{50} for HeLa and HeLa/CP cells was 7 μM vs. 30 μM or approximately a 4.3-fold difference.

Table 3.9: Cytotoxicity of Δ–[MP$_p$]$^{2+}$ and $\Delta\Delta$–[P$_p$]$^{4+}$ against cisplatin sensitive HeLa cells and cisplatin resistant HeLa/CP cells

Complex	Cisplatin Parental HeLa cells IC$_{50}$ (in µM)[*]	Cisplatin Resistant HeLa/CP cells IC$_{50}$ (in µM)[*]
Cisplatin	7.0	30.0
Δ–[MP$_p$]$^{2+}$	15.03	34.03
$\Delta\Delta$–[P$_p$]$^{4+}$	16.07	**1.86**

[*]The data represents mean value of 3 determinations

The two HeLa cells lines, HeLa and HeLa/CP, were treated with Δ–[MP$_p$]$^{2+}$ and $\Delta\Delta$–[P$_p$]$^{4+}$ and the data is collected in Table 3.9. Both complexes exhibit similar IC$_{50}$ values for the parental HeLa cells at ~16 µM. Interestingly, they differ considerably in their activity against HeLa/CP cells. Cisplatin resistant HeLa cells are very sensitive to dinuclear complex, $\Delta\Delta$–[P$_p$]$^{4+}$, showing an IC$_{50}$ value of 1.86 µM, which is approximately an 8-fold increase in sensitivity for the HeLa/CP cells over parental HeLa cells. In contrast, the HeLa/CP cells are less sensitive to Δ–[MP$_p$]$^{2+}$ with an IC$_{50}$ of 34.03 µM compared to 15.03 μM for parental HeLa cells. The earlier studies with H226 and H358 cell lines suggested that the dinuclear complexes offered little advantage over the mononuclear ones. In this study, we observed that the dinuclear structure may have a distinct advantage in cases were drug-resistance is observed.

3.6 Classification of Chemotherapy Agents

Before proceeding further to discuss the results of NCI 60-cell line panel, we introduce some common mechanisms of action known for several classes of anti-cancer drugs.

3.6.1 Alkylating Agents

Alkylating agents are the oldest class of anticancer drugs and are defined as drugs which modify DNA bases by the formation of alkyl-adducts. This alkylation leads to inhibition of DNA replication. The DNA sites at which most adducts are formed are N-7 of guanine, N-7, N-3 and N-1 of adenine, the N-3 of cytosine, and O-4 of thymidine. Alkylating agent drugs include mustards (mechloethamine, melphalan, chlorambucil, cyclophosphamide, ifosfamide, and busulfan), nitrosoureas (BCNU, CCNU, meCCNU, fotemustine, and streptozocin), tetrazines (dacarbazine, temozolomide), aziridines (thiotepa, mitomycin-C, and diaziquone), and others. Many compounds in this class are monofunctional alkylators (CCNU, BCNU)[111,112] that cannot form cross-links, and others are bi-(melphalan, chlorabucil, MeCCNU)[113,114] and tri-functional (thiotepa)[115] alkylators that do form intra- and inter-strand cross-links. Alkylating agents (Figure 3.13) are still among the most frequently used chemotherapy drugs for most solid tumors as well as hematological malignancies.

Cyclophosphamide

CCNU

Mitomycin C
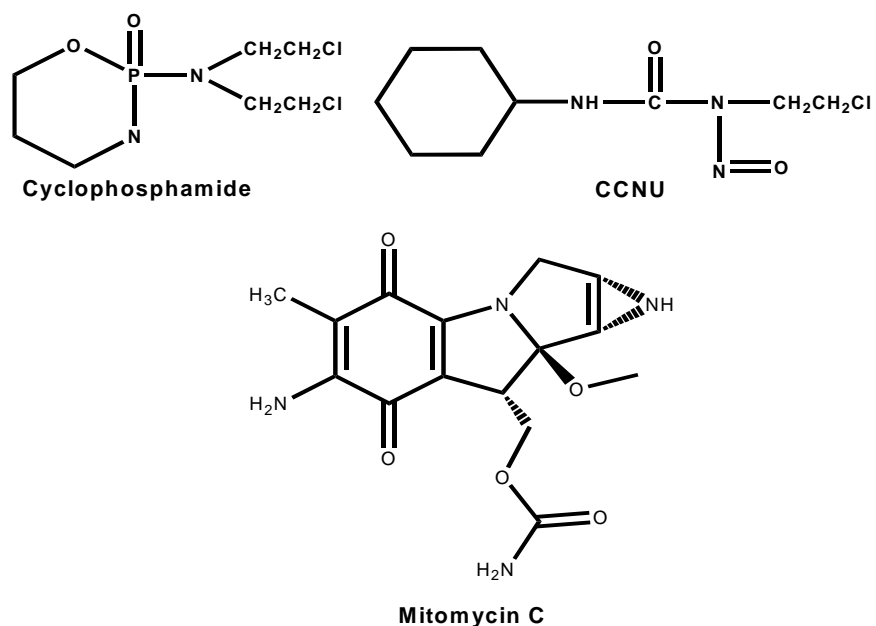
Figure 3.13: Alkylating agents

3.6.2 Topoisomerase I and II Inhibitors

Topoisomerases are an essential class of enzymes which are responsible for catalyzing a number of conformational and topological changes in DNA. Topoisomerase I (Topo I) functions to relieve tortional stress in DNA caused by unwinding. Topo I functions through creation of transient single-strand DNA breaks that allow the nicked DNA strand to rotate about the complementary strand before re-ligation. Topoisomerase II (Topo II) functions to prevent knotting and catenation by transiently inducing a double-strand break in duplex DNA and allowing another duplex to pass through before religation of the original DNA. Compounds which interfere with the action of topoisomerases are often lethal to the cell and thus they are attractive targets for chemotherapeutic drug

75

development. One structural feature common to most topoisomerase inhibitors is the presence of a large planar aromatic group, which is thought to favor intercalation into DNA.

Camptothecin (Figure 3.14) was originally identified as the active antitumor component in the extract of the plant Camptotheca acuminate[116] and is know known to function via inhibition of Topo I.[117] The camptothecin derivatives Irinotecan (CPT-11) and Topotecan are widely used drugs in chemotherapy.

Camptothecin

Irenotecan
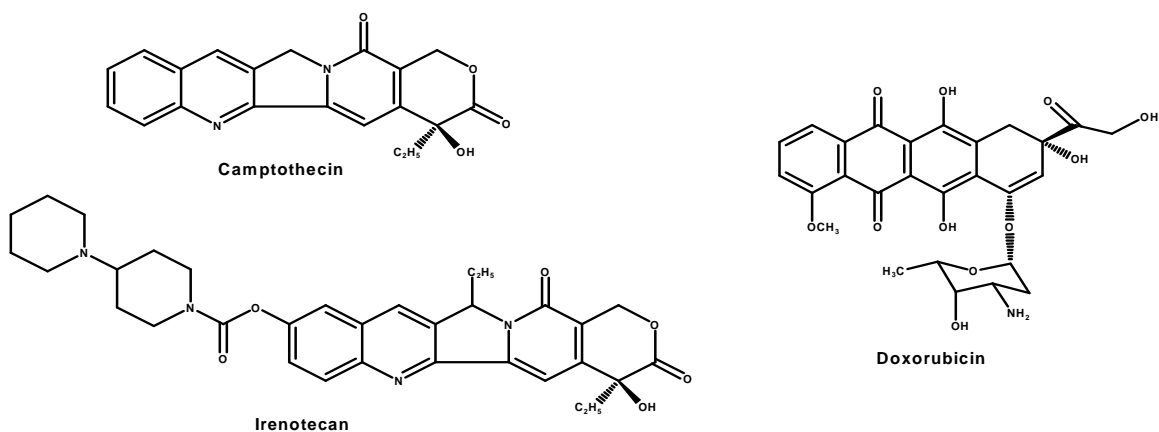
Doxorubicin

Figure 3.14: Topoisomerase inhibitors

Doxorubicin, also shown in Figure 3.14, was the first identified anthracycline drug. Although a number of mechanisms have been proposed for the in vivo antitumor activity of doxorubicin, the primary mechanism of biological activity has been identified as the inhibition and poisoning of Topo II.[118] Doxorubicin stabilizes the so-called "cleavable-complex" between DNA polymerase and topoisomerase II resulting in the formation of protein-linked DNA

double-strand breaks.[119] This compound was first isolated from pigment-producing Streptomyces sp. in the early 1960's and still remain in widespread clinical use today.[120] It is most widely used in the treatment of lymphoma, breast cancer and sarcomas.

3.6.3 Antimetabolites

The antimetabolite class of chemotherapy drugs is varied in structure, but is generally targeted at the metabolic pathways for the synthesis of precursors and DNA or RNA. Rapidly dividing tumor cells consume more metabolites for production of precursor nucleotides for DNA and RNA than normal resting cells and therefore are more susceptible to these agents. These compounds act as either inhibitors or false substrates for a number of nucleotide synthesis or salvage pathway enzymes including thymidilate synthase (5-fluorouracil)[121], dihydrofolate reductase (methotrexate, trimetrexate)[122,123], deoxycytidine kinase (cytarabine), glutamine phosphoribosylamido transferase (6-mercaptopurine)[124] and ribonucleotide reductase (hydroxyurea)[124]. In addition to enzyme inhibition, false substrates are incorporated into DNA resulting in alterations in DNA replication, transcription, and repair that lead to apoptosis.

5-Fluorouracil, shown in Figure 3.15, is the best known and most widely-used antimetabolite. As a pyrimidine analog, the drug is transformed inside the cell into different cytotoxic metabolites which are then incorporated into DNA and

77

RNA inducing cell cycle arrest and apoptosis. Currently, it is most widely used to

treat colorectal and pancreatic cancer
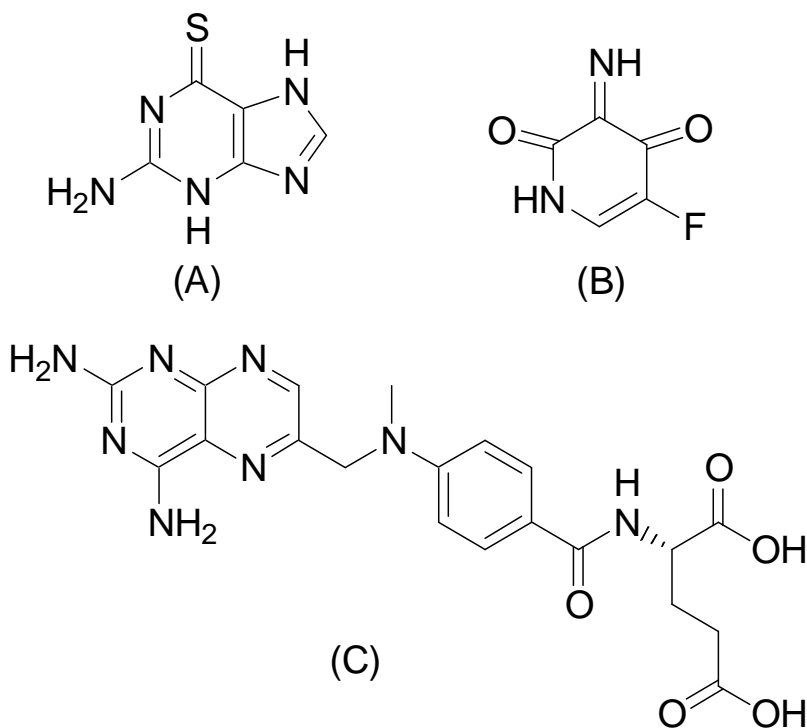
Figure 3.15: Antimetabolites
A) thioguanine B) 5-fluorouracil and C) methotrexate

3.6.4 Antimitotic Agents

Antimitotic agents function by changing the polymerization kinetics of tubulin

forming the process of forming or deconstructing microtubules. Tubulin is a

protein of molecular weight 100,000, and is the principal protein subunit of

microtubules. Microtubules are vital to the performance of many critical cellular

functions, particularly mitosis, and also play an important role in the maintenance

of cell shape and intracellular transport. They are present within the cell in dynamic equilibrium with tubulin heterodimers and many of their unique functional properties are the result of their ability to polymerize and depolymerize in response to critical physiological messages in the cell, including those related to cell cycle progression.[125] Antimitotic agents, such as paclitaxel (Figure 3.16) and docetaxel, preferentially bind to and stabilize microtubules thereby shifting the dynamic equilibrium between tubulin dimers and microtubules towards polymerization.[126,127] This perturbation of the microtubule-tubulin equilibrium, especially during cell division, prevents mitosis and results in cell death.
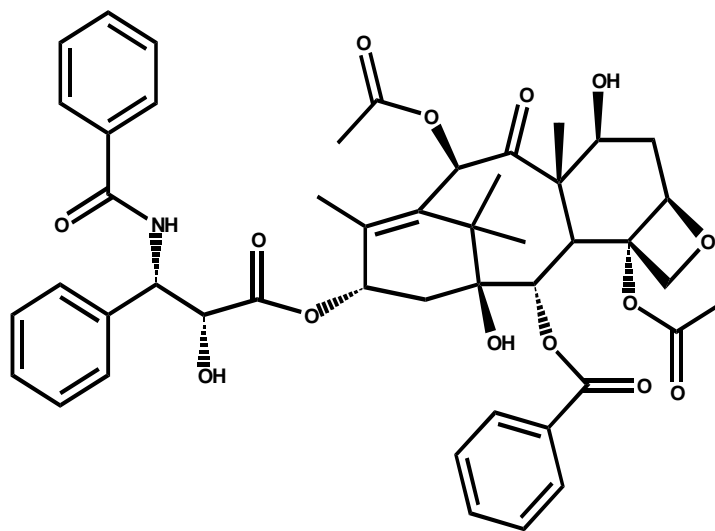
Figure 3.16: Antimitotic agent- paclitaxel

3.6.5 DNA Cleaving Anti-Cancer Drugs

One obvious way to prevent DNA replication is to cleave the biopolymer into pieces. A number of anti-tumor agents function along this principle with Fe-bleomycin (Figure 3.17) being one well-known example.
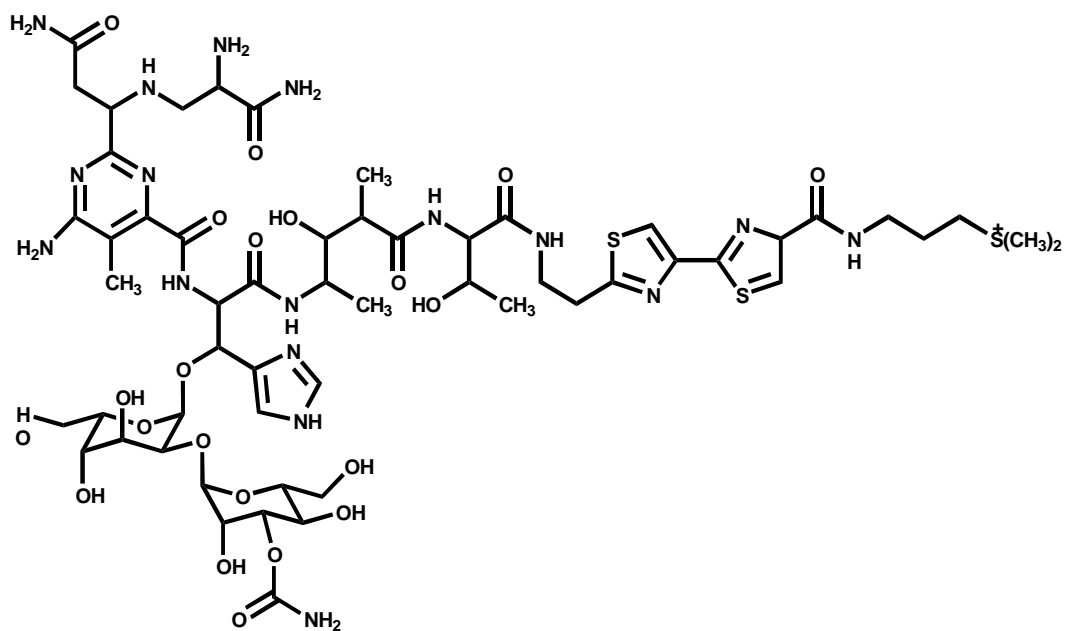
Figure 3.17: Chemical structure of bleomycin

The metal-free bleomycin, shown in Figure 3.17, is a glycopeptide

antibiotic produced by the bacterium Streptomyces verticillus. When used for

treatment, the bleomycin binds Fe(II) in situ to form a Fe(II)BLM complex which

binds DNA via intercalation of the bithiazole group into the minor groove of

DNA.[128] This DNA bound drug complex can react with [O_2] at the Fe(II) site to

produce reactive oxygen species that attack the nearby deoxyribose units in the

DNA, ultimately leading to both single and double-strand cleavage. The drug is

used in the treatment of Hodgkin's lymphoma (as a component of the ABVD

regimen), squamous cell carcinomas, and testicular cancer.

3.6.6 Platinum Complexes

As mentioned previously, cisplatin, or cis-$[PtCl_2(NH_3)_2]$, is a remarkably effective and widely-used chemotherapeutic agent. It is known to kill cancer cells by the formation of DNA adduct between guanine bases and the Pt(II) center. Because of its remarkable effectiveness, this drug has become one of the 'gold standards' in cancer chemotherapy and it continues to be the treatment of choice for testicular and ovarian cancer and is also used in treating cervical, bladder and head/neck tumors.[83,129-131] The neutral complex is thought to passively diffuse through cell membranes into the cytoplasm where the chloride concentration is markedly lower than in the extra-cellular fluids. Because of this concentration drop, the labile chloride ligands are lost to form the cationic monoaqua and diaqua species, cis-$[(NH_3)_2Pt(H_2O)Cl]^+$ and $[(NH_3)_2Pt(H_2O)_2]^{2+}$.[82] These cationic species are electrostatically attracted to the DNA and eventually lose the aqua ligands and coordinate to the basic N7 on adjacent guanine residues to form DNA inter- and intra-strand crosslinks.

Cisplatin has well-known toxic side-effects which primarily target the nervous system and the kidneys in a dose dependent fashion.[132] Derivatives which partially alleviate these side-effects are known and are in clinical use. For example, carboplatin which is shown in Figure 3.18, retains the basic structural elements of cisplatin yet is less toxic effect and thus allows a higher dose to be administered.[83,133] Oxaliplatin, also shown in Figure 3.18, is another derivative which has shown efficacy against many tumor cell lines including some that are

either insensitive or resistant to cisplatin and carboplatin. Studies have further

suggested that oxaliplatin has different molecular targets and/or different

mechanisms of resistance.[84,134]
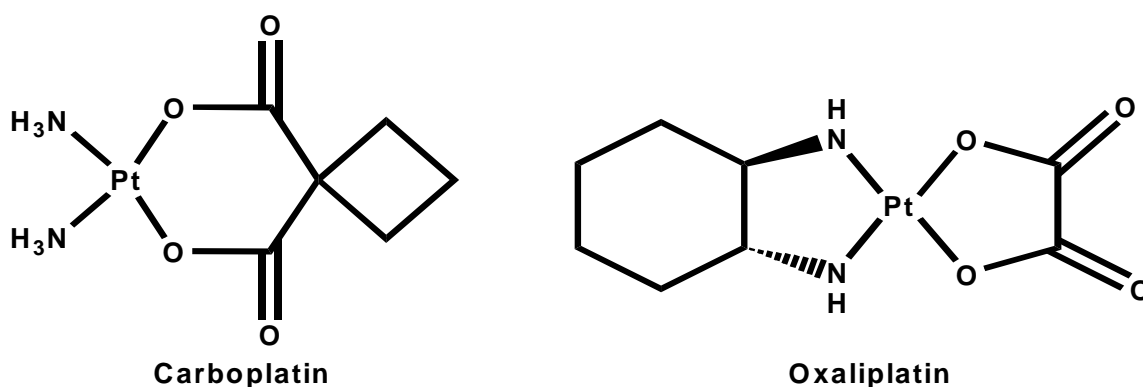
Figure 3.18: Second generation platinum drugs

3.6.7 Ruthenium-Based Drugs

The clinical success of cisplatin demonstrated the potential of metal-based

compounds as drugs. Literally thousands of cisplatin analogues have been

examined for antitumor activity since the clinical introduction of cisplatin in the

1970's. Despite all this activity, only carboplatin and oxaliplatin have shown

enough promise to make it to clinical use. Looking to other metals in the periodic

table, ruthenium complexes were an obvious choice given that Ru(II) and Pt(II)

share similar ligand substitution kinetics. Ruthenium(II) compounds, like Pt(II)

compounds, have different substitution kinetics with different ligands. For

example, ligands containing nitrogen-bases (donor-atoms) are typically much

slower to dissociate than ligands with oxygen or halogen donor atoms. When multidentate ligands containing N-donor atoms, such as bipyridine, are used it becomes very difficult to displace these ligands under normal conditions. Thus it is possible to prepare relatively stable complexes with different sets of ligands and which will react in predictable ways.[135]

Two classes of ruthenium-based drugs are in active development. One class includes complexes with substitutionally labile ligands, such as chloride, which are intended to react with biological targets, including DNA, via the formation of new metal-ligand bonds with the biological target. The other promising class of ruthenium complex drugs is those based on substitutionally inert ruthenium(II)polypyridyl complexes. These complexes are not designed to undergo ligand exchange in situ but instead rely on the nature of the multidentate ligands, the cationic charge, the good lipophilicity and high stability of the complex to interact with specific biological targets.

Keppler and coworkers were the first to describe the anti-cancer activity of substitutionally-labile ruthenium complexes which incorporated imidazole and/or indazole ligands. The complexes were shown to possess anti-cancer activity against the Walker 256 carcinosarcoma, MAC 15A colon tumor, B16 melanoma and solid sarcoma 180.[136] The complex KP1019 (Figure 3.19) is known to interact with and inhibit DNA synthesis[86] as well as being a potent topo II poison.[137] It was reported to be in Phase I clinical trials in 2001, however the results of this study are unknown.

Another promising substitutionally-labile ruthenium drug would be

ImH[trans-RuCl$_4$(DMSO)Im] (NAMI) which is shown in Figure 3.20. This complex

has shown anti-tumor activity against some metastasizing tumors from which it

draws its nickname, NAMI (New-Anti-tumor Metastasis Inhibitor). This

compound has shown enough promise that it has passed phase I clinical trials in

1999 and has been entered into phase II clinical trials in 2003.[135,138]
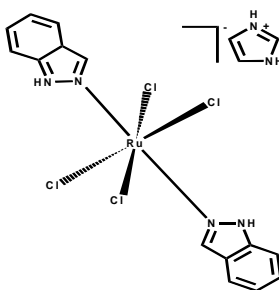
Figure 3.19: Ruthenium metallopharmaceutical, KP1019
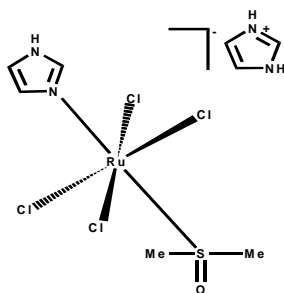
Figure 3.20: Ruthenium metallopharmaceutical, NAMI

Hind trans-[RuCl$_4$(ind)$_2$], KP1019 has also shown remarkable

antiproliferative activity in vitro in human carcinoma cell lines SW707 and

SW948[139] which was very similar to standard chemotherapeutic drug 5-

fluorouracil.

3.7 Developmental Therapeutics Program of the National Cancer Institute

The evolution of strategies at the National Cancer Institute (NCI) illustrates the changes in screening that have resulted from advances in cancer biology. The Developmental Therapeutics Program (DTP) operates a tiered anti-cancer compound screening program with the goal of identifying novel chemical leads and biological mechanisms. The DTP screen is a three phase screen which includes: an initial screen which first involves a single dose cytotoxicity screen with the 60 cell line assay. Those passing certain thresholds are subjected to a 5 dose screen of the same 60 cell-line panel to determine a more detailed picture of the biological activity. A second phase screen establishes the Maximum Tolerable Dosage and involves in vivo examination of tumor regression using the Hollow fiber assay. The third phase of the study is the human tumor xenograft evaluation.

Active compounds are selected for testing based on several criteria: disease type specificity in the in vitro assay, unique structure, potency, and demonstration of a unique pattern of cellular cytotoxicity or cytostasis, indicating a unique mechanism of action or intracellular target.

Some of the approved cancer treatment drugs developed with DTP involvement are: Fluorouracil (1962, NSC-19893), Bleomycin (1973, NSC-125066), Doxorubicin (1974, NSC-123127), cis-Platinum (1978, NSC-119875), Carboplatin (1989, NSC-241240), Taxol (1992, NSC-192573) and Erbitux (2004, NSC-632307).

We submitted two lead compounds to this program $\Delta-[Ru(phen)_2(tatpp)]Cl_2$, $\Delta-[MP_p]^{2+}$ and $\Delta\Delta-[(phen)_2Ru(tatpp)(phen)_2]Cl_4$, $\Delta\Delta-[P_p]^{4+}$ for this screen. Both compounds were accepted for the initial one dose screen and given an NSC number for identification. $\Delta-[MP_p]^{2+}$ was designated as NSC 747949 and $\Delta\Delta-[P_p]^{4+}$ was designated as NSC 747950. The data from the one dose screen warranted further investigation for only one compound, $\Delta-[MP_p]^{2+}$ (NSC 747949). This compound was subjected to a 5-dose cytotoxicity screen against the 60 cell line panel.

Drug testing data are represented as a mean graph that displays growth inhibition in a standard bar graph representation. The mean graph is constructed by projecting bars to the right or left of the mean, depending on whether an individual cell line is more or less sensitive than the average line in the panel. Further the length of each bar is proportional to the relative sensitivity of the cell lines. Thus, each agent can be represented by a characteristic fingerprint of cell-line responsiveness, indicated by the bar graph presentation.

These data are presented and analyzed in this section. The broad screen provides a basis for comparison with other compounds, many of which have a known mechanism of action. The NCI COMPARE program is an online database and comparison tool which analyzes both one-dose and five-dose data cytotoxicity data for the 60 cell line panel for similar activity profiles with all the compounds screened previously by the DTP.

A compound is entered into the program as a seed, and the computer database elicits a list of those agents that have similar patterns of cellular cytotoxicity. A correlation coefficient is also expressed relating the closeness of the seed to those agents listed by the computer program. Close correlations between agents demonstrates biological and pharmacological importance and implies a common intracellular target despite dissimilarity in structure.

A high correlation of cytotoxicity with compounds of known biological mechanism is often predictive of the drugs mechanism of action and thus a tool to aid in the drug development and testing. It also tells if there is any unique response of the drug which is not similar to any of the standard prototype compounds in the NCI database.

This section discusses the results of 60 human tumor cell line (NCI-60) screen employed by NCI. The cell lines are grouped into nine disease subpanels including: Leukemia, Lung (non small cell lung and small cell lung), Central Nervous System, Colon, Melanoma, Ovarian, Renal, Breast and Prostate.

3.7.1 Methodology of the in-vitro Cancer Screen

The protocol for the NCI-60 screen is as follows. The human tumor cell lines are grown in RPMI 1640 medium containing 5% fetal bovine serum and 2 mM L-glutamine. For a typical screening experiment, cells are inoculated into 96 well microtiter plates in 100 μL at plating densities ranging from 5,000 to 40,000 cells/well depending on the doubling time of individual cell lines. After cell

inoculation, the microtiter plates are incubated at 37°C, 5 % CO_2, 95 % air and 100 % relative humidity for 24 h prior to addition of experimental drugs.

After 24 h, two plates of each cell line are fixed in situ with TCA, to represent a measurement of the cell population for each cell line at the time of drug addition (T_z). Experimental drugs are solubilized in dimethyl sulfoxide at 400-fold the desired final maximum test concentration and stored frozen prior to use. At the time of drug addition, an aliquot of frozen concentrate is thawed and diluted to twice the desired final maximum test concentration with complete medium containing 50 µg/mL gentamicin. Additional four, 10-fold or ½ log serial dilutions are made to provide a total of five drug concentrations plus control. Aliquots of 100 µl of these different drug dilutions are added to the appropriate microtiter wells already containing 100 µl of medium, resulting in the required final drug concentrations.

Following drug addition, the plates are incubated for an additional 48 h at 37°C, 5 % CO_2, 95 % air, and 100 % relative humidity. For adherent cells, the assay is terminated by the addition of cold TCA. Cells are fixed in situ by the gentle addition of 50 µl of cold 50 % (w/v) TCA (final concentration, 10 % TCA) and incubated for 60 minutes at 4°C. The supernatant is discarded, and the plates are washed five times with tap water and air dried. Sulforhodamine B (SRB) solution (100 µl) at 0.4 % (w/v) in 1 % acetic acid is added to each well, and plates are incubated for 10 minutes at room temperature. After staining, unbound dye is removed by washing five times with 1 % acetic acid and the

plates are air dried. Bound stain is subsequently solubilized with 10 mM trizma base, and the absorbance is read on an automated plate reader at a wavelength of 515 nm. For suspension cells, the methodology is the same except that the assay is terminated by fixing settled cells at the bottom of the wells by gently adding 50 µl of 80 % TCA (final concentration, 16 % TCA). Using the seven absorbance measurements [time zero, (T_z), control growth, (C), and test growth in the presence of drug at the five concentration levels (T_i)], the percentage growth is calculated at each of the drug concentrations levels. Percentage growth inhibition is calculated as:

$[(T_i-T_z)/(C-T_z)]$ x 100 for concentrations for which $T_i >/= T_z$

$[(T_i-T_z)/T_z]$ x 100 for concentrations for which $T_i < T_z$.

Three dose response parameters are calculated for each experimental agent.

1) GI_{50}

Growth inhibition of 50 % (GI_{50}) is calculated from $[(T_i-T_z)/(C-T_z)]$ x 100 = 50, which is the drug concentration resulting in a 50% reduction in the net protein increase (as measured by SRB staining) in control cells during the drug incubation.

2) TGI

The drug concentration resulting in total growth inhibition (TGI) is calculated from $T_i = T_z$.

3) LC$_{50}$

The LC$_{50}$ (concentration of drug resulting in a 50% reduction in the measured protein at the end of the drug treatment as compared to that at the beginning) indicating a net loss of cells following treatment is calculated from $[(T_i-T_z)/T_z] \times 100 = -50$.

Values are calculated for each of these three parameters if the level of activity is reached; however, if the effect is not reached or is exceeded, the value for that parameter is expressed as greater or less than the maximum or minimum concentration tested.

3.7.2 NCI Screen Data

The compound NSC 747950 and NSC 747949 was tested at an initial high dose of 10 µM in the full NCI-60 cell panel and the data was reported as a mean graph of percent growth of treated cells.

It was found that mean percent growth for cells treated with $\Delta\Delta-[P_p]^{4+}$ (NSC 747950) was 79.61% as compared to 42.03% for $\Delta-[MP_p]^{2+}$ (Figure 3.21 and Figure 3.22)

Developmental Therapeutics Program	NSC: 747950 / 1	Conc: 1.00E-5 Molar	Test Date: Jul 07, 2008
One Dose Mean Graph	Experiment ID: 0807OS66		Report Date: Aug 05, 2008

Panel/Cell Line	Growth Percent	Mean Growth Percent - Growth Percent
Non-Small Cell Lung Cancer		
A549/ATCC	103.65	
EKVX	94.89	
HOP-62	69.14	
HOP-92	62.73	
NCI-H226	104.01	
NCI-H23	71.52	
NCI-H322M	91.93	
NCI-H460	78.00	
NCI-H522	108.23	
Colon Cancer		
COLO 205	92.07	
HCC-2998	71.70	
HCT-116	41.15	
HCT-15	99.36	
HT29	76.92	
KM12	44.91	
SW-620	22.27	
Breast Cancer		
BT-549	88.93	
HS 578T	101.10	
MCF7	100.99	
MDA-MB-231/ATCC	94.70	
MDA-MB-435	49.44	
MDA-MB-468	85.46	
NCI/ADR-RES	87.55	
T-47D	95.07	
Ovarian Cancer		
IGROV1	66.58	
OVCAR-3	87.28	
OVCAR-4	94.62	
OVCAR-5	84.20	
OVCAR-8	113.77	
SK-OV-3	96.67	
Leukemia		
CCRF-CEM	48.86	
HL-60(TB)	45.82	
K-562	28.33	
MOLT-4	28.23	
RPMI-8226	9.67	
SR	88.93	
Renal Cancer		
786-0	57.03	
A498	115.66	
ACHN	91.62	
CAKI-1	58.59	
RXF 393	126.44	
SN12C	85.28	
TK-10	127.95	
UO-31	75.28	
Melanoma		
LOX IMVI	53.05	
M14	51.23	
MALME-3M	97.55	
SK-MEL-2	125.64	
SK-MEL-28	30.03	
SK-MEL-5	97.23	
UACC-257	110.58	
UACC-62	65.61	
Prostate Cancer		
DU-145	100.79	
PC-3	72.13	
CNS Cancer		
SF-268	92.62	
SF-295	50.45	
SF-539	97.97	
SNB-19	98.47	
SNB-75	73.27	
U251	93.22	
Mean	79.61	
Delta	69.94	
Range	118.28	

150   100   50   0   -50   -100   -150

Figure 3.21: One dose mean graph for $\Delta\Delta-[P_p]^{4+}$ (NSC 747950)

91

Panel/Cell Line	Growth Percent
Non-Small Cell Lung Cancer	
A549/ATCC	51.71
EKVX	67.85
HOP-92	59.72
NCI-H226	82.18
NCI-H23	26.97
NCI-H322M	28.12
NCI-H460	-31.50
NCI-H522	73.71
Colon Cancer	
COLO 205	12.97
HCC-2998	79.84
HCT-116	106.39
HCT-15	12.19
HT29	13.67
KM12	22.17
SW-620	4.47
Breast Cancer	
BT-549	-3.85
HS 578T	2.42
MCF7	29.00
MDA-MB-231/ATCC	66.59
MDA-MB-435	47.28
NCI/ADR-RES	144.70
T-47D	73.68
Ovarian Cancer	
IGROV1	56.74
OVCAR-3	20.23
OVCAR-4	62.79
OVCAR-5	-13.34
OVCAR-8	55.55
SK-OV-3	65.95
Leukemia	
CCRF-CEM	38.17
HL-60(TB)	49.34
K-562	19.00
MOLT-4	46.45
RPMI-8226	19.27
SR	10.52
Renal Cancer	
786-0	67.32
A498	28.01
ACHN	41.49
CAKI-1	25.27
RXF 393	83.96
SN12C	26.41
TK-10	60.41
UO-31	98.04
Melanoma	
LOX IMVI	7.97
MALME-3M	54.95
SK-MEL-2	110.92
SK-MEL-28	34.33
SK-MEL-5	46.36
UACC-257	106.48
UACC-62	38.51
Prostate Cancer	
DU-145	5.47
PC-3	43.93
CNS Cancer	
SF-268	40.39
SF-295	3.51
SF-539	2.58
SNB-19	30.80
SNB-75	6.74
U251	31.00
Mean	42.03
Delta	73.53
Range	176.20

Mean Growth Percent - Growth Percent

150   100   50   0   -50   -100   -150

Figure 3.22: One dose mean graph for $\Delta-[MP_p]^{2+}$ (NSC 747949)

92

3.7.2.1 One Dose Screen Results for $\Delta\Delta-[P_p]^{4+}$

A COMPARE analysis of the one screen data for $\Delta\Delta-[P_p]^{4+}$ was performed using the NCI database.

The results of this analysis are tabulated in Table 3.10 for all the three parameters GI_{50}, TGI and LC_{50} tabulated in one long table. Only compounds with a correlation coefficient of 0.2 or greater are listed and these are listed in order of the highest correlation to the least.

Table 3.10: DTP Compare All-Correlation results for one dose screen-complex $\Delta\Delta-[P_p]^{4+}$

Rank	Vector	Correlation	Mechanism of Action
1	3-deazauridine	0.517	Unknown
2	Fostriecin	0.483	Unknown
3	Methotrexate	0.48	RNA/DNA Antimetabolite
4	Rhizoxin	0.474	Antimitotic Agent
5	emofolin sodium	0.453	Unknown
6	Spirogermanium	0.442	Unknown
7	"N,N-dibenzyldaunomycin"	0.434	Topo II
8	Cyclopentenylcytosine	0.433	Unknown

Table 3.10- Continued

Rank	Vector	Correlation	Mechanism of Action
9	Trimetrexate	0.427	RNA/DNA Antimetabolite
10	DON	0.359	Unknown
11	Menogaril	0.356	Topo II
12	methyl-CCNU	0.352	Alkylating Agent
13	Maytansine	0.352	Antimitotic Agent
14	L-cysteine analogue	0.349	Unknown
15	Didemnin B	0.334	Unknown
16	m-AMSA (amsacrine)	0.332	Topo II
17	Cyclocytidine	0.322	DNA Antimetabolite
18	Homoharringtonine	0.206	Unknown

As can be seen from the data in Table 3.10, none of the correlations are high. This suggests either that a novel mechanism of activity and thus spectrum of activity is occurring or that the data set is weak or both. We suspect the latter as this is for a single dose screen. Of the compounds in which a correlation is observed and a mechanism of biological activity is known, we see no mechanism is predominant as shown in Table 3.10 which summarizes the number of times a

particular mechanism was correlated with the activity of $\Delta\Delta-[P_p]^{4+}$. The table

3.11 represents the results of 9 different drugs with known mechanisms of action.

Table 3.11: Predicted mechanism of action of $\Delta\Delta-[P_p]^{4+}$ based on one dose screen results

Alkylating agent	Topo I inhibitor	Topo II inhibitor	DNA/RNA anti-metabolite	DNA anti-metabolite	Antimitotic agent
1	0	3	2	1	2

Complex $\Delta\Delta-[P_p]^{4+}$ could not pass the one dose screen and so no data is

available for the five dose assay for this complex.

3.7.2.2 Five Dose Screen Results for $\Delta-[MP_p]^{2+}$

Complex $\Delta-[MP_p]^{2+}$ (NSC-747949) passed the minimum standards in the one

dose screen and was subjected to the more detailed 5-dose assay. The data for

the GI_{50}, TGI and LC_{50} are shown in Figure 3.23, 3.24, and 3.25 respectively.

Developmental Therapeutics Program Mean Graph
Selected Data Vectors

Prefix/Nsc: S747949 Endpoint:GI50 ExperimentIdAVGDATA logHiConc:-4.0

vectorId: 1265202
count expts: 1
count cell lines: 57
std dev: 0.596

Leukemia		
CCRF-CEM	-5.10	
HL-60(TB)	-4.79	
K-562	-5.21	
MOLT-4	-4.68	
RPMI-8226	-5.54	
SR	-8.00	
Non-SmallCellLung		
A549/ATCC	-5.46	
EKVX	-4.46	
HOP-62	-6.37	
NCI-H226	-4.71	
NCI-H23	-5.93	
NCI-H322M	-5.17	
NCI-H460	-5.59	
NCI-H522	-4.78	
Colon		
COLO205	-5.62	
HCC-2998	-6.40	
HCT-116	-5.50	
HCT-15	-5.54	
HT29	-5.34	
KM12	-5.26	
SW-620	-5.72	
CNS		
SF-268	-5.03	
SF-295	-5.67	
SF-539	-5.46	
SNB-19	-5.76	
SNB-75	-4.91	
U251	-5.48	
Melanoma		
LOXIMVI	-5.65	
MALME-3M	-4.85	
M14	-5.69	
SK-MEL-2	-4.30	
SK-MEL-28	-5.15	
SK-MEL-5	-5.01	
UACC-257	-4.54	
UACC-62	-5.42	
Ovarian		
IGROV1	-5.38	
OVCAR-3	-5.12	
OVCAR-4	-4.46	
OVCAR-5	-5.47	
OVCAR-8	-4.94	
SK-OV-3	-4.77	
Renal		
786-0	-4.81	
A498	-5.43	
ACHN	-5.45	
CAKI-1	-5.36	
RXF393	-5.51	
SN12C	-5.52	
TK-10	-4.91	
UO-31	-5.54	
Prostate		
DU-145	-5.52	
Breast		
MCF7	-5.71	
NCI/ADR-RES	-4.97	
MDA-MB-231/ATCC	-4.34	
HS578T	-5.51	
MDA-MB-435	-5.09	
BT-549	-5.57	
T-47D	-4.18	
summary		
MG_MID	-5.29	
Delta	1.11	
Range	3.82	

3 2 1 0 -1 -2 -3

Figure 3.23: Five dose all compare analysis of $\Delta-[MP_p]^{2+}$ (GI_{50})

96

Developmental Therapeutics Program Mean Graph
Selected Data Vectors

Prefix/Nsc: S747949 Endpoint:TGI ExperimentIdAVGDATA logHiConc:-4.0

vectorId: 1265203
count expts: 1
count cell lines: 57
std dev: 0.559

Leukemia
CCRF-CEM   -4.36
HL-60(TB)   -4.33
K-562   -4.42
MOLT-4   -4.05
RPMI-8226   -4.86
SR   -7.05
Non-SmallCellLung
A549/ATCC   -4.50
EKVX   -4.00
HOP-62   -5.54
NCI-H226   -4.08
NCI-H23   -4.57
NCI-H322M   -4.19
NCI-H460   -4.75
NCI-H522   -4.26
Colon
COLO205   -5.12
HCC-2998   -6.02
HCT-116   -4.69
HCT-15   -4.00
HT29   -4.00
KM12   -4.45
SW-620   -4.64
CNS
SF-268   -4.00
SF-295   -4.67
SF-539   -4.59
SNB-19   -4.00
SNB-75   -4.00
U251   -4.00
Melanoma
LOXIMVI   -4.81
MALME-3M   -4.16
M14   -5.19
SK-MEL-2   -4.00
SK-MEL-28   -4.23
SK-MEL-5   -4.59
UACC-257   -4.00
UACC-62   -4.00
Ovarian
IGROV1   -4.48
OVCAR-3   -4.37
OVCAR-4   -4.00
OVCAR-5   -4.64
OVCAR-8   -4.00
SK-OV-3   -4.00
Renal
786-0   -4.10
A498   -4.76
ACHN   -4.00
CAKI-1   -4.00
RXF393   -5.02
SN12C   -4.00
TK-10   -4.00
UO-31   -4.49
Prostate
DU-145   -4.68
Breast
MCF7   -4.00
NCI/ADR-RES   -4.30
MDA-MB-231/ATCC -4.00
HS578T   -4.03
MDA-MB-435   -4.26
BT-549   -4.75
T-47D   -4.00
summary
MG_MID   -4.42
Delta   0.42
Range   3.05

3   2   1   0   -1   -2   -3

Figure 3.24: Five dose all compare analysis of $\Delta-[MP_p]^{2+}$ (TGI)

97

Prefix/Nsc: S747949 Endpoint:LC50 ExperimentIdAVGDATA logHiConc:-4.0

vectorId: 1265204
count expts: 1
count cell lines: 57
std dev: 0.147

Leukemia	
CCRF-CEM	-4.00
HL-60(TB)	-4.00
K-562	-4.00
MOLT-4	-4.00
RPMI-8226	-4.00
SR	-4.00
Non-SmallCellLung	
A549/ATCC	-4.00
EKVX	-4.00
HOP-62	-4.00
NCI-H226	-4.00
NCI-H23	-4.00
NCI-H322M	-4.00
NCI-H460	-4.00
NCI-H522	-4.00
Colon	
COLO205	-4.00
HCC-2998	-5.09
HCT-116	-4.00
HCT-15	-4.00
HT29	-4.00
KM12	-4.00
SW-620	-4.00
CNS	
SF-268	-4.00
SF-295	-4.00
SF-539	-4.00
SNB-19	-4.00
SNB-75	-4.00
U251	-4.00
Melanoma	
LOXIMVI	-4.00
MALME-3M	-4.00
M14	-4.16
SK-MEL-2	-4.00
SK-MEL-28	-4.00
SK-MEL-5	-4.17
UACC-257	-4.00
UACC-62	-4.00
Ovarian	
IGROV1	-4.00
OVCAR-3	-4.00
OVCAR-4	-4.00
OVCAR-5	-4.00
OVCAR-8	-4.00
SK-OV-3	-4.00
Renal	
786-0	-4.00
A498	-4.00
ACHN	-4.00
CAKI-1	-4.00
RXF393	-4.00
SN12C	-4.00
TK-10	-4.00
UO-31	-4.00
Prostate	
DU-145	-4.00
Breast	
MCF7	-4.00
NCI/ADR-RES	-4.00
MDA-MB-231/ATCC	-4.00
HS578T	-4.00
MDA-MB-435	-4.00
BT-549	-4.00
T-47D	-4.00
summary	
MG_MID	-4.02
Delta	0.02
Range	1.09

3 2 1 0 -1 -2 -3

Figure 3.25: Five dose all compare analysis of $\Delta-[MP_p]^{2+}$ (LC_{50})

98

A COMPARE analysis using the all compare data set was carried out for

NSC-747949 using the 5-dose assay data and the results summarized in Table

3.12.

Table 3.12: DTP Compare All-Correlation results for five dose screen-complex $\Delta-[MP_p]^{2+}$

Rank	Vector	Correlation	Mechanism of Action
1	Paclitaxel (Taxol)	0.909	Antimitotic Agent
2	Pyrazofurin	0.666	RNA/DNA Antimetabolite
3	Bruceantin	0.63	Unknown
4	didemnin B	0.616	Unknown
5	Cyclodisone	0.616	Alkylating Agent
6	flavoneacetic acid	0.588	Unknown
7	2'-deoxycoformycin	0.579	Unknown
8	Piperazine alkylator	0.57	Alkylating Agent
9	vincristine sulfate	0.553	Antimitotic Agent
10	5-FUDR	0.532	DNA Antimetabolite
11	5-fluorouracil	0.529	RNA/DNA Antimetabolite
12	Pyrazine diazohydroxide	0.527	Unknown

Table 3.12- Continued

Rank	Vector	Correlation	Mechanism of Action
13	mitomycin C	0.52	Alkylating Agent
14	Ftoafur	0.518	RNA/DNA Antimetabolite
15	"N,N-dibenzyldaunomycin"	0.515	Topo II
16	Porfiromycin	0.505	Alkylating Agent
17	CCNU	0.502	Alkylating Agent
18	Echinomycin	0.487	Antimitotic Agent
19	Cisplatin	0.473	Alkylating Agent
20	Phyllanthoside	0.469	Unknown
21	Chlorambucil	0.432	Alkylating Agent
22	Thio-tepa	0.431	Alkylating Agent
23	Tetraplatin	0.42	Alkylating Agent
24	Thioguanine	0.413	DNA Antimetabolite
25	Pancratiastatin	0.405	Unknown
26	Chlorozotocin	0.395	Alkylating Agent

The combined data for predicting the mechanism category of $\Delta-[MP_p]^{2+}$ is given in Table 3.13 which represents the results of 19 different drugs.

Table 3.13: Predicted mechanism of action of $\Delta-[MP_p]^{2+}$ based on five dose screen results

Alkylating agent	Topo I inhibitor	Topo II inhibitor	DNA/RNA anti-metabolite	DNA anti-metabolite	Antimitotic agent
10	0	1	3	2	3

3.8 Conclusions

Based on the COMPARE results $\Delta-[MP_p]^{2+}$ is likely to be acting as an alkylating agent. As discussed before in the earlier section, by definition, alkylating agents are compounds which result in the alkylation of DNA phosphate or base moiety, such and mustard agents. However as a mechanism of action, a number of other non-alkylating agents are classified as alkylating agents. For example, cisplatin form adducts with guanine bases in DNA resulting in a DNA modification which behaves, to some extent, as if the DNA was alkylated.

Therefore, while $\Delta-[MP_p]^{2+}$ has no obvious mechanism by which alkyl transfer would occur, it is possible that the complex forms covalent adducts with DNA that cause the mechanism of drug action to mimic alkylation to some extent.

CHAPTER 4

PHARMACOLOGY AND TOXICOLOGY OF RUTHENIUM(II)

POLYPYRIDYL COMPLEXES

4.1 Introduction

Medical oncologists prescribe and administer those drugs with the narrowest therapeutic index in all of medicine. Thus, understanding variability in toxicity and response is of utmost importance. Such variability can be divided into two components: pharmacokinetics and pharmacodynamics.

Pharmacokinetics, the relationship between time and plasma concentration, is concerned with understanding issues such as metabolism and excretion. It can be simply described as what the body does to the drug.

The clinical interpretation of pharmacokinetic results requires another set of information, the relationship between plasma concentrations (or dose) and effect, or pharmacodynamics. This can be described as what the drug does to the body.[140]

In phase I clinical trials, the primary pharmacological objective is to define pharmacokinetics to optimize scheduling and dosing for subsequent studies. Phase II trials offer a different opportunity, as all patients are generally treated at

the same dose. Thus, variability in toxicity or response may potentially be related to variability in pharmacokinetics.[141]

4.2 Why are Pharmacokinetic and Pharmacodynamic Studies Important?

By understanding the pharmacokinetic and pharmacodynamic principles of drug action, one can optimize dosing of these often highly toxic agents for optimal therapeutic effect. The dose modifications comprise of the following major factors:

1)   Dose modification for toxicity

Reducing the drug dosage is a common practice for excessive toxicity of clinically important agents. However, the toxicity response may differ from one patient to another, hence parameters such as age, diet, genetics are important while treatment.

2)   Dose modification for impaired clearance

Normally prior to treatment it is important to consider hepatic and renal functions. Dose modifications or reductions are then quite useful for the drug to avoid accumulation resulting in organ toxicity.

3)   Dose modification for altered pharmacodynamics

Heavily pre-treated patients have a lower chance of response which is due to altered pharmacodynamics; increased sensitivity or tumor resistance. Thus achieving response is very difficult since patient's tolerance is less while tumor's tolerance has increased.

4)   Dose modification for adaptive control of chemotherapy

Dosing of drugs with a relatively narrow therapeutic index (TI), is carefully

monitored and controlled. Cytotoxic therapy normally has a narrow therapeutic

index, and is often given as a combination treatment.

4.3 Metal Based Complexes as Drugs

Compounds containing heavy metals have long been considered poor

candidates for drugs because of the toxicity generally associated with the metal.

That said many early treatments involved the use of heavy-metal based

compounds. For example, arsenic and mercury based compounds use to be

common treatments for syphilis. There are many other areas where metal

compounds continue to make significant contributions to medical treatment.

Examples include the use of cisplatin for cancer therapy, gold compounds for

treatment of rheumatoid arthritis, silver compounds for wound healing,

radioactive technetium compounds for imaging, among others.[142]

Many metals and metal compounds are known to be acutely toxic at low

doses, e.g. mercury compounds. Long term toxicity commonly arises due to

accumulation over time as in the case of osteomalaca in which aluminium(III) is

accumulated by patients with end stage renal disease.

Many of the modern MRI contrast agents use metal ions, such as Gd^{3+},

that are tightly held by multidentate chelate ligands to prevent their escaping in to

the body as free metal ions. In this case the use of the strongly chelating ligand

results in a compound which is useful and non-toxic even though the free metal ion is toxic.

Four Gd(III) complexes (Magnevist, Dotarem, Omniscan and Prohance) have been approved for clinical use and are widely used in the detection of the abnormalities of the blood-brain barrier.[144] ^{99m}Tc-based radiopharmaceutical and several other radionuclides are currently used in clinical diagnosis. Ceretec is an approved cerebral perfusion imaging agent for evaluation of stroke. Another analog Cardiolite is used for myocardial perfusion imaging.[145] Silver and its compounds are long used as antimicrobial agents in medicine. Silver sulfadiazine is used clinically as an anti-microbial and anti-fungal agent.[144]

Two antimony(V) based drugs N-methylglucamine antimonite (Glucantime) and sodium stibogluconate (Pentostam) are used clinically for the treatment of leishmaniasis, a disease caused by intracellular parasites.[144] The iron chelator desferrioxamine is clinically approved for the treatment of malaria. The low-spin Fe(II) complex sodium nitroprusside is the only clinically used metal-nitrosyl complex and is used to lower blood pressure in humans.[144]

The Bleomycins are a group of glycopeptides antibiotics which posses anti-tumor activity against several types of tumors.[2] The cytotoxicity of BLM is believed to result from its ability to bind Fe, activate oxygen and cleave DNA.[146] Apart from cisplatin, one other metal-based complex titanocenedichloride which has shown activity for gastrointestinal and breast carcinomas is in phase II clinical trials. Gold(I) anticancer drugs are also known which target mitochondria

105

and hence results in cell death.[144] Gold(III) porphyrins studied by Che et. al. exhibit potent in-vitro and in-vivo anti-cancer activity towards hepatocellular and nasopharyngeal carcinoma.

While we can design many anti-cancer drugs which may have significant efficacy in terms of in vitro cytotoxicity, questions regarding the toxicity and ability to selectively target cancer cells in vivo are critical for true clinical efficacy. The ability to mediate tumor growth lies in administering the right doses over the right intervals of time. In this chapter, we establish the maximum tolerable dosage of several of our ruthenium-based complexes and examine some of the more promising ones for their ability to inhibit tumor progression in live mice.

4.4 Toxicity of Some Well Known Anti-Cancer Drugs

One of the most commonly used anti-cancer drug is doxorubicin which is an anthracycline widely used in the treatment of breast and ovarian cancer[147]. Doxorubicin has problems related to a dose-limiting toxicity leading to myelosuppression and cardiomyopathy.   A lifetime dose of 550 mg/m^2 is recommended for doxorubicin as further treatment can lead to congestive heart failure.[148] Many formulations like Myocet and Doxil have since been introduced to minimize doxorubicin toxicity.[149] The cytotoxicity of doxorubicin is not cycle-dependent and the maximum dosage that can be administered to patients is between 9 mg/Kg-18 mg/Kg.[150]

The anti-tumor activity of cisplatin is ascribed to reaction of the platinum complex with nucleophilic sites on the DNA. The major adduct is an intra-strand cross links formed by the binding of cisplatin to two neighboring guanines.[151] The clinical use of cisplatin is restricted due to the emergence of intrinsic and acquired resistance and severe side effects such as nephrotoxicity and neurotoxicity.[152] Research has focused on increasing the efficacy of the drug and reducing its toxicity. One way is encapsulating the drug in long circulating liposomes. One of the formulation of this type is SPI-077 in which cisplatin is encapsulated in Stealth liposomes.[153-156] Another way is encapsulating cisplatin in polymeric micelles.

4.5 Toxicity of Ruthenium Based Complexes

A number of ruthenium-based compounds have been evaluated for potential use as anti-tumor drugs. Ruthenium(III)-ammine complexes[157] and ruthenium red ($[(NH_3)_5Ru\text{-}O\text{-}Ru(NH_3)_4\text{-}O\text{-}Ru(NH_3)_5]Cl_6$)[158] are active against a number of tumors, however for this class of compounds the therapeutic doses were relatively close to the toxic dose. Complexes such as [trans-$RuCl_4(ImH)_2]ImH$[159,160] and NAMI[161,162] are promising drug candidates but some toxic side-effects were discovered in the phase I clinical studies for NAMI including phlebitis, hypersensitivity reactions and blister formation. Gastrointestinal toxicity was also observed at significantly higher doses.[163]

Dwyer and coworkers were the first to examine the toxicity of simple ruthenium polypyridyl complexes such as $[Ru_b]^{2+}$ and $[Ru_p]^{2+}$.[8] Both complexes were found to be acutely toxic at relatively low doses. Both the symptoms observed during death (seizures) and the demonstrated inhibitory activity against acetylcholinesterase in vitro[9] suggest that these complexes are potent neurotoxins. Using radiolabeled $[^{106}Ru(phen)_3]^{2+}$, Dwyer and coworkers were also able to show that the complex does not accumulate in any organs or tissue and the majority of the complex is excreted in the urine. Furthermore, the complex isolated from the urine was intact indicating that it is not metabolized by mammalian tissues (mice). This result shows the biological activity of the complex is due to the complex cation as a whole and not some metabolized derivative. When the two enantiomers were studies for toxicity in mice, it was found that the $\square-$ enantiomer is more toxic than the $\Delta-$ enantiomer which appears to be related to the faster absorbance of the $\Lambda-$ enantiomer into the blood stream.[10]

The selective cytotoxicity of $[MP_p]^{2+}$ and $[P_p]^{4+}$ towards cancer cell lines obviously suggests potential as anti-tumor agents, however if the toxicity of these complexes is similar to that reported for $[Ru_b]^{2+}$ and $[Ru_p]^{2+}$ their utility as drugs may be severely limited. In this chapter, we performed a structure-toxicity study of our ruthenium polypyridyl complexes in mice. In this study, we examined the effect of the following factors on the animal toxicity of this class of ruthenium(II) compounds: nuclearity (monomers vs. dimers), ligands (bpy, phen, tpphz, and

tatpp) and stereochemistry. Toxicity was examined by single dose i.p. injections of the various complexes, as the chloride salt, in a buffer solution. Toxicity was determined by survival for 24 hours and no significant morbidity on the animal and is reported as the maximum tolerable dose at which the mouse survived. All the experiments were done in triplicate.

In three cases, $[Ru_p]^{2+}$, $[Z_p]^{4+}$ and $[P_p]^{4+}$ the complexes biodistribution was determined by injecting the animals with the complexes at ½ the MTD and then sacrificing them at time intervals of 5 min (0 hr data), 24h and 48 h. Various organs including the brain, heart, kidney, liver, lungs, spleen and intestine were collected by dissection and analyzed for ruthenium content by flameless atomic absorption spectroscopy. The results are discussed herein.

4.6 Materials and Methods

4.6.1 Animal Studies

Animal studies were carried out according to the protocol approved by the Institutional Animal Care and Use Committee. C57 BL/6 mice were obtained from Harlan (Indianapolis, Indiana).

4.6.2 Biodistribution Studies

Ruthenium concentration was determined by Atomic Absorption Spectroscopy using a Varian SpectrAA-300 instrumentation, supplied with graphite furnace mod GTA-96, an autosampler mod PSD-96 and a specific ruthenium emission

lamp (Hollow cathode lamp). A standard curve for ruthenium concentration was determined using a custom grade ruthenium standard of 998 µg/mL in 3.3% HCl (Inorganic Ventures Inc., Christiansburg, VA) as a stock solution.

The following procedure for the preparation of the tissue samples for ruthenium analysis was used here:

1. A fragment of each wet organ was taken and carefully weighed. This was put in a cryovial and heated at 105^oC until completely dried. Mass measurements were taken periodically until no change is mass was observed between measurements.

2. The dried tissue sample was then digested by addition of 0.5 ml of 25% tetramethylammonium hydroxide and then completely dissolved in the same closed cryovial by the addition of water. The solution should be clear and no heating was required to dissolve the samples.

3. Once the sample is completely digested, the total solution volume was adjusted to 1.0 mL using Millipore water.

4. The ruthenium content was determined by atomic AAS as follows: 10 µL aliquots of the sample solutions were introduced into the graphite furnace and atomized at a temperature of 2500^0C. The furnace was continuously purged with argon gas at a flow rate of 3.0 L min^{-1} and the atomized sample analyzed at a wavelength of 349.9 nm. Ruthenium concentration was determined by comparison of the absorbance reading with that on the standard curve.

4.7 Results and Discussion:

4.7.1 Toxicity and Maximum Tolerable Dose Studies

4.7.1.1 Acute Toxicity Studies

An initial toxicity screen was performed for the Ru(II) compounds by intraperitoneal injection to a single mouse (C57BL/6NTac mice, ~ 30 g) with 0.2 mg of the ruthenium complex in 200 µL Tris buffer, pH 7.5. This dose corresponds to about 6 mg complex per kilogram of mouse body weight. The outcome of this experiment as judged by the survival or death of the animal after 24 hr. The data are tabulated in Table 4.1

Table 4.1: Animal survival after intraperitoneal injection of 6 mg/Kg of a Ru(II) polypyridyl complex

Compound	Result for 1 mg/mL dose (6 mg/Kg)
$[Ru_p]^{2+}$	Survived
$[Ru_b]^{2+}$	Survived
$[Z_p]^{4+}$	Died
$[Z_b]^{4+}$	Died
$[MP_p]^{2+}$	Survived
$[MP_b]^{2+}$	Survived
$[P_p]^{4+}$	Survived
$[P_b]^{4+}$	Survived

At this dose, only the complexes containing the tpphz ligand were lethal. In this case, the toxicity was acute with the animals observed to have seizures and die within 5 minutes of the injection.

4.7.1.2 Maximum Tolerable Dose

The maximum tolerable dose (MTD) for the compounds was determined in the following manner. At 10 weeks of age, the mice were randomly allocated into treatment groups (3 per group). Stock solutions of ruthenium complexes were prepared. After intraperitoneal doses of 100 μL, animals were observed and animal appearing moribund, if any, were sacrificed. Drug concentrations examined were 50 mg/mL, 25 mg/mL, 10 mg/mL, 5 mg/mL, 2.5 mg/mL and 1 mg/mL. At first a single mouse was treated with a single dose of the drug complex and observed. If the mouse died in short order, this dosage was considered lethal and the next smaller dosage was examined. If the mouse survived, then two additional mice were injected and the group monitored. This assay was performed for the racemates of the monometallic complexes $[Ru_p]^{2+}$, $[Ru_b]^{2+}$, $[MP_p]^{2+}$ and $[MP_b]^{2+}$ and the diastereomeric mixtures of $[Z_p]^{4+}$, $[Z_b]^{4+}$, $[P_p]^{4+}$ and $[P_b]^{4+}$. The MTD's for all these complexes are shown graphically in Figure 4.1.
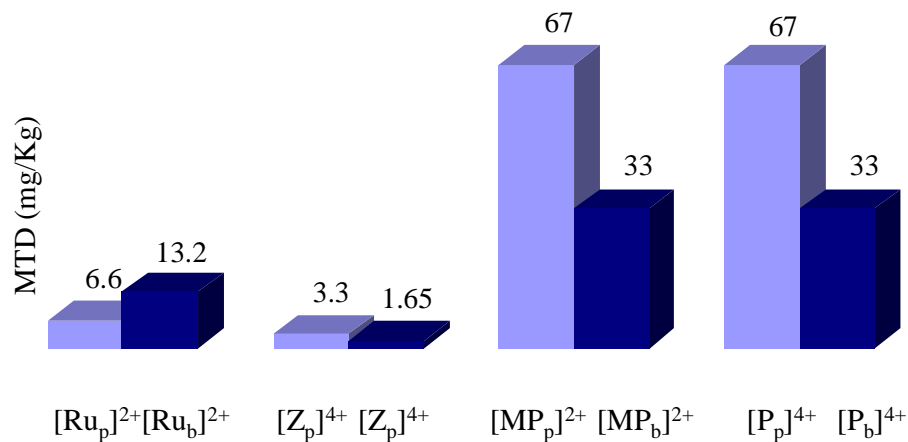
Figure 4.1: Maximum tolerable dose (mg/Kg) for rac/mix- Ru(II) complexes

From the Figure 4.1 we see that there is a clear difference in the tolerance dose with phenanthroline and bipyridyl analogs with the phenanthroline analogs having higher MTD than bipyridyl except in case of $[Ru_b]^{2+}$. Ru(II) complexes with longer bridging ligand, tatpp are tolerated 20 fold better than if the length of bridging ligand is short i.e. for tpphz. Also we see there is no difference in the toxicity for structures containing two ruthenium centers over those with one. The data clearly supports the evidence as was seen with cytotoxicity and hence the types of ligands surrounding the metal center are a key factor in determining the toxicity of the complex.

Our next objective was to examine the effect of chirality and hence we took two lead compounds one $[Ru_p]^{2+}$ as a control and the other complex $[P_p]^{4+}$ as the test compound.
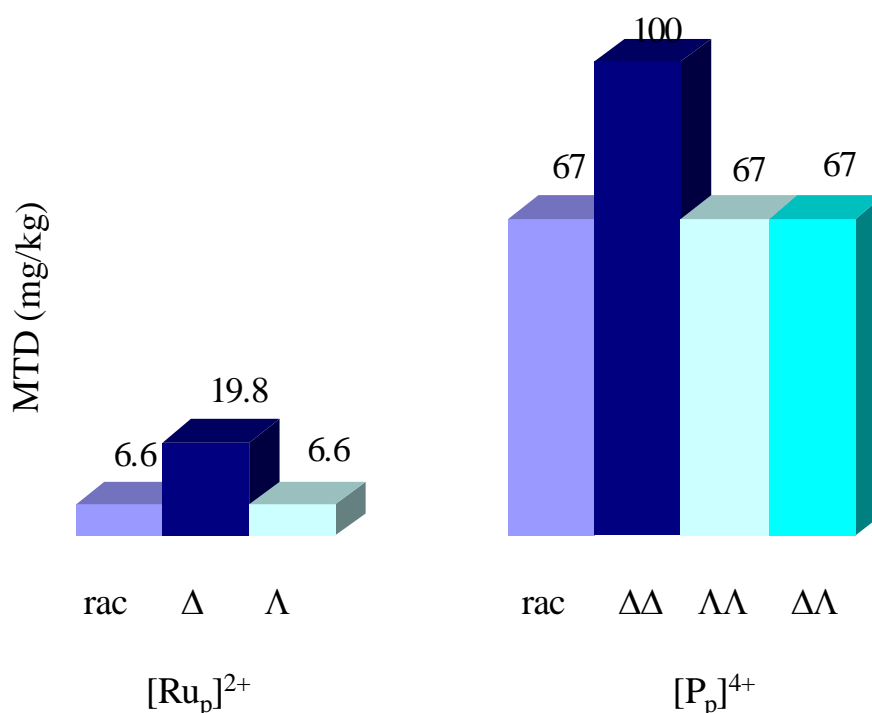
Figure 4.2: Maximum tolerable dose (mg/Kg) for chiral Ru(II) complexes

From Figure 4.2 we see that though we found a three fold increase in MTD value with $\Box-[Ru_p]^{2+}$ as compared to rac or $\tilde{\Box}$ analog. The difference was also there in $[P_p]^{4+}$ but was less profound with $\Delta\Delta-$ showing a slight higher MTD of 100 mg/Kg than the rest of the complexes under investigation, establishing that both metal centers need to be $\Delta-$ to get the difference.

4.8 Biodistribution of Ruthenium Polypyridyl Complexes

Dwyer et. al. described chromatographic experiments to study the metabolic fate of the complex $[Ru_p]^{2+}$. Mice were injected intraperitoneally about 400 μL of $\Delta-$ or $\Lambda-$ form of the radiolabelled ^{106}Ru complex at the concentration of 0.25 mg/mL. Chromatograms were used to examine the nature of complexes excreted in urine. Samples were collected for upto 24 hours and the ruthenium complexes were identified by their yellow color in the chromatogram. From these experiments it was known that the complex is not metabolized by the mammalian tissues of mice and rats. It was thus suggested that any biological activity is due to complex cation as a whole. The complex was mainly excreted in the urine and no trace of the complex was found in the nervous system. Radioactivity experiments also revealed that accumulation occurred appreciably in kidney and liver and the amounts found in other tissues were below that in blood[10].

Fate of the antimetastatic ruthenium complex ImH [trans-RuCl$_4$(DMSO)Im] was determined after acute i.v. treatment in mice by atomic absorption spectrometry. It was found that ruthenium concentration was maximum after about 10 minutes of i.v. treatment and was about 0.35 μg/mg wet weight of tissue higher in kidney as compared to 0.15 μg/mg for liver, accounting for approximately 13% and 5% of the administered dose. No ruthenium content was detected in the brain. Also ruthenium concentration in blood fell rapidly within 10 minutes after i.v. injection.

For biodistribution experiments by atomic absorption spectrometry, a fragment of each wet organ was taken, dried at 105°C and carefully weighed, this was followed by digestion with 25% tetrabutyl ammonium hydroxide. Ruthenium was then measured in 10 µL samples and the dissolved samples were analyzed for Ru content using a graphite furnace and ruthenium emission lamp at 379.9 nm.

Two animals were autopsied after administration of the dose which corresponded to one dose lower than their MTD, so 3.3 mg/Kg for rac–$[Ru_p]^{2+}$, 1.65mg/Kg for mix–$[Z_p]^{4+}$ and 33.3 mg/Kg for mix–$[P_p]^{4+}$. The organs collected for the study were: liver, lungs, spleen, intestine, kidneys, heart and brain.

Before daily analysis, a five point calibration curve was performed by Ruthenium Custom-Grade Standard 998 µg ml^{-1} in 3.3 % HCl. (Figure 4.3)

$$y = 0.0027x$$
$$R^2 = 0.9915$$

Legend:
- ♦ 379.9nm
- ■ 392.6 nm
- —— Linear (379.9nm)
- —— Linear (392.6 nm)
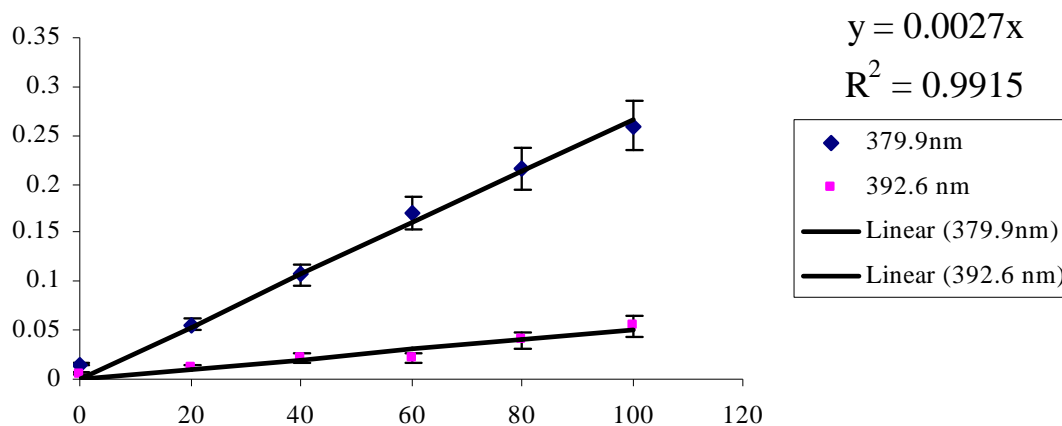
Figure 4.3: Standard curve for determining ruthenium content performed by ruthenium custom-grade standard 998 µg ml^{-1} in 3.3% HCl

4.8.1 Biodistribution of rac–[Ru$_p$]$^{2+}$
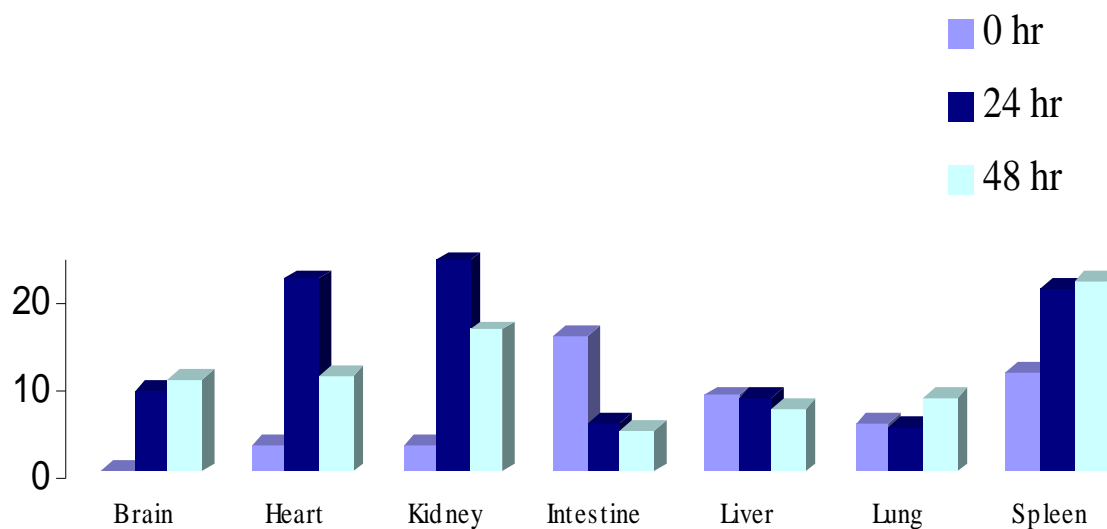
Figure 4.4: Biodistribution of [Ru$_p$]$^{2+}$ after 0, 24 and 48 hours of administration

From Figure 4.4 we see that [Ru$_p$]$^{2+}$ is mainly accumulated in kidney as compared to any other tissue. After the i.p. injection only ~10% of the [Ru$_p$]$^{2+}$ is recovered in the tissues of mice within 24 hr or 48 hr. We speculate the rest 90% of the ruthenium complex may be either excreted in the urine as evident by radiolabelling experiments done by Dwyer et al or they may be in blood.

4.8.2 Biodistribution of mix–[Z$_p$]$^{4+}$
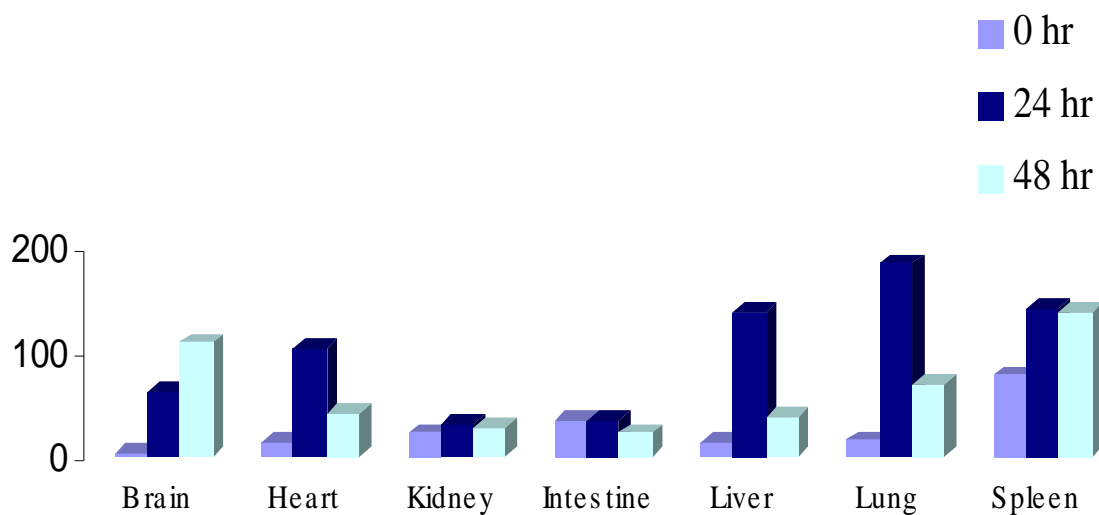
Figure 4.5: Biodistribution of [Z$_p$]$^{4+}$ after 0, 24 and 48 hours of administration

From Figure 4.5 we see that rac–[Z$_p$]$^{4+}$ is accumulated in liver and lung which may account for its higher toxicity, there is no appreciable accumulation of [P$_p$]$^{4+}$ in any organ. We see about 70% accumulations occurring for [Z$_p$]$^{4+}$ within 24 hours of drug administration which drops to 45% in 48 hours.

4.8.3 Biodistribution of mix−$[P_p]^{4+}$
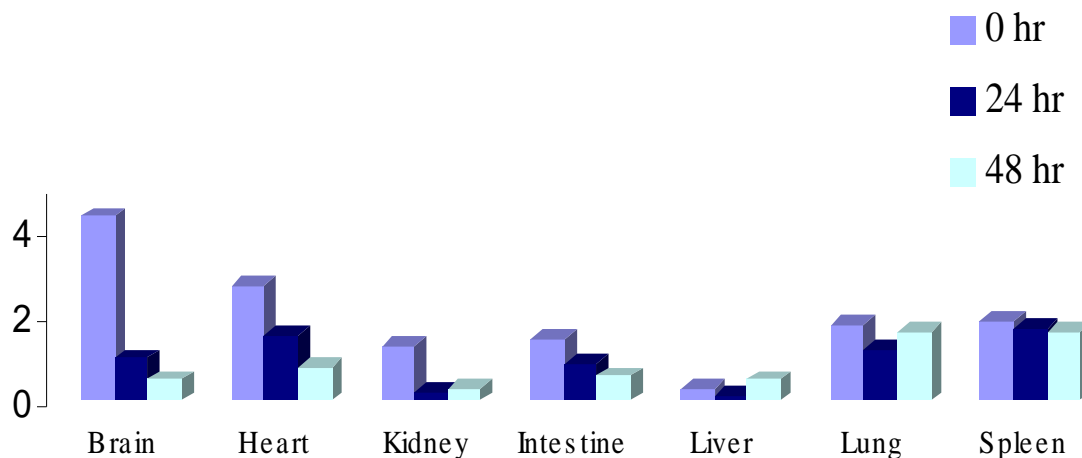
Figure 4.6: Biodistribution of $[P_p]^{4+}$ after 0, 24 and 48 hours of administration

From Figure 4.6 we see that $[P_p]^{4+}$ is not accumulated in any organ even after 48 hours. We see only 1% accumulation for $[P_p]^{4+}$ as compared to about 70% accumulation occurring for $[Z_p]^{4+}$ and 9% occurring for $[Ru_p]^{2+}$ within 24 hours of drug administration. One more observation was that surprisingly amount found in brain is higher than any other organ minutes after administration.

4.9 Conclusions

As we discussed in earlier portion of the chapter the ruthenium complexes with the longer bridging ligand, tatpp were well tolerated in mice as compared to shorter bridging ligands, tpphz, phen or bpy. Lastly, another important

experimental observation can be concluded if we compare the biodistribution of the Ru(II) complexes with time. (Table 4.2)

Table 4.2: Accumulation of Ru(II) complexes after 24 hours

24 hour	Accumulation (µg/mg) of tissue		
	rac–$[Ru_p]^{2+}$	mix– $[Z_p]^{4+}$	mix– $[P_p]^{4+}$
Brain	9.37	61.18	1.01
Heart	22.06	102.70	1.53
Kidney	24.14	28.77	0.20
Intestine	5.61	32.82	0.89
Liver	8.54	134.91	0.15
Lung	5.35	182.43	1.22
Spleen	20.97	139.78	1.73
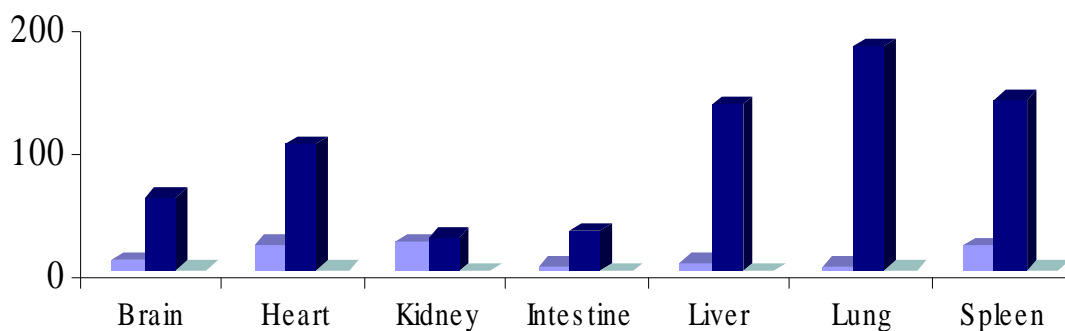
Figure 4.7: Fate of Ru(II) complexes after 24 hours of drug administration

Figure 4.7 represents the distribution in graphical format for comparison. After 24 hours we see accumulation of $[Ru_p]^{2+}$ in heart and kidney while for the complex $[Z_p]^{4+}$ the accumulation is in liver and lung. After 48 hours we do see decrease in Ruthenium content in tissues but complex $[Z_p]^{4+}$ starts accumulation in brain which may account for its unreasonably high toxicity. As we did not find any detectable amount of complex $[P_p]^{4+}$ we speculate it to be found more in blood and excreted in urine within this time course of experiment.

CHAPTER 5

TUMOR REGRESSION OF MOUSE MELANOMA AND LUNG CANCER XENOGRAFTS BY RUTHENIUM(II) POLYPYRIDYL COMPLEXES

5.1 Introduction

Delivery of cytotoxic chemotherapeutic agents in the treatment of human cancer is often accompanied by acute and cumulative toxicities to normal tissues that limit the dose and duration of treatment. Cisplatin is one of the most effective anti-cancer drugs, but its severe toxic effects, including depletion of immune-competent cells, limits its efficacy.[164]

In this chapter, we examine the in vivo anti-tumor activity of two promising ruthenium polypyridyl complexes, $\Delta\Delta-[P_p]^{4+}$ and $\Delta-[MP_p]^{2+}$, using two mouse models. One model uses the highly tumorigenic and poorly immunogenic murine B16 mouse melanoma cell line that originated in the syngeneic C57BL/6 mouse stain model. These model systems are well-established models for the study of experimental cancer therapies.[165-167] The other model examines the anti-tumor activity of these complexes on human cancers, specifically non small cell lung cancer, H358, developed as xenograft tumors in nude mice. Nude mice have severe combined immune deficiency (SCID) which allows human tumors to be established and studied in mice.[168-171]

122

5.2 IACUC Protocol

The tumor regression studies were necessary for development of the ruthenium polypyridyl complexes as potential anti-cancer drugs. All the studies were conducted in accordance with the Institutional Animal Care and Use Committee, IACUC protocol # A08.018- Ruthenium polypyridyl complexes as potential anti-cancer drugs.

The cell lines were grown in culture and harvested cells were injected subcutaneously into bilateral flanks of mice. The tumors were allowed to grow ~10 mm^3. The ruthenium polypyridyl complexes were then injected subcutaneously at a site away from the subcutaneous tumor. Injections were performed using a dose strategy which was different for syngeneic and xenograft model. Tumor growths were monitored by calipers. The experiments lasted 30 days for syngeneic model and 60 days for xenograft model. The remaining animals left after study were sacrificed by cervical dislocation after CO_2 asphyxiation, and death was ensured by opening the thorax. Animals were routinely monitored on a daily basis for signs of tumor growth and during the study if there occurred signs of distress or moribund nature, the animals were sacrificed. The experimental endpoints included tumor size and survival. Comparisons were then made between the experimental and control groups by drawing tumor growth curves. Tumor weights were also determined and compared between control and treated groups.

5.3 Materials and Methods

5.3.1 Reagents

RPMI-1640 and DMEM medium, PBS, penicillin/streptomycin solution (P/S), fetal bovine serum (FBS), trypsin-EDTA and trypan blue were purchased from Life Sciences Technologies, Inc., Grand Island, NY. DMSO and 3-(4,5-dimethylthiazol-2-yl)-2,5-diphenyltetrazolium bromide (MTT) were obtained from Sigma.

5.3.2 Cell Lines and Cultures

The cell lines non-small cell lung cancer NSCLC-H358 (bronchioalveolar) and B-16 mouse melanoma were kindly donated by Dr. Sanjay Awasthi.

The NSCLC cells were cultured in RPMI 1640 medium supplemented with 10% (v/v) heat-inactivated Fetal Bovine Serum (FBS), 1% (v/v) Penicillin/Streptomycin solution (P/S), 2 mmol/L L-glutamine, 10 mmol/L HEPES, 1 mmol/L sodium pyruvate, 4.5 g/L glucose, and 1.5 g/L sodium bicarbonate and the B16 cells were cultured in DMEM medium supplemented with 10% (v/v) FBS and 1% (v/v) P/S solution. All the cells were cultured at 37℃ in a humidified atmosphere of 5% CO_2.

5.3.3 Animal Model: Syngeneic Mouse Melanoma Model

C57 BL/6 mice were obtained from Harlan (Indianapolis, Indiana) and were kept at the animal care facility, University of Texas at Arlington, Arlington, TX.

Fourteen week old mice were divided into 3 groups of three animals (treated with PBS, Δ–$[MP_p]^{2+}$ and $\Delta\Delta$–$[P_p]^{4+}$). All animals were injected with 1 X 10^6 B16 mouse melanoma cell suspensions in 100µL of PBS subcutaneously. Animals were examined daily for signs of tumor growth and treatments were administered after 14 days of developing the tumors ($\sim$ 10 mm^2). Tumors were measured in two dimensions using vernier calipers.

5.3.4 Animal Model: Xenograft Lung Cancer Model

Hsd: athymic nude nu/nu mice were obtained from Harlan (Indianapolis, Indiana) and were kept at the animal care facility of University of North Texas Health Science Center at Fort Worth, Fort Worth, TX.

Fourteen week old mice were divided into 3 groups of three animals (treated with PBS, Δ–$[MP_p]^{2+}$ and $\Delta\Delta$–$[P_p]^{4+}$). All animals were injected with 1 X 10^6 NSCLC H358 human lung cancer cell suspensions in 100 µL of PBS subcutaneously. Animals were examined daily for signs of tumor growth and treatment was administered after 14 days of developing the tumors ($\sim$ 10 mm^2). Tumors were measured in two dimensions using vernier calipers.

5.4 Results and Discussion

5.4.1 Antineoplastic Effects of Ruthenium (II) Polypyridyl Complexes-Syngeneic Mouse Melanoma Model

The complexes' antitumor activities were investigated using an orthotopic syngeneic mouse melanoma model. C57BL/6 mice were used in these

experiments according to a protocol approved by the Institutional Animal Care and Use Committee. A total of nine 14 week-old male mice were divided into three groups of three each:

Group 1: Control Group

Group 2: Mice treated with $\Delta-[MP_p]^{2+}$

Group 3: Mice treated with $\Delta\Delta-[P_p]^{4+}$

All animals were injected with 1 million B16 mouse melanoma cell suspensions in 100 µL of PBS, subcutaneously in the rear thigh and were examined daily for signs of tumor growth. Treatment was administered when the tumor surface area exceeded 10 mm^2 as measured in two dimensions using calipers. It typically took 14 days for the tumors to reach this size.

At this time, each mouse was injected intraperitoneally with 1.0 mg complex $\Delta-[MP_p]^{2+}$ (Group 2) or $\Delta\Delta-[P_p]^{4+}$ (Group 3) dissolved in 200 µL Tris buffer, which corresponds to ~33 mg drug complex per Kg mouse body weight or approximately one-half the observed MTD. The control group 1 was injected with Tris buffer alone. This time was considered Day 0, coinciding with the initial drug treatment.

Thereafter, groups 2 and 3 were administered an additional 1.0 mg of the drug complexes on days 3, 10, 14, 21 and 24 for a total of 6 doses (6 mg total drug administered). Similarly, the control group was given 200 µL injections of the carrier solutions on these days also. Every other day mice were weighed and tumor dimensions were recorded with calipers. Deaths were also recorded.

126

Dose and day of dosage are shown in Table 5.1

Table 5.1: Day dose administered for syngeneic mouse melanoma model

Day	Control	$\Delta-[MP_p]^{2+}$	$\Delta\Delta-[P_p]^{4+}$
0	0 mg (n=3)	1 mg (n=3)	1 mg (n=3)
3	0 mg (n=3)	1 mg (n=3)	1 mg (n=3)
10	0 mg (n=3)	1 mg (n=3)	1 mg (n=3)
14	0 mg (n=3)	1 mg (n=3)	1 mg (n=3)
21	0 mg (n=2)	1 mg (n=3)	1 mg (n=3)
24	All animals died	1 mg (n=2)	1 mg (n=2)
Total dose as of day 31	0 mg	6 mg	6 mg

The results of this anti-tumor study are summarized by three factors: tumor volume, animal survival and animal average body weight.

Change in Tumor Volume after injecting B-16 mouse melanoma cells
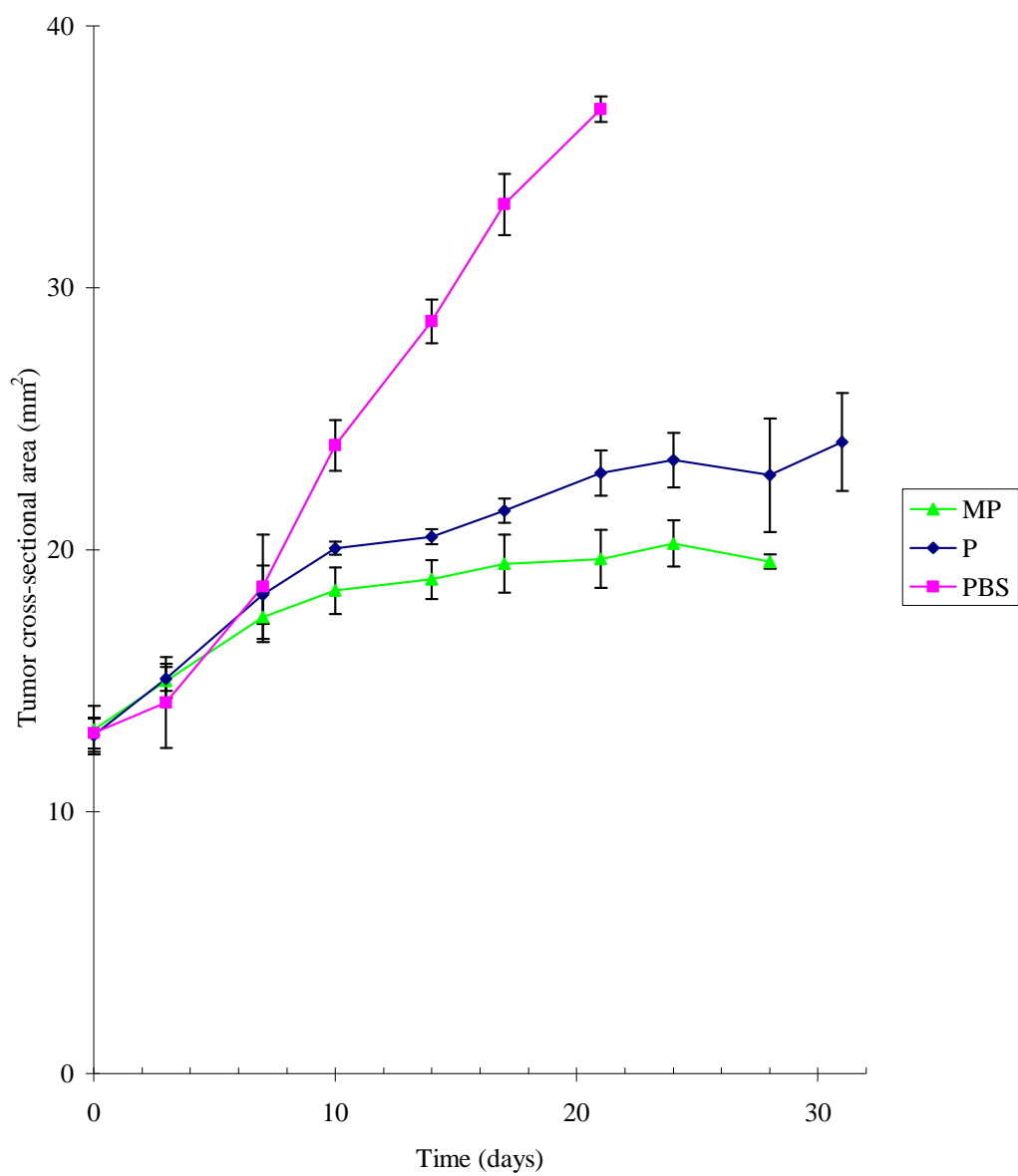
Figure 5.1: Change in B-16 melanoma tumor volume after treatment with
ruthenium-tatpp complexes.

Squares represent the mean tumor volume for Group 1 (control); triangles for Group 2
($\Delta- [MP_p]^{2+}$); and diamonds for Group 3 ($\Delta\Delta-[P_p]^{4+}$)

The tumor volume data is shown graphically in Figure 5.1. Importantly, both of the treated groups (2 and 3) show significantly lees tumor growth relative to the control (Group 1). This data shows that both $\Delta-[MP_p]^{2+}$ and $\Delta\Delta-[P_p]^{4+}$ are able to inhibit growth of the B-16 melanoma in vivo. Of the two complexes, $\Delta-[MP_p]^{2+}$ is slight more effective as noted by the smaller overall tumor growth over the time period examined.

It can be seen that the mice in groups 2 and 3 also survived longer from the data in Figure 5.1, however this data is shown explicitly in Figure 5.2. All of the mice in the control group were dead by day 24, whereas all of the mice in groups 2 and 3 were still alive at this time. One mouse from both groups 2 and 3 died on day 28 and another mouse in group 2 died on day 30. The remaining mice were sacrificed on day 31 due to their moribund behavior.
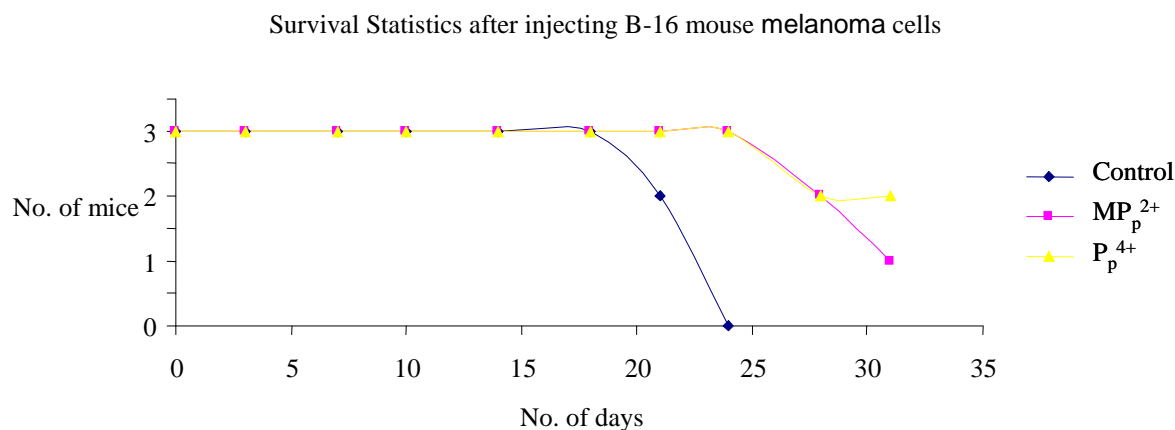
Figure 5.2: Survival statistics for mice with B-16 melanoma tumors after treatment with ruthenium-tatpp complexes.

Clearly, the mice treated with $\Delta-[MP_p]^{2+}$ or $\Delta\Delta-[P_p]^{4+}$ show enhanced survival rates further demonstrating the anti-cancer potential of these two complexes.

Average Body Weight after injecting B-16 mouse melanoma cells
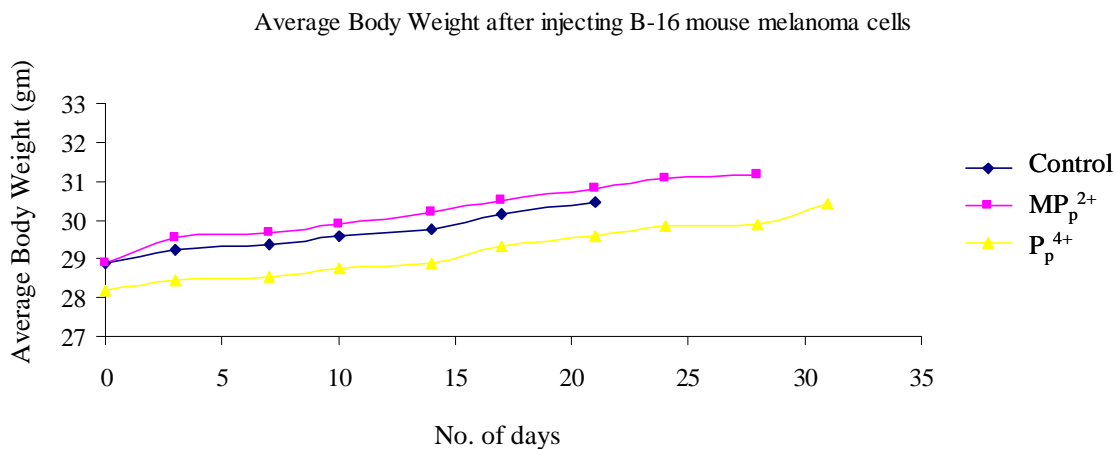
5.3: Average body weights of mice with B-16 melanoma tumors after treatment with ruthenium-tatpp complexes

The mouse body weight data for the syngeneic mouse melanoma model is shown in Figure 5.3. Importantly, none of the mice, treated or control, lost weight during the course of the experiment. This is considered as a positive sign in that the mice continued to eat and drink regularly despite the treatments. With time, all three groups of mice showed some minor weight gain, which simply appears to reflect the growth in tumor volume.

In summary, both $\Delta-[MP_p]^{2+}$ and $\Delta\Delta-[P_p]^{4+}$ show promising anti-proliferative activity on this nominally aggressive and resilient B-16 tumor cell line in vivo. Treated mice not only showed considerably less tumor growth, they also slightly survived longer. The mouse body weight data reveals that the two complexes do not appear to affect normal eating and drinking behavior. This

130

study shows the two complexes clearly warrant further investigation into their potential as anti-cancer drugs. In particular, different dosing regimes as well as both i.v. administrations could be explored to improve the efficacy. Given the robust nature of these complexes towards enzymatic and chemical degradation, we could even explore oral administration.

5.4.2 Antineoplastic Effects of Ruthenium (II) Polypyridyl Complexes-Xenograft Lung Cancer Model

After the promising results we obtained in the syngeneic mouse melanoma model we decided to investigate the effect in a human xenograft mouse model. In this case, human H358 NSCLC bronchio-alveolar non small cell lung cancer cells were introduced into nude mice and the resulting tumors were treated with $\Delta-[MP_p]^{2+}$ and $\Delta\Delta-[P_p]^{4+}$.

As with the B-16 melanoma study, a total of nine 14 week-old male nude mice were divided into three groups of three:

Group 1: Control Group

Group 2: Mice treated with $\Delta-[MP_p]^{2+}$

Group 3: Mice treated with $\Delta\Delta-[P_p]^{4+}$

All animals were injected with 1 million human lung cancer H358 NSCLC, bronchio-alveolar cell suspensions in 100 µL of PBS, subcutaneously in the rear thigh and were examined daily for signs of tumor growth. Treatment was

administered when the tumor surface area exceeded 40 mm^2 which usually occurred approximately 14 days after the cancer cells were injected.

On day 0, the mice in groups 2 and 3 were given i.p. injections of 2.0 mg each of complex $\Delta-[MP_p]^{2+}$ (Group 2) and $\Delta\Delta-[P_p]^{4+}$ (Group 3) dissolved in 200 μL Tris buffer. The control group 1 was injected with 200 μL Tris buffer alone. A second dose of 2.0 mg each of the drugs were given on day 14 and a third dose of 2.0 mg each given on day 30 for groups 2 and 3. Total dosage was 6.0 mg per animal. The mice in the control group were similarly injected with the carrier solution alone. Every other day mice were weighed and tumor dimensions were recorded with calipers. Deaths were also recorded.

Dose and day of treatments are shown in Table 5.2

Table 5.2: Day dose administered for xenograft human lung cancer model

Day	Control	$\Delta-[MP_p]^{2+}$	$\Delta\Delta-[P_p]^{4+}$
0	0 mg (n=3)	2 mg (n=3)	2 mg (n=3)
14	0 mg (n=3)	2 mg (n=3)	2 mg (n=3)
30	0 mg (n=1)	2 mg (n=2)	2 mg (n=2)
Total dose as of day 60	0 mg	6 mg	6 mg

The results of this anti-tumor study are summarized by three factors: tumor volume, animal survival, and animal average body weight.
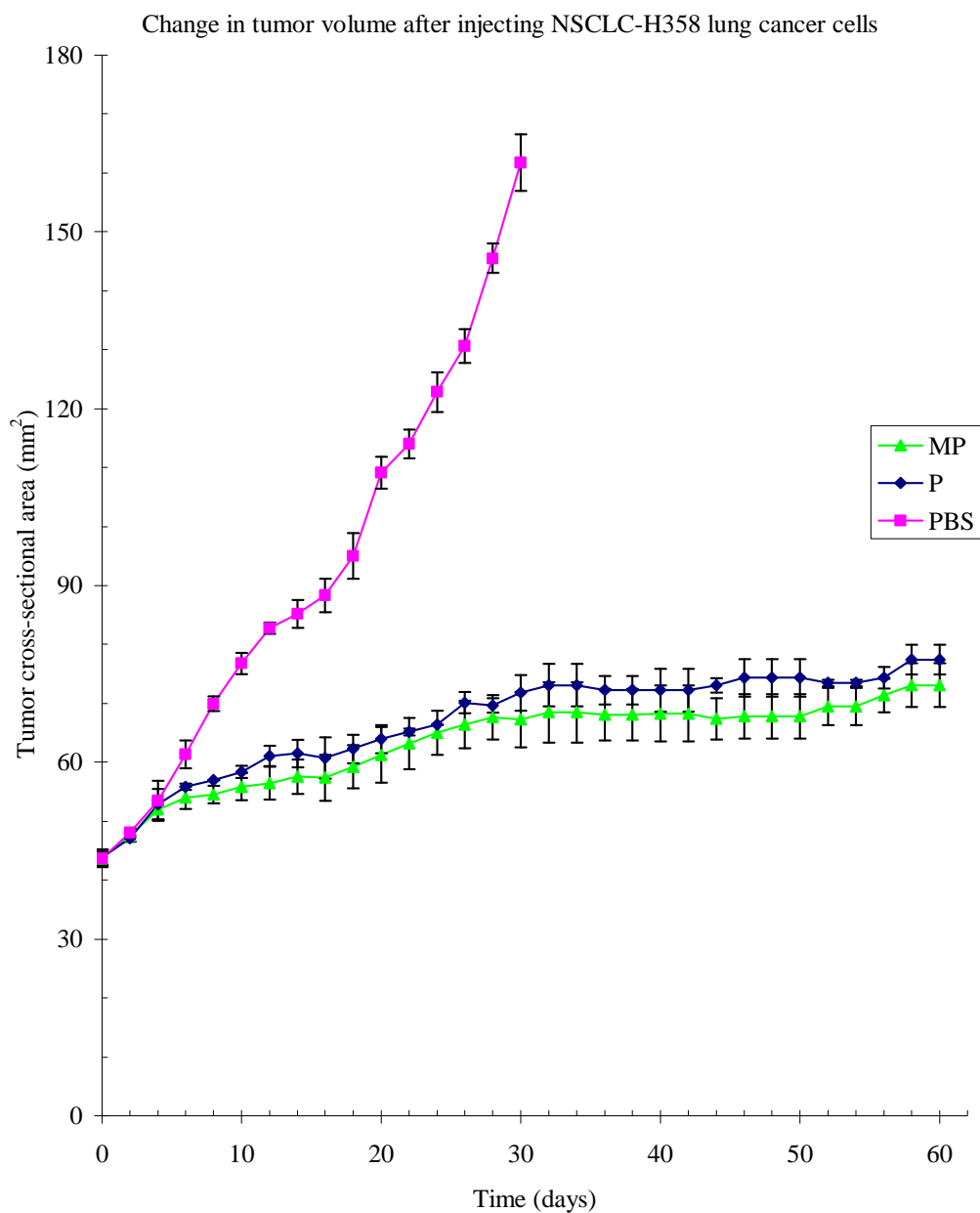
Figure 5.4: Change in H358 lung cancer tumor volume after treatment with ruthenium-tatpp complexes.

Squares represent the mean tumor volume for Group 1 (control); triangles for Group 2 ($\Delta-[MP_p]^{2+}$); and diamonds for Group 3 ($\Delta\Delta-[P_p]^{4+}$)

The results on the tumor volume study were striking as shown in Figure 5.4. Treatment with either $\Delta-[MP_p]^{2+}$ or $\Delta\Delta-[P_p]^{4+}$ prevented any significant tumor growth after the first few days. By comparison, the control group showed rapid increases in tumor volume demonstrating the anti-proliferative activity of $\Delta-[MP_p]^{2+}$ and $\Delta\Delta-[P_p]^{4+}$ in this in vivo model. While similar results were seen in the B-16 syngeneic mouse model, we observed an even more dramatic effect here. This is likely due to the greater cytotoxicity of $\Delta-[MP_p]^{2+}$ and $\Delta\Delta-[P_p]^{4+}$ towards H358 cells (IC_{50}'s of 9 and 9 μM, respectively) over B-16 cells (IC_{50}'s of 41 and 36 μM, respectively). As with the B-16 study, the complex $\Delta-[MP_p]^{2+}$ shows slightly better activity, although this is less pronounced in this case.

The data from the survival study is shown in Figure 5.5. As can be seen, two of the mice in the control group died on day 30 and the last one on day 32. For groups 2 and 3, one mouse from each of groups 2 and 3 died on day 30 and the remaining two mice in each group went on to survive up through day 60 at which point the experiment was ended and the mice sacrificed. Clearly, the survival rate of the treated mice was significantly better than that observed for the control. The death of one mouse from both group 2 and 3 each on day 30 coincided with the day of their last drug injection. As the individual doses of 66 mg/kg were near the MTD for these complexes and that this was their third such dose, it is possible that these deaths may be related to the complexes toxicity rather than the tumor which was still quite modest in size for these two groups.

Additional studies into the dosing are warranted to clarify this survival and efficacy data.

Survival Statistics after injecting human NSCLC lung cancer cells
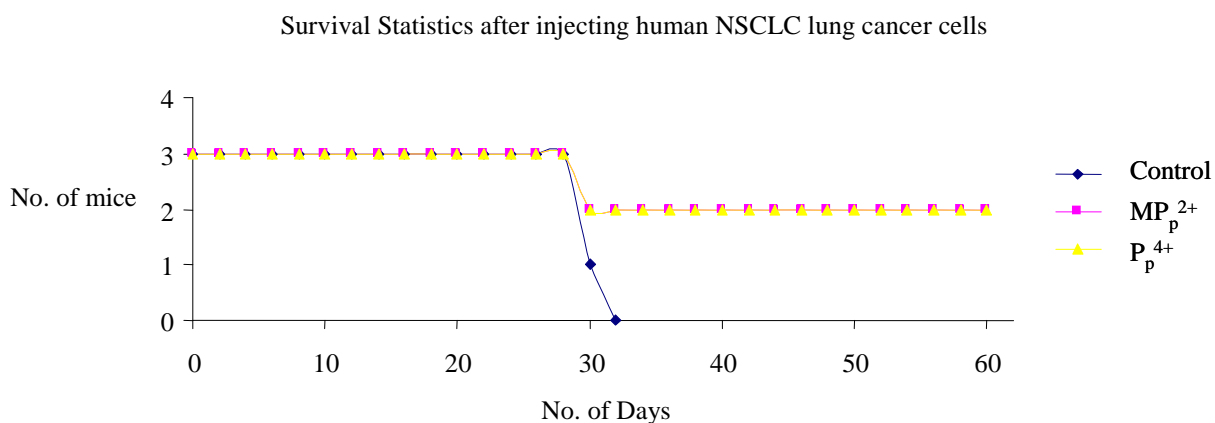
Figure 5.5: Survival statistics for mice with NSCLC H358 tumors after treatment with ruthenium-tatpp complexes.

Finally, we followed the average mouse body weight during the course of this experiment and the data are shown in Figure 5.6. None of the treated mice lost weight during the treatments, which were considered a positive sign as this meant that the mice continued to eat and drink despite repeated injections of these complexes. With time, all three groups of mice showed weight gain, which approximately mirrored the growth in tumor volume, suggesting that the weight gain was largely due to the tumor growth.

Average Body Weight after injecting NSCLC- H358 lung cancer cells
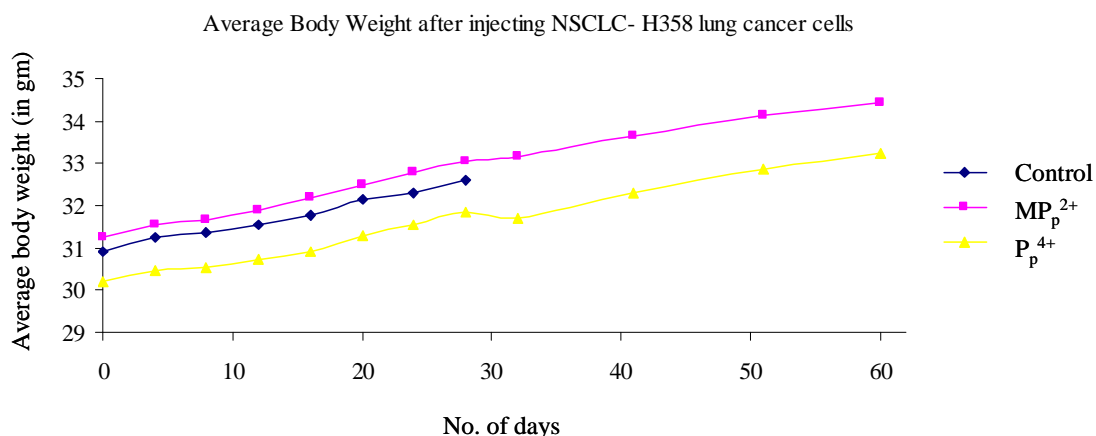
Figure 5.6: Average body weights of mice with NSCLC H358 tumors after treatment with ruthenium-tatpp complexes

5.5 Conclusions

We have investigated a novel class of potential anti-tumor drugs- ruthenium polypyridyl complexes. In our screen we found two ruthenium complexes $\Delta-[MP_p]^{2+}$ and $\Delta\Delta-[P_p]^{4+}$ inhibited the regression of tumor growth in two designed models: syngeneic B16 mouse melanoma model and xenograft H358 non small cell lung cancer model. The complexes were also shown to be comparatively non-toxic with maximum tolerable dose as high as 100 mg/Kg for the two complexes, very rare for this class of complexes. The IC_{50} values were investigated and the two complexes were found to have an IC_{50} in the range of 9 µM in non small cell lung cancer cell lines (H358 and H226). Another study investigated towards a potential mechanism of the anti-cancer activity and it was found that the complexes cleave DNA under hypoxic conditions with a carbon centered radical being involved in the cleavage.

Further study needs to be done to find a mechanistic route of the DNA cleavage through EPR and electrochemistry experiments. As the potential activity of these complexes is due to the presence of redox-active tatpp bridging ligand, one can further explore this possibility by removing the ruthenium centers and seeing if the activity is still there or not, this will answer whether ruthenium is needed at all or not for the anti-cancer activity.

REFERENCES

1.   *Cancer Facts and Figures 2008*; American Cancer Society: Atlanta, 2008; pp 1-72.

2.   Yang, X. L.; Wang, A. H. J., Structural studies of atom-specific anticancer drugs acting on DNA. *Pharmacology & Therapeutics* **1999,** *83* (3), 181-215.

3.   Kumar, C. V.; Barton, J. K.; Turro, N. J., Photophysics of ruthenium complexes bound to double helical DNA. *Journal of the American Chemical Society* **1985,** *107* (19), 5518-23.

4.   Friedman, A. E.; Kumar, C. V.; Turro, N. J.; Barton, J. K., Luminescence of ruthenium(II) polypyridyls: evidence for intercalative binding to Z-DNA. *Nucleic Acids Res* **1991,** *19* (10), 2595-602.

5.   Hiort, C.; Lincoln, P.; Norden, B., DNA binding of D- and L-[Ru(phen)2DPPZ]2+. *Journal of the American Chemical Society* **1993,** *115* (9), 3448-54.

6.   Lincoln, P.; Norden, B., Binuclear ruthenium(II) phenanthroline compounds with extreme binding affinity for DNA. *Chem. Comm.* **1996,** *18*, 2145-2146.

7.   Wilhelmsson, L. M.; Esbjorner, E. K.; Westerlund, F.; Norden, B.; Lincoln, P., Meso Stereoisomer as a Probe of Enantioselective Threading Intercalation of

Semirigid Ruthenium Complex [μ-(11,11'-bidppz)(phen)4Ru2]4+. *J. Phys. Chem. B* **2003,** *107* (42), 11784-11793.

8.   Dwyer, F. P.; Gyarfas, E. C.; Rogers, W. P.; Koch, J. H., Biological activity of complex ions. *Nature* **1952,** *170*, 190-1.

9.   Koch, J. H.; Gyarfas, E. C.; Dwyer, F. P. A., Biological activity of complexions. Mechanism of inhibition of acetylcholinesterase. *Australian J. Biol. Sci.* **1956,** *9*, 371-81.

10.   Koch, J. H.; Rogers, W. P.; Dwyer, F. P.; Gyarfas, E. C., The metabolic fate of tris-1,10-phenanthroline ruthenium-106 (II) perchlorate, a compound with anticholinesterase and curare-like activity. *Australian J. Biol. Sci.* **1957,** *10*, 342-50.

11.   Novakova, O.; Kasparkova, J.; Vrana, O.; van Vliet, P. M.; Reedijk, J.; Brabec, V., Correlation between cytotoxicity and DNA binding of polypyridyl ruthenium complexes. *Biochemistry* **1995,** *34* (38), 12369-78.

12.   Norden, B.; Lincoln, P.; Akerman, B.; Tuite, E., DNA interactions with substitution-inert transition metal ion complexes. *Metal ions in biological systems* **1996,** *33*, 177-252.

13.   Haq, I.; Lincoln, P.; Suh, D.; Norden, B.; Chowdhry, B. Z.; Chaires, J. B., Interaction of Delta - and L-[Ru(phen)2DPPZ]2+ with DNA: A Calorimetric and Equilibrium Binding Study. *Journal of the American Chemical Society* **1995,** *117* (17), 4788-96.

14.   Lincoln, P.; Norden, B. Preparation of transition metal binuclear complexes as antitumor and anti-infective agents. 98-SE1655 9915535, 19980916., 1999.

15.   Janaratne, T. K. Investigation of ruthenium (II) polypyridyl dimers as potential chemotherapeutic agents. . University of Texas at Arlington, Arlington, 2006.

16.   Krishnan, A. Effect of structure and stereochemistry on cytotoxicity of ruthenium polypyridyl complexes. University of Texas at Arlington, Arlington, 2007.

17.   Eriksson, M.; Mehmedovic, M.; Westman, G.; Akerman, B., Time-resolved electrophoretic analysis of mobility shifts for dissociating DNA ligands. *Electrophoresis* **2005,** *26* (3), 524-32.

18.   Rajput, C.; Rutkaite, R.; Swanson, L.; Haq, I.; Thomas, J. A., Dinuclear monointercalating RuII complexes that display high affinity binding to duplex and quadruplex DNA. *Chem. Eur. J.* **2006,** *12* (17), 4611-4619.

19.   Janaratne, T. K.; Yadav, A.; Ongeri, F.; MacDonnell, F. M., Preferential DNA Cleavage under Anaerobic Conditions by a DNA-Binding Ruthenium Dimer. *Inorg. Chem.* **2007,** *46*, 3420-3422.

20.   MacDonnell, F. M.; Janaratne, T. K.; Awashti, S. Ruthenium complexes with modifying activity enhanced under hypoxic conditions. 2006-496837 2007082881, 20060801., 2007.

21.   Kim, M.-J. Chiral metallodendrimers and oligomers containing ruthenium(II) polypyridyl complexes

University of Texas at Arlington, Arlington, 2000.

22.   Konduri, R. Novel ruthenium (II) polypyridyl supramolecules capable of storing multiple electrons upon photoirradiation

University of Texas at Arlington, Arlington, 2003.

23.   Wouters, K. L. Assemblies of assemblies: Supramolecular ordering of nanoscopic ruthenium polypyridyl building blocks

University of Texas at Arlington, Arlington, 2007.

24.   Chitakunye, R. Investigation of the photochemistry of ruthenium complexes containing unusual acceptor ligands

University of Texas at Arlington, Arlington, 2006.

25.   Wong, E.; Giandomenico, C. M., Current Status of Platinum-Based Antitumor Drugs. *Chemical Reviews (Washington, D. C.)* **1999,** *99* (9), 2451-2466.

26.   Farrell, N., Metal complexes as drugs and chemotherapeutic agents. *Comp.Coord. Chem. II* **2004,** *9*, 809-840.

27.   Clarke, M. J., Ruthenium Metallopharmaceuticals. *Coord. Chem. Rev.* **2003,** *236*, 207-231.

28.   Blower, P. J., Inorganic pharmaceuticals. *Ann. Rep. Prog. Chem., Sec A.* **2002,** *98*, 615-633.

29.   Long, E. C.; Barton, J. K., Metallointercallators as probes of DNA structure. *Acc. Chem. Res.* **1990,** *23*, 273-279.

30.   Thorp, H. H., New mechanisms in DNA cleavage by metal complexes. *J. Inorg. Organomet. Polymers* **1993,** *3* (1), 41-57.

31.   Norden, B.; Tjerneld, F., Binding of inert metal complexes to deoxyribonucleic acid detected by linear dichroism. *FEBS Letters* **1976,** *67* (3), 368-70.

32.   Barton, J. K., Metals and DNA: molecular left-handed complements. *Science (Washington, DC, United States)* **1986,** *233* (4765), 727-34.

33.   Barton, J. K. D., A. T. and Goldberg, J. M., Tris(phenanthroline)ruthenium(II): Stereoselectivity in binding to DNA. *J. Am. Chem. Soc.* **1984,** *106*, 2172-2176.

34.   Barton, J. K.; Basile, L. A.; Danishefsky, A.; Alexandrescu, A., Chiral probes for the handedness of DNA helixes: enantiomers of tris(4,7-diphenylphenanthroline)ruthenium(II). *Proceedings of the National Academy of Sciences of the United States of America* **1984,** *81* (7), 1961-5.

35.   Hiort, C.; Lincoln, P.; Nordén, B., DNA Binding of □- and □-[Ru(phen)$_2$DPPZ]$^{2+}$. *J. Am. Chem. Soc.* **1993,** *115*, 3448-3454.

36.   Satyanarayana, S.; Dabrowiak, J. C.; Chaires, J. B., Neither DELTA- nor LAMBDA-tris(phenanthroline)ruthenium(II) binds to DNA by classical intercalation. *Biochemistry* **1992,** *31* (39), 9319 - 9324.

37.   Norden, B. L., Per.; Akerman, B.; Tuite, E. , *DNA Transitions with Substitution-Inert Metal Ion Complexes.*

38.   Sigman, D. S.; Mazumder, A.; Perrin, D. M., Chemical nucleases. *Chemical Reviews (Washington, DC, United States)* **1993,** *93* (6), 2295-316.

39.   Gupta, N.; Grover, N.; Neyhart, G. A.; Liang, W.; Singh, P.; Thorp, H. H., [RuO(dppz)(tpy)]2+ (dppz = dipyridophenazine): a DNA cleavage reagent with high DNA affinity. *Angew. Chem.* **1992,** *104* (8), 1058-60 (See also Angew Chem , Int Ed Engl , 1992, 31(8), 1048-50).

40.   Gupta, N.; Grover, N.; Neyhart, G. A.; Singh, P.; Thorp, H. H., Synthesis and properties of new DNA cleavage agents based on oxoruthenium(IV). *Inorg Chem* **1993,** *32* (3), 310-16.

41.   Sadler, P. J.; Guo, Z., Metal complexes in medicine: design and mechanism of action. *Pure Appl. Chem.* **1998,** *70* (4), 863-871.

42.   Heo, J.; Raines, K. W.; Mocanu, V.; Campbell, S. L., Redox Regulation of RhoA. *Biochemistry* **2006,** *45* (48), 14481-14489.

43.   Pogozelski, W. K.; Tullius, T. D., Oxidative Strand Scission of Nucleic Acids: Routes Initiated by Hydrogen Abstraction from the Sugar Moiety. *Chem. Rev.* **1998,** *98* (3), 1089-1107.

44.   Floyd, R. A.; Watson, J. J.; Wong, P. K.; Altmiller, D. H.; Rickard, R. C., Hydroxyl free radical adduct of deoxyguanosine: sensitive detection and mechanisms of formation. *Free Radic Res Commun* **1986,** *1* (3), 163-72.

45.   Zelenko, O.; Gallagher, J.; Sigman, D. S., Scission of DNA with bis(1,10-phenanthroline)copper without intramolecular hydrogen migration. *Angew. Chem., Int. Ed. Engl.* **1998,** *36* (24), 2776-2778.

46.   Meijler, M. M.; Zelenko, O.; Sigman, D. S., Chemical Mechanism of DNA Scission by (1,10-Phenanthroline)copper. Carbonyl Oxygen of 5-Methylenefuranone Is Derived from Water. *J. Am. Chem. Soc.* **1997,** *119* (5), 1135-1136.

47.   Maeda, M.; Nushi, K.; Kawazoe, Y., Chemical alterations of nucleic acids and their components. VII. C-Alkylation of purine bases through free radical process catalyzed by ferrous ion. *Tetrahedron* **1974,** *30* (16), 2677-82.

48.   Mohler, D. L.; Dain, D. R.; Kerekes, A. D.; Nadler, W. R.; Scott, T. L., Organometallic photonucleases: a novel class of DNA-cleaving agents. *Bioorganic & Medicinal Chemistry Letters* **1998,** *8* (7), 871-874.

49.   Hatayama, T.; Goldberg, I. H., Deoxyribonucleic acid sugar damage in the action of neocarzinostatin. *Biochemistry* **1980,** *19* (25), 5890-8.

50.   Povirk, L. F.; Dattagupta, N.; Warf, B. C.; Goldberg, I. H., Neocarzinostatin chromophore binds to deoxyribonucleic acid by intercalation. *Biochemistry* **1981,** *20* (14), 4007-14.

51.   Grover, N.; Thorp, H. H., Efficient electrocatalytic and stoichiometric oxidative cleavage of DNA by oxoruthenium(IV). *J. Am. Chem. Soc.* **1991,** *113* (18), 7030-1.

52.   Gupta, N.; Grover, N.; Neyhart, G. A.; Liang, W.; Singh, P.; Thorp, H. H., [RuO(dppz)(tpy)]2+ (dppz = dipyridophenazine): a DNA cleavage reagent with high DNA affinity. *Angew. Chem., Int. Ed. Engl.* **1992,** *31* (8).

53.   Neyhart, G. A.; Cheng, C.-C.; Thorp, H. H., Kinetics and Mechanism of the Oxidation of Sugars and Nucleotides by Oxoruthenium(IV): Model Studies for Predicting Cleavage Patterns in Polymeric DNA and RNA. *J. Am. Chem. Soc.* **1995,** *117* (5), 1463-71.

54.   Carter, P. J.; Cheng, C.; Thorp, H. H., Oxidation of DNA and RNA by Oxoruthenium(IV) Metallointercalators: Visualizing the Recognition Properties of Dipyridophenazine by High-Resolution Electrophoresis. *J. Am. Chem. Soc.* **1998,** *120* (4), 632-642.

55.   Fu, K.-L. P.; Bradley, P. M.; Turro, C., *Inorg. Chem.* **2001,** *40*, 2476-.

56.   Fu, P. K. L.; Bradley, P. M.; van Loyen, D.; H. Duerr; Bossmann, S. H.; Turro, C., DNA Photocleavge by a Supramolecular Ru(II)-Viologen Complex. *Inorg. Chem.* **2002,** *41*, 3808-3810.

57.   Holder, A. A.; Swavey, S.; Brewer, K. J., Design Aspects for the Development of Mixed Metal Supramolecular Complexes Capable of Visible Light Induced Photocleavage of DNA. *Inorg. Chem.* **2004,** *43,* 303-308.

58.   Elias, B.; Kirsch-De Mesmaeker, A., Photo-reduction of polyazaaromatic Ru(II) complexes by biomolecules and possible applications. *Coord. Chem. Rev.* **2006,** *250* (13-14), 1627-1641.

59.   Pierard, F.; Kirsch-De Mesmaeker, A., Bifunctional transition metal complexes as nucleic acid photoprobes and photoreagents. *Inorg. Chem. Comm.* **2006,** *9* (1), 111-126.

60.   Hergueta-Bravo, A.; Jimenez-Hernandez, M. E.; Montero, F.; Oliveros, E.; Orellana, G., Singlet Oxygen-Mediated DNA Photocleavage with Ru(II) Polypyridyl Complexes. *J. Phys. Chem. B.* **2002,** *106* (15), 4010-4017.

61.   Mei, H. Y.; Barton, J. K., Tris(tetramethylphenanthroline)ruthenium(II): a chiral probe that cleaves A-DNA conformations. *Proc. Natl. Acad. Sci. U. S. A.* **1988,** *85* (5), 1339-43.

62.   Holder, A. A.; Zigler, D. F.; Tarrago-Trani, M. T.; Storrie, B.; Brewer, K. J., Photobiological Impact of [{(bpy)2Ru(dpp)}2RhCl2]Cl5 and [{(bpy)2Os(dpp)}2RhCl2]Cl5 [bpy = 2,2'-Bipyridine; dpp = 2,3-Bis(2-pyridyl)pyrazine] on Vero Cells. *Inorg. Chem.* **2007,** *46*, 4760 - 4762.

63.   Swavey, S.; Brewer, K. J., Visible Light Induced Photocleavage of DNA by a Mixed-Metal Supramolecular Complex: [{(bpy)2Ru(dpp)}2RhCl2]5+. *Inorg. Chem.* **2002,** *41* (24), 6196-6198.

64.   de Tacconi, N. R.; Lezna, R. O.; Chitakunye, R.; MacDonnell, F. M., Electroreduction of the Ruthenium Complex [(bpy)2Ru(tatpp)]Cl2 in Water: Insights on the Mechanism of Multielectron Reduction and Protonation of the Tatpp Acceptor Ligand as a Function of pH. *Inorg. Chem. (Washington, DC, U. S.)* **2008,** *47* (19), 8847-8858.

65.   Kim, M.-J.; Konduri, R.; Ye, H.; MacDonnell, F. M.; Puntoriero, F.; Serroni, S.; Campagna, S.; Holder, T.; Kinsel, G.; Rajeshwar, R., Dinuclear Ru(II) Polypyridyl Complexes Containing Large, Redox-Active Aromatic Bridging Ligands. Synthesis, Characterization and Intramolecular Quenching of MLCT Excited States. *Inorg. Chem.* **2002,** *41* (9), 2471-2476.

66.   de Tacconi, N. R.; Lezna, R. O.; Konduri, R.; Ongeri, F.; Rajeshwar, K.; MacDonnell, F. M., Influence of pH on the photochemical and electrochemical reduction of the dinuclear ruthenium complex, [(phen)2Ru(tatpp)Ru(phen)2]Cl4, in water: Proton-coupled sequential and concerted multi-electron reduction. *Chem.--Eur. J.* **2005,** *11* (15), 4327-4339.

67.   Janaratne, T. K. Investigation of ruthenium(II) polypyridyl dimers as potential chemotherapeutic agents University of Texas at Arlington, Arlington, 2006.

68.   Konduri, R.; de Tacconi, N. R.; Rajeshwar, K.; MacDonnell, F. M., Multielectron photoreduction of a bridged ruthenium dimer, [(phen)2Ru(tatpp)Ru(phen)2][PF6]4: aqueous reactivity and chemical and spectroelectrochemical identification of the photoproducts. *J. Am. Chem. Soc.* **2004,** *126* (37), 11621-9.

69.   Tu, C.; Shao, Y.; Gan, N.; Xu, Q.; Guo, Z., Oxidative DNA Strand Scission Induced by a Trinuclear Copper(II) Complex. *Inorg. Chem.* **2004,** *43*, 4761-4766.

70.   Ren, R.; Yang, P.; Zheng, W.; Hua, Z., A simple copper(II)-L-histidine system for efficient hydrolytic cleavage of DNA. *Inorg Chem* **2000,** *39* (24), 5454-63.

71.   Mohler, D. L.; Shell, T. A., The hydrogen peroxide induced enhancement of DNA cleavage in the ambient light photolysis of CpFe(CO)2Ph: A potential strategy for targeting cancer cells. *Bioorganic & Medicinal Chemistry Letters* **2005,** *15* (20), 4585-4588.

72.   Yamaguchi, T.; Kashige, N.; Mishiro, N.; Miake, F.; Watanabe, K., Dihydropyrazine derivatives as a new type of DNA strand breaking agent. *Biol. Pharm. Bull.* **1996,** *19* (10), 1261-1265.

73.   Yamaguchi, T.; Matsumoto, S.; Watanabe, K., Generation of free radicals from dihydropyrazines with DNA strand-breakage activity. *Tetrahedron Lett.* **1998,** *39* (45), 8311-8312.

74.   Yamaguchi, T.; Ito, S.; Iwase, Y.; Watanabe, K.; Harano, K., Products from a novel reaction of dihydropyrazines with vicinal diamines. *Heterocycles* **1999,** *51* (10), 2305-2309.

75.   Yamaguchi, T.; Eto, M.; Harano, K.; Kashige, N.; Watanabe, K.; Ito, S., New compounds derived from dihydropyrazines having DNA strand-breakage activity. *Tetrahedron* **1999,** *55* (3), 675-686.

76.   Yamaguchi, T. I., S.; Iwase, Y.; Watanabe, K.; Harano, K., A diamine-exchange reaction of dihydropyrazines. *Heterocycles* **2000,** *53* (8), 1677-1680.

148

77.   Yamaguchi, T.; Nomura, H.; Matsunaga, K.; Ito, S.; Takata, J.; Karube, Y., The behavior of dihydropyrazine with DNA strand-breakage activity in vivo. *Biol. Pharm. Bull.* **2003,** *26* (11), 1523-1527.

78.   Kashige, N.; Takeuchi, T.; Matsumoto, S.; Takechi, S.; Miake, F.; Yamaguchi, T., Radical species in DNA strand-cleavage caused by dihydropyrazines. *Biol. Pharm. Bull.* **2005,** *28* (3), 419-423.

79.   Takeda, O.; Takechi, S.; Katoh, T.; Yamaguchi, T., The role of dihydropyrazines in accelerated death of Escherichia coli on addition of copper(II). *Biol. Pharm. Bull.* **2005,** *28* (7), 1161-1164.

80.   Tossi, A. B.; Kelly, J. M., A study of some polypyridylruthenium(II) complexes as DNA binders and photocleavage reagents. *Photochem. Photobiol.* **1989,** *49* (5), 545-56.

81.   Rosenberg, B.; VanCamp, L.; Trosko, J. E.; Mansour, V. H., Platinum compounds: a new class of potent antitumour agents. *Nature* **1969,** *222* (5191), 385-6.

82.   Brabec, V., DNA Modifications by antitumor platinum and ruthenium compounds: their recognition and repair *Progress in nucleic acid research and molecular biology* **2002,** *71*, 1-68.

83.   Reedijk, J., Improved understanding in platinum antitumor chemistry. *Chem. Commun.* **1996**, 801-806.

84.   Raymond, E. F., S.; Woynarowski, J. M. and Chaney, S. G., Oxaliplatin: Mechanism of action and antineoplastic activity. *Seminars in oncology* **1998,** *25* (2), 4-12.

85.   Fruhauf, S.; Zeller, W. J., In vitro evaluation of platinum, titanium and ruthenium metal complexes in cisplatin-sensitive and -resistant rat ovarian tumors. *Cancer Chemother Pharmacol* **1991,** *27* (4), 301-7.

86.   Fruhauf, S.; Zeller, W. J., New platinum, titanium, and ruthenium complexes with different patterns of DNA damage in rat ovarian tumor cells. *Cancer Res* **1991,** *51* (11), 2943-8.

87.   Gallori, E.; Vettori, C.; Alessio, E.; Vilchez, F. G.; Vilaplana, R.; Orioli, P.; Casini, A.; Messori, L., DNA as a possible target for antitumor ruthenium(III) complexes. *Arch Biochem Biophys* **2000,** *376* (1), 156-62.

88.   Clarke, M. J.; Zhu, F.; Frasca, D. R., Non-Platinum Chemotherapeutic Metallopharmaceuticals. *Chem. Rev.* **1999,** *99* (9), 2511-2533.

89.   Tuite, E.; Lincoln, P.; Norden, B., Photophysical Evidence that Delta - and L-[Ru(phen)2(dppz)]2+ Intercalate DNA from the Minor Groove. *J. Am. Chem. Soc.* **1997,** *119* (1), 239-240.

90.   Mishra, L.; Sinha, R.; Itokawa, H.; Bastow, K. F.; Tachibana, Y.; Nakanishi, Y.; Kilgore, N.; Lee, K. H., Anti-HIV and Cytotoxic Activities of Ru(II)/Ru(III) Polypyridyl Complexes Containing 2,6-(2'-Benzimidazolyl)-pyridine/chalcone as Co-Ligand. *Bioorganic & Medicinal Chemistry* **2001,** *9* (7), 1667-1671.

91.   Mazumder, U. K.; Gupta, M.; Karki, S. S.; Bhattacharya, S.; Rathinasamy, S.; Thangavel, S., Synthesis, anticancer and antibacterial activity of some novel mononuclear Ru(II) complexes. *Chemical & Pharmaceutical Bulletin* **2004,** *52* (2), 178-185.

92.   Mishra, L.; Singh, A. K.; Trigun, S. K.; Singh, S. K.; Pandey, S. M., Anthi-HIV and cytotoxic ruthenium(II) complexes containing flavones: biochemical evaluation in mice. *Indian Journal of Experimental Biology* **2004,** *42* (7), 660-666.

93.   MacDonnell, F. M.; Bodige, S., Efficient Stereospecific Syntheses of Chiral Ruthenium Dimers. *Inorg. Chem.* **1996,** *35*, 5758-5759.

94.   Bodige, S.; MacDonnell, F. M., Synthesis of Free and Ruthenium Coordinated 5,6-Diamino-1,10-Phenanthroline. *Tetrahedron Lett.* **1997,** *38* (47), 8159-8160.

95.   MacDonnell, F. M.; Kim, M.-J.; Bodige, S., Substitutionally Inert Metal Complexes as Chiral Synthons for Stereospecific Supramolecular Syntheses. *Coord. Chem. Rev.* **1999,** *185-186*, 535-549.

96.   Sun, P.; Krishnan, A.; Yadav, A.; Singh, S.; MacDonnell, F. M.; Armstrong, D. W., Enantiomeric Separations of Ruthenium(II) Polypyridyl Complexes Using High-Performance Liquid Chromatography (HPLC) with Cyclodextrin Chiral Stationary Phases (CSPs). *Inorg. Chem. (Washington, DC, U. S.)* **2007,** *46* (24), 10312-10320.

97.   Sun, P.; Krishnan, A.; Yadav, A.; MacDonnell, F. M.; Armstrong, D. W., Enantioseparations of chiral ruthenium(II) polypyridyl complexes using HPLC

with macrocyclic glycopeptide chiral stationary phases (CSPs). *J. Mol. Struct.* **2008,** *890* (1-3), 75-80.

98.   Henderson, G. G.; Ewing, A. R., Action of Acidic Oxides on Salts of Hydroxy-acids. Part I. Metallic Tartraarsenites. *J. Chem. Soc.* **1895,** *67*, 102-108.

99.   Bolger, J.; Gourdon, A.; Ishow, E.; Launay, J.-P., Stepwise syntheses of mono- and di-nuclear ruthenium tpphz complexes [(bpy)2Ru(tpphz)]2+ and [(bpy)2Ru(tpphz)Ru(bpy)2]4+ {tpphz = tetrapyrido[3,2-a:2',3'-c:3'',2''-h:2''',3'''-j]phenazine}. *J. Chem. Soc., Chem. Commun.* **1995,** (17), 1799-800.

100.   Bolger, J.; Gourdon, A.; Ishow, E.; Launay, J.-P., Mononuclear and Binuclear Tetrapyrido[3,2-a:2',3'-c:3'',2''-h:2''',3'''-j]phenazine (tpphz) Ruthenium and Osmium Complexes. *Inorg. Chem.* **1996,** *35* (10), 2937-44.

101.   Kim, M.-J. Chiral metallodendrimers and oligomers containing Ru(II) polypyridyl complexes. University of Texas at Arlington, Arlington, 2000.

102.   Awasthi, S.; Singhal, S. S.; He, N.-g.; Chaubey, M.; Zimniak, P.; Srivastava, S. K.; Singh, S. V.; Awasthi, Y. C., Modulation of doxorubicin cytotoxicity by ethacrynic acid. *International Journal of Cancer* **1996,** *68* (3), 333-339.

103.   Satyanarayana, S.; Dabrowiak, J. C.; Chaires, J. B., Tris(phenanthroline)ruthenium(II) enantiomer interactions with DNA: Mode and specificity of binding. *Biochemistry* **1993,** *32* (10), 2573-2584.

104. Puckett, C. A.; Barton, J. K., Methods to Explore Cellular Uptake of Ruthenium Complexes. *J. Am. Chem. Soc.* **2007,** *129* (1), 46-47.

105. de Tacconi, N. R.; Lezna, R. O.; Konduri, R.; Ongeri, F.; Rajeshwar, K.; MacDonnell, F. M., Influence of pH on the Photochemical and Electrochemical Reduction of the Dinuclear Ruthenium Complex, [(phen)$_2$Ru(tatpp)Ru(phen)$_2$]Cl$_4$, in Water: Proton-Coupled Sequential and Concerted Multi-Electron Reduction. *Chem. Eur. J.* **2005,** *11*, 4327-4339.

106. Ishow, E.; Gourdon, A.; Launay, J.-P.; Lecante, P.; Verelst, M.; Chiorboli, C.; Scandola, F.; Bignozzi, C.-A., Tetranuclear Tetrapyrido[3,2-a:2',3'-c:3'',2''-h:2''',3'''-j]phenazine ruthenium Complex: Synthesis, Wide Angle Scattering, and Photophysical Studies. *Inorg. Chem.* **1998,** *37*, 3603-3609.

107. Alberts, D. S.; Garcia, D.; Mason-Liddil, N., Cisplatin in advanced cancer of the cervix: an update. *Seminars in oncology* **1991,** *18* (1 Suppl 3), 11-24.

108. Chu, G., Cellular responses to cisplatin. The roles of DNA-binding proteins and DNA repair. *J Biol Chem* **1994,** *269* (2), 787-90.

109. Huang, J.; Mohanty, S.; Basu, A., Cisplatin resistance is associated with deregulation in protein kinase C-delta. *Biochemical and Biophysical Research Communications* **2004,** *316* (4), 1002-1008.

110. Johnson, C. L.; Lu, D.; Huang, J.; Basu, A., Regulation of p53 stabilization by DNA damage and protein kinase C. *Molecular Cancer Therapeutics* **2002,** *1* (10), 861-867.

111.   Wasserman, T. H.; Slavik, M.; Carter, S. K., Methyl-CCNU inclinical cancer therapy. *Cancer treatment reviews* **1974,** *1* (4), 251-69.

112.   Salmon, S. E., Nitrosoureas in multiple myeloma. *Cancer treatment reports* **1976,** *60* (6), 789-94.

113.   Hoogstraten, B.; Sheehe, P. R.; Cuttner, J.; Cooper, T.; Kyle, R. A.; Oberfield, R. A.; Townsend, S. R.; Harley, J. B.; Hayes, D. M.; Costa, G.; Holland, J. F., Melphalan in multiple myeloma. *Blood* **1967,** *30* (1), 74-83.

114.   Begleiter, A.; Goldenberg, G. J., Uptake and decomposition of chlorambucil by L5178Y lymphoblasts in vitro. *Biochemical Pharmacology* **1983,** *32* (3), 535-9.

115.   Egorin, M. J.; Snyder, S. W.; Wietharn, B. E., Effects of ethanolamine and choline on thiotepa cellular accumulation and cytotoxicity in L1210 cells. *Cancer Research* **1990,** *50* (14), 4322-7.

116.   Wall, M. E.; Wani, M. C.; Cook, C. E.; Palmer, K. H.; McPhail, A. T.; Sim, G. A., Plant antitumor agents. I. Isolation and structure of camtothecin, a novel alkaloidal leukemia and tumor inhibitor from Camptotheca acuminata. *Journal of the American Chemical Society* **1966,** *88* (16), 3888-90.

117.   Potmesil, M., Camptothecins: from bench research to hospital wards. *Cancer Research* **1994,** *54* (6), 1431-9.

118.   Wang, J. C., *Annu. Rev. Biochem.* **1996,** *65*, 635-692.

119. Beer, E. L. D. B., A. E.; Voest, E. E., Doxorubicin and mechanical performance of cardiac trabeculae after acute and chronic treatment: a review. *Eur. J. Pharma.* **2001,** *415*, 1-11.

120. Binaschi, M. B., M.; Cipollone, A.; Rossi, C.; Goso, C.; Maggi, C. A.; Capranico, G. and Animati, F., Anthracyclines: Selected New Developments. *Curr. Med. Chem.- Anti-Cancer Agents* **2001,** *1*, 113-130.

121. Heidelberger, C.; Chaudhuri, N. K.; Danneberg, P.; Mooren, D.; Griesbach, L.; Duschinsky, R.; Schnitzer, R. J.; Pleven, E.; Scheiner, J., Fluorinated pyrimidines, a new class of tumor-inhibitory compounds. *Nature (London, United Kingdom)* **1957,** *179*, 663-6.

122. Chu, E.; Drake, J. C.; Boarman, D.; Baram, J.; Allegra, C. J., Mechanism of thymidylate synthase inhibition by methotrexate in human neoplastic cell lines and normal human myeloid progenitor cells. *Journal of Biological Chemistry* **1990,** *265* (15), 8470-8.

123. Arkin, H.; Ohnuma, T.; Kamen, B. A.; Holland, J. F.; Vallabhajosula, S., Multidrug resistance in a human leukemic cell line selected for resistance to trimetrexate. *Cancer Research* **1989,** *49* (23), 6556-61.

124. Hitchings, G. H.; Elion, G. B., The chemistry and biochemistry of purine analogs. *Annals of the New York Academy of Sciences* **1954,** *60* (2), 195-9.

125. Jordan, M. A.; Wilson, L., Microtubules and actin filaments: dynamic targets for cancer chemotherapy. *Current opinion in cell biology* **1998,** *10* (1), 123-30.

126.   Hamel, E., Antimitotic natural products and their interactions with tubulin. *Medicinal research reviews* **1996,** *16* (2), 207-31.

127.   Altmann, K. H., Microtubule-stabilizing agents: a growing class of important anticancer drugs. *Current Opinion in Chemical Biology* **2001,** *5* (4), 424-431.

128.   Povirk, L. F.; Hogan, M.; Dattagupta, N., Binding of bleomycin to DNA: intercalation of the bithiazole rings. *Biochemistry* **1979,** *18* (1), 96-101.

129.   Reedijk, J., *Inorg. Chim. Acta* **1992,** *873*, 198-200.

130.   Barnard, C. F. J., *Plat. Met. Rev.* **1989,** *33*, 162.

131.   Christian, M. C., *Semin. Oncol.* **1992,** *19*, 720.

132.   Lipp, H.-P. a. H., J. T., Toxicity of platinum compounds. *Expert Opin. Pharmacother.* **2003,** *4* (6), 889-901.

133.   O'Dwyer, P. J. S., J. P. and Johnson, S. W. , Clinical pharmocokinetics and administration of established platinum drugs. *Drugs* **2000,** *59(Suppl. 4)*, 19-27.

134.   Cvitkovic, E. a. B., M., Oxaliplatin: a new therapeutic option in colorectal cancer. *Semin Oncol* **1999,** *26*, 647-662.

135.   Galanski, M.; Arion, V. B.; Jakupec, M. A.; Keppler, B. K., Recent developments in the field of tumor-inhibiting metal complexes. *Curr. Pharmaceu. Design* **2003,** *9* (25), 2078-2089.

136.   Keppler, B. K.; Henn, M.; Juhl, U. M.; Berger, M. R.; Niebl, R.; Wagner, F. E., New ruthenium complexes for the treatment of cancer. *Prog. Clin. Biochem.*

Med. **1989,** *10* (Ruthenium Other Non-Platinum Met. Complexes Cancer Chemother.), 41-69.

137.   Froelich-Ammon, S. J.; Osheroff, N., Topoisomerase poisons: harnessing the dark side of enzyme mechanism. *Journal of Biological Chemistry* **1995,** *270* (37), 21429-32.

138.   Sava, G.; Zorzet, S.; Turrin, C.; Vita, F.; Soranzo, M.; Zabucchi, G.; Cocchietto, M.; Bergamo, A.; DiGiovine, S.; Pezzoni, G.; Sartor, L.; Garbisa, S., Dual Action of NAMI-A in Inhibition of Solid Tumor Metastasis: Selective Targeting of Metastatic Cells and Binding to Collagen. *Clinical Cancer Research* **2003,** *9* (5), 1898-1905.

139.   Kreuser, E. D. K., B. K.; Berdel, W. E.; Piest, A. and Thiel, E., *Semin. Oncol.* **1992,** *19*, 73-81.

140.   Kobayashi, K.; Jodrell, D. I.; Ratain, M. J., Pharmacodynamic-pharmacokinetic relationships and therapeutic drug monitoring. *Cancer Surveys* **1993,** *17* (Pharmacokinetics and Cancer Chemotherapy), 51-78.

141.   Ratain, M. J.; Rosner, G.; Allen, S. L.; Costanza, M.; Van Echo, D. A.; Henderson, I. C.; Schilsky, R. L., Population pharmacodynamic study of amonafide: a Cancer and Leukemia Group B study. *Journal of clinical oncology official journal of the American Society of Clinical Oncology* **1995,** *13* (3), 741-7.

142.   Fox, J., Clinical delivery of therapeutic agents based on metals. *Metal-Based Drugs* **1997,** *4* (3), 133-135.

143.   Sava, G.; Bergamo, A., Ruthenium-based compounds and tumor growth control (review). *Int. J. Oncol.* **2000,** *17* (2), 353-365.

144.   Guo, Z.; Sadler, P. J., Metals in medicine. *Angewandte Chemie, International Edition* **1999,** *38* (11), 1512-1531.

145.   Cohen, S. M., New approaches for medicinal applications of bioinorganic chemistry. *Curr. Opin. Chem. Biol.* **2007,** *11* (2), 115-120.

146.   Burger, R. M.; Berkowitz, A. R.; Peisach, J.; Horwitz, S. B., Origin of malondialdehyde from DNA degraded by Fe(II) x bleomycin. *J Biol Chem* **1980,** *255* (24), 11832-8.

147.   Vermorken, J. B., The role of anthracyclines in second-line therapy of ovarian cancer. *Int J Gynecol Cancer* **2003,** *13 Suppl 2*, 178-84.

148.   Von Hoff, D. D.; Layard, M. W.; Basa, P.; Davis, H. L., Jr.; Von Hoff, A. L.; Rozencweig, M.; Muggia, F. M., Risk factors for doxorubicin-induced congestive heart failure. *Ann Intern Med* **1979,** *91* (5), 710-7.

149.   Harris, L.; Batist, G.; Belt, R.; Rovira, D.; Navari, R.; Azarnia, N.; Welles, L.; Winer, E., Liposome-encapsulated doxorubicin compared with conventional doxorubicin in a randomized multicenter trial as first-line therapy of metastatic breast carcinoma. *Cancer (N. Y., NY, U. S.)* **2002,** *94* (1), 25-36.

150.   Charrois, G. J. R.; Allen, T. M., Multiple injections of pegylated liposomal doxorubicin: Pharmacokinetics and therapeutic activity. *J. Pharmacol. Exp. Ther.* **2003,** *306* (3), 1058-1067.

151.   Fruehauf, S.; Zeller, W. J., New platinum, titanium, and ruthenium complexes with different patterns of DNA damage in rat ovarian tumor cells. *Cancer Res.* **1991,** *51* (11), 2943-8.

152.   Nishiyama, N.; Okazaki, S.; Cabral, H.; Miyamoto, M.; Kato, Y.; Sugiyama, Y.; Nishio, K.; Matsumura, Y.; Kataoka, K., Novel Cisplatin-Incorporated Polymeric Micelles Can Eradicate Solid Tumors in Mice. *Cancer Res.* **2003,** *63* (24), 8977-8983.

153.   Bandak, S.; Goren, D.; Horowitz, A.; Tzemach, D.; Gabizon, A., Pharmacokinetic and therapeutic studies with cisplatin encapsulated in liposomes. *Proc. Int. Symp. Controlled Release Bioact. Mater.* **1999,** *26th*, 771-772.

154.   Vaage, J.; Donovan, D.; Wipff, E.; Abra, R.; Colbern, G.; Uster, P.; Working, P., Therapy of a xenografted human colonic carcinoma using cisplatin or doxorubicin encapsulated in long-circulating pegylated stealth liposomes. *Int J Cancer* **1999,** *80* (1), 134-7.

155.   Newman, M. S.; Colbern, G. T.; Working, P. K.; Engbers, C.; Amantea, M. A., Comparative pharmacokinetics, tissue distribution, and therapeutic effectiveness of cisplatin encapsulated in long-circulating, pegylated liposomes (SPI-077) in tumor-bearing mice. *Cancer Chemother. Pharmacol.* **1999,** *43* (1), 1-7.

156.   Working, P. K.; Newman, M. S.; Sullivan, T.; Brunner, M.; Podell, M.; Sahenk, Z.; Turner, N., Comparative intravenous toxicity of cisplatin solution and

cisplatin encapsulated in long-circulating, pegylated liposomes in cynomolgus monkeys. *Toxicol. Sci.* **1998,** *46* (1), 155-165.

157.   Clarke, M. J., Ruthenium chemistry pertaining to the design of anticancer agents. *Prog. Clin. Biochem. Med.* **1989,** *10* (Ruthenium Other Non-Platinum Met. Complexes Cancer Chemother.), 25-39.

158.   Anghileri, L. J., The in vivo inhibition of tumor growth by ruthenium red: its relationship with the metabolism of calcium in the tumor. *Z Krebsforsch Klin Onkol Cancer Res Clin Oncol* **1975,** *83* (3), 213-7.

159.   Keppler, B. K.; Rupp, W., Antitumor activity of imidazolium-bisimidazole-tetrachlororuthenate(III). A representative of a new class of inorganic antitumor agents. *J. Cancer Res. Clin. Oncol.* **1986,** *111* (2), 166-8.

160.   Fruehauf, S.; Zeller, W. J., In vitro evaluation of platinum, titanium and ruthenium metal complexes in cisplatin-sensitive and -resistant rat ovarian tumors. *Cancer Chemother. Pharmacol.* **1991,** *27* (4), 301-7.

161.   Sava, G.; Pacor, S.; Mestroni, G.; Alessio, E., Effects of the Ru(III) complexes [mer-RuCl3(DMSO)2Im]degrees and Na[trans-RuCl4(DMSO)Im] on solid mouse tumors. *Anticancer Drugs* **1992,** *3* (1), 25-31.

162.   Sava, G.; Bergamo, A., Ruthenium-based compounds and tumour growth control (review). *Int J Oncol* **2000,** *17* (2), 353-65.

163.   Rademaker-Lakhai, J. M.; Van Den Bongard, D.; Pluim, D.; Beijnen, J. H.; Schellens, J. H. M., A Phase I and Pharmacological Study with Imidazolium-

trans-DMSO-imidazole-tetrachlororuthenate, a Novel Ruthenium Anticancer Agent. *Clin. Cancer Res.* **2004,** *10* (11), 3717-3727.

164. Perrotta, C.; Bizzozero, L.; Falcone, S.; Rovere-Querini, P.; Prinetti, A.; Schuchman, E. H.; Sonnino, S.; Manfredi, A. A.; Clementi, E., Nitric Oxide Boosts Chemoimmunotherapy via Inhibition of Acid Sphingomyelinase in a Mouse Model of Melanoma. *Cancer Research* **2007,** *67* (16), 7559-7564.

165. Yang, Y.; Yang, S.; Ye, Z.; Jaffar, J.; Zhou, Y.; Cutter, E.; Lieber, A.; Hellstroem, I.; Hellstroem, K. E., Tumor Cells Expressing Anti-CD137 scFv Induce a Tumor-Destructive Environment. *Cancer Research* **2007,** *67* (5), 2339-2344.

166. Singhal, S. S.; Awasthi, Y. C.; Awasthi, S., Regression of Melanoma in a Murine Model by RLIP76 Depletion. *Cancer Research* **2006,** *66* (4), 2354-2360.

167. Akazawa, T.; Masuda, H.; Saeki, Y.; Matsumoto, M.; Takeda, K.; Tsujimura, K.; Kuzushima, K.; Takahashi, T.; Azuma, I.; Akira, S.; Toyoshima, K.; Seya, T., Adjuvant-Mediated Tumor Regression and Tumor-Specific Cytotoxic Response Are Impaired in MyD88-Deficient Mice. *Cancer Research* **2004,** *64* (2), 757-764.

168. Anderson, W. K., Activity of bis-carbamoyloxymethyl derivatives of pyrroles and pyrrolizines against human tumor xenografts in nude mice. *Cancer Research* **1982,** *42* (6), 2168-70.

169. Dalal, M.; Plowman, J.; Breitman, T. R.; Schuller, H. M.; Del Campo, A. A.; Vistica, D. T.; Driscoll, J. S.; Cooney, D. A.; Johns, D. G., Arabinofuranosyl-5-

azacytosine: antitumor and cytotoxic properties. *Cancer Research* **1986,** *46* (2), 831-8.

170.   Hjarnaa, P.-J. V.; Jonsson, E.; Latini, S.; Dhar, S.; Larsson, R.; Bramm, E.; Skov, T.; Binderup, L., CHS 828, a novel pyridyl cyanoguanidine with potent antitumor activity in vitro and in vivo. *Cancer Research* **1999,** *59* (22), 5751-5757.

171.   Singhal, S. S.; Singhal, J.; Yadav, S.; Dwivedi, S.; Boor, P. J.; Awasthi, Y. C.; Awasthi, S., Regression of lung and colon cancer xenografts by depleting or inhibiting RLIP76 (ral-binding protein 1). *Cancer Research* **2007,** *67* (9), 4382-4389.

BIOGRAPHICAL INFORMATION

Abhishek Yadav was born on October 20, 1981 in Delhi, India. He received his Bachelor's Degree with Honors and Masters Degree in Chemistry from University of Delhi in 2001 and 2003 respectively. From 2003-2004, he did research as a Junior Research Fellow under the supervision of Prof. Amarnath Maitra, FNA, Department of Chemistry, University of Delhi, India in a project titled "Targeted delivery of Amphotericin-B drug through polymeric nanoparticles as drug delivery carriers".

Starting fall of 2004 he started attending the University of Texas at Arlington for his Doctoral of Philosophy in Chemistry under the supervision of Prof. Frederick M. MacDonnell. He worked primarily on development of novel cancer therapies using DNA-binding chiral coordination complexes.

Abhishek Yadav went to Bristol Myers Squibb, Co. New York for his research internship at the Department of Biotechnology in Summer of 2008.

Abhishek Yadav graduated from University of Texas at Arlington in 2008.